

REPORT DOCUMENTATION PAGE

AD-A228 746

1. AGENCY USE ONLY (Leave blank)		2. REPORT DATE August 1990	3. REPORT TYPE AND DATES COVERED Final 15 May 88 - 14 Oct 89
4. TITLE AND SUBTITLE New Non-Linear Optical Polymers			5. FUNDING NUMBERS 61102F 2303/A3
6. AUTHOR(S) I. Gorodisher (For G. E. Wnek and D. R. Uhlmann, P.I.'s)			
7. PERFORMING ORGANIZATION NAME(S) AND ADDRESS(ES) Rensselaer Polytechnic Institute University of Arizona			8. PERFORMING ORGANIZATION REPORT NUMBER AFOSR-TR- 90 1070
9. SPONSORING MONITORING AGENCY NAME(S) AND ADDRESS(ES) AFOSR/NC Bolling AFB Washington, D.C. 20332-6448			10. SPONSORING MONITORING AGENCY REPORT NUMBER F49620-88-C-0078
11. SUPPLEMENTARY NOTES			
12a. DISTRIBUTION AVAILABILITY STATEMENT Approved for Public Release: Distribution is unlimited			12b. DISTRIBUTION CODE
13. ABSTRACT (Maximum 200 words) New polyurethanes were prepared which exhibit non-linear optical activity. The polymers were poled during synthesis, advantage being taken of the fast polymerization kinetics. Second harmonic generation (SHG) was observed from these polymers. In selected cases, no decrease in the SHF signal (due to depolarization) was observed at room temperature for up to one month. The SHG activity of a series of organic model compounds was also investigated.			
14. SUBJECT TERMS Non-Linear Optical Polymers; Polyurethanes, Second Harmonic Generation			15. NUMBER OF PAGES 143
			16. PRICE CODE
17. SECURITY CLASSIFICATION OF REPORT UNCLASSIFIED	18. SECURITY CLASSIFICATION OF THIS PAGE UNCLASSIFIED	19. SECURITY CLASSIFICATION OF ABSTRACT UNCLASSIFIED	20. LIMITATION OF ABSTRACT SAR

DTIC
ELECTE
NOV 16 1990
S E D

New Non-Linear Optical Polymers
~~NOVEL POLYMERS AND ORGANICS FOR
OPTICAL SECOND HARMONIC GENERATION~~



by

ILYA GORODISHER

S.M. Materials Science and Engineering
Massachusetts Institute of Technology
(1986)
S.B. Materials Science and Engineering
Massachusetts Institute of Technology
(1985)

Accession For	
DTIS GRA&I	<input checked="" type="checkbox"/>
DTIC TAB	<input checked="" type="checkbox"/>
Unannounced	<input type="checkbox"/>
Justification	
By _____	
Distribution/	
Availability Codes	
Dist	Avail and/or Special
A-1	

Submitted to the Department of Materials Science and Engineering in
Partial Fulfillment of the Requirements of the Degree of
Doctor of Philosophy in Polymers at the
Massachusetts Institute of Technology
June 1990

© Massachusetts Institute of Technology

Signature of Author _____
Department of Materials Science and Engineering
May 4, 1990

Certified by _____
Michael F. Rubner
Thesis Supervisor

Accepted by _____
Thomas W. Eagar
Chairman, Departmental Committee on Graduate Students

Approved for public release;
distribution unlimited.

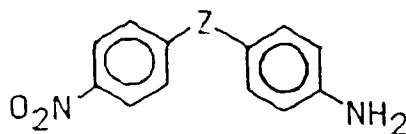
Novel Non-Linear Optical Polymers
**NOVEL POLYMERS AND ORGANICS FOR
 OPTICAL SECOND HARMONIC GENERATION**

by
 ILYA GORODISHER

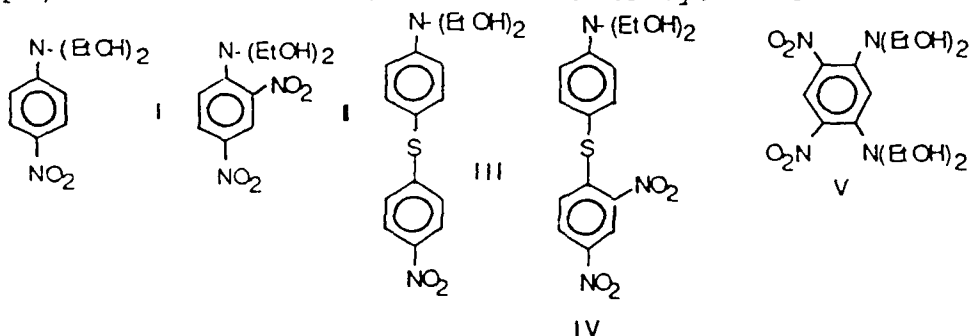
Submitted to the Department of Materials Science and Engineering
 in Partial Fulfillment of the Requirements of the
 Degree of Doctor of Philosophy in Polymers

ABSTRACT

A series of bridged amino nitro diphenyl compounds (below) was studied to determine the effect of the bridging entity Z on the hyperpolarizability of the molecule.



Several series of novel polyesters and polyurethanes were prepared by condensation of five alcohol monomers (below), containing second harmonic generation (SHG) active groups, with diacid chlorides and diisocyanates.



Four novel diols and a novel tetrol were designed to covalently incorporate nitroanilines and aminonitrodiphenyl sulfides into the polymeric backbone.

Polymer structures were confirmed by NMR, IR and UV spectroscopies and elemental analysis. Polymers were characterized by X-ray scattering and DSC. Diols and diisocyanates were corona poled during the course of the polymerization. This approach showed improved active group alignment vs the conventionally corona poled polymers as indicated by an up to 500% increase of the SHG. Polyurethanes showed excellent stability of the SHG signal at room and at elevated temperatures due to the hydrogen bonding "locking in" the SHG active dipole. Crosslinked polyurethanes showed no SHG signal relaxation after 1000 second exposure to 120°C.

Thesis Supervisor: Prof. M.F. Rubner

Associate Professor of Materials Science

TABLE OF CONTENTS

Title page.....	1
Abstract.....	2
Table of Contents.....	3
List of Figures.....	6
List of Tables.....	10
Acknowledgements.....	12
 I. Introduction.....	 13
1.1 VLSI Technology and Its Limitations.....	13
1.2 NLO Systems for SHG.....	15
1.3 Polymeric SHG Systems.....	16
 II. SHG Theory.....	 18
2.1 Material Requirements for SHG.....	18
2.2 Lorenz Model.....	19
2.3 SHG Measurement Techniques.....	21
2.3.1 Pockel's Effect.....	21
2.3.2 DC Induced SHG.....	21
2.3.3 Solvatochromism.....	22
2.3.4 Maker Fringe Method.....	22
 III. Bridged Diphenyl Compounds.....	 29
3.1 Type I Molecule	29
3.2 Investigation of the Polarization Mechanism of Type I Molecule	30
3.2.1 UV Spectroscopy Study.....	30
3.2.2 Nucleophilicity of the Amine Study.....	33
3.2.3 Dipole Moment Study.....	35
3.2.4 NMR Study.....	36
3.3 Synthesis of Some Type I Molecules.....	39
3.4 Investigation of Their Polarization.....	47
3.4.1 UV Spectroscopy Study.....	47
3.4.2 Solvatochromism.....	48

IV.	Alcohol Monomers.....	50
	4.1 Synthesis of Diols I - V	50
	4.2 Characterization and Discussion.....	52
V.	Diallyl Compounds and Cyclopolymerization.....	55
VI.	Polyesters.....	58
	6.1 Synthesis.....	59
	6.2 Characterization and Discussion.....	60
	6.3 SHG Evaluation.....	61
VII.	Polymers with Increased Concentration of SHG Active Groups per Repeat Unit.....	62
	7.1 Poly(ANDS)	62
	7.1.1 Monomer Synthesis.....	62
	7.1.2 Polymer Synthesis.....	64
	7.1.2.1 Lantz Method.....	64
	7.1.2.2 Wolfe Method.....	65
	7.2 Poly(ANDS Vinylene).....	66
	7.3 Poly(DNDS).....	68
VIII.	Polyurethanes.....	70
	8.1 Synthesis.....	70
	8.2 Characterization.....	79
	8.2.1 HUPEG.....	79
	8.2.2 NMR.....	80
	8.2.3 Elemental Analysis.....	85
	8.2.4 UV and IR Spectroscopies.....	85
	8.2.5 DSC.....	87
	8.2.6 Wide Angle X-Ray Scattering.....	88
	8.3 Poling.....	89
IX.	Polyurethane SHG Evaluation and Discussion.....	94
	9.1 Reference Materials.....	96
	9.2 SHG Relaxation Studies.....	96
	9.2.1 At Room Temperature.....	97
	9.2.2 At Elevated Temperatures.....	98

9.3 Poling Field Strength Effect.....	100
9.4 Film Thickness Dependence.....	102
9.5 Alignment vs Conventional Corona Poling.....	104
9.6 Polyesters vs polyurethanes for SHG.....	105
9.7 Effect of the Second Nitro Group on SHG.....	105
9.8 Anilines vs Diphenyl Sulfides for SHG.....	108
9.9 Effect of the SHG Active Group Density on SHG...	112
IX. Conclusions and Directions for Future Research.....	116
Appendix.....	117
References.....	134

LIST OF FIGURES

FIGURE #	DESCRIPTION	PAGE#
FIGURE 1	χ_2 of various materials	p. 2
FIGURE 2	Non vs Centrosymmetric Crystallization	p. 6
FIGURE 3	Schematic of the Maker Fringe SHG Experiment	p. 12
FIGURE 4	Typical Maker Fringe Result for a Poled Polymer	p. 14
FIGURE 5	Type I Molecule	p. 16
FIGURE 6	Possible Polarizations for a Type I Molecule	p. 17
FIGURE 7	Modena's Chromophore XI	p. 18
FIGURE 8	Typical NMR Spectrum of a Type I Molecule	p. 23
FIGURE 9	NMR Shifts for the Proton Ortho to Amine	p. 28
FIGURE 10	NMR of 2,2'-dimethyl-4-amino-4'-nitro diphenyl sulfide	Appdx
FIGURE 11	NMR of 2-methyl-4-amino-4'-nitro diphenyl sulfide	Appdx
FIGURE 12	NMR of 2'-methyl-4-amino-4'-nitro diphenyl sulfide	Appdx
FIGURE 13	NMR of 2-amino-7-nitro dibenzothiophene	Appdx
FIGURE 14	NMR of 4-hydroxy-4'-nitro diphenyl sulfide	Appdx
FIGURE 15	NMR of 4-chloro-4'-nitro diphenyl sulfide	Appdx
FIGURE 16	Various Alcohols for Polymerization	p. 37
FIGURE 17	Reaction of 4-chloro-4'-nitrodiphenyl Sulfide	p. 40
FIGURE 18	NMR of I	Appdx
FIGURE 19	NMR of II	Appdx
FIGURE 20	NMR of III	Appdx
FIGURE 21	NMR of IV	Appdx
FIGURE 22	NMR of V	Appdx
FIGURE 23	Potential SHG Compounds for Cyclopolymerization	p. 42
FIGURE 24	NMR of VI	Appdx
FIGURE 25	NMR of VII	Appdx
FIGURE 26	Ketene Side Reaction	p. 45
FIGURE 27	NMR of Diphenyl Malonate	Appdx
FIGURE 28	Intrinsic Viscosity of Sln and Melt Polyesters	p. 47
FIGURE 29	NMR of VIII	Appdx
FIGURE 30	NMR of IX	Appdx
FIGURE 31	NMR of Clean IX	Appdx

FIGURE 32	NMR of X	Appdx
FIGURE 33	NMR of XI	Appdx
FIGURE 34	Synthetic Route to Diaminodithiophenoxide salts	p. 52
FIGURE 35	Synthetic Route to Poly(Phenylene Vinylene)	p. 53
FIGURE 36	NMR of dichlorinated B	Appdx
FIGURE 37	DSC of Poly(DNDS)	Appdx
FIGURE 38	SAX of Poly(DNDS)	Appdx
FIGURE 39	NMR of Poly(DNDS)	Appdx
FIGURE 40	PU1	p. 57
FIGURE 41	Corona Alignment Polymerization	p. 58
FIGURE 42	PU2	p. 59
FIGURE 43	PU3	p. 59
FIGURE 44	PU4	p. 60
FIGURE 45	PU5	p. 60
FIGURE 46	DU1	p. 61
FIGURE 47	DU2	p. 61
FIGURE 48	DU3	p. 62
FIGURE 49	DU4	p. 62
FIGURE 50	DU5	p. 63
FIGURE 51	HU1	p. 63
FIGURE 52	HU2	p. 63
FIGURE 53	HU3	p. 64
FIGURE 54	HU4	p. 64
FIGURE 55	HU5	p. 65
FIGURE 56	NMR of PU1	Appdx
FIGURE 57	NMR of PU2	Appdx
FIGURE 58	NMR of PU3	Appdx
FIGURE 59	NMR of PU4	Appdx
FIGURE 60	NMR of HU1	Appdx
FIGURE 61	NMR of HU2	Appdx
FIGURE 62	NMR of HU3	Appdx
FIGURE 63	NMR of HU4	Appdx
FIGURE 64	NMR of DU1	Appdx
FIGURE 65	NMR of DU2	Appdx
FIGURE 66	NMR of DU3	Appdx
FIGURE 67	NMR of DU4	Appdx
FIGURE 68	IR of PU1	Appdx
FIGURE 69	IR of PU2	Appdx
FIGURE 70	IR of PU3	Appdx
FIGURE 71	IR of PU4	Appdx
FIGURE 72	UV of PU1	Appdx
FIGURE 73	UV of PU2	Appdx

FIGURE 74	UV of PU3	Appdx
FIGURE 75	UV of PU4	Appdx
FIGURE 76	UV of PU5	Appdx
FIGURE 77	DSC of PU1	Appdx
FIGURE 78	DSC of PU2	Appdx
FIGURE 79	DSC of PU3	Appdx
FIGURE 80	DSC of PU4	Appdx
FIGURE 81	SAX of PU1	Appdx
FIGURE 82	SAX of PU2	Appdx
FIGURE 83	SAX of PU3	Appdx
FIGURE 84	SAX of PU4	Appdx
FIGURE 85	Parallel Plates Poling	Appdx
FIGURE 86	Parallel Plates Alignment Polymerization w/ PET	Appdx
FIGURE 87	Par. Plates Align. Polymerization, Wnek Method	Appdx
FIGURE 88	SHG from PU1C15	Appdx
FIGURE 89	SHG from PU2C15	Appdx
FIGURE 90	SHG from PU3C15	Appdx
FIGURE 91	SHG from PU4C15	Appdx
FIGURE 92	SHG from PU5C15	Appdx
FIGURE 93	SHG from DU1C15	Appdx
FIGURE 94	SHG from DU2C15	Appdx
FIGURE 95	SHG from DU3C15	Appdx
FIGURE 96	SHG from DU4C15	Appdx
FIGURE 97	SHG from DU5C15	Appdx
FIGURE 98	SHG from HU1C15	Appdx
FIGURE 99	SHG from HU2C15	Appdx
FIGURE 100	SHG from HU3C15	Appdx
FIGURE 101	SHG from HU4C15	Appdx
FIGURE 102	SHG from HU5C15	Appdx
FIGURE 103	SHG from Repoled PU1C15	Appdx
FIGURE 104	SHG from Repoled PU4C15	Appdx
FIGURE 105	SHG from PE1C15	Appdx
FIGURE 106	PU SHG Signal Relaxations at 25°C	p. 84
FIGURE 107	DU5 SHG Signal Relaxation at 120°C	p. 85
FIGURE 108	PU SHG Signal Relaxations at 100°C	p. 86
FIGURE 109	PU SHG Signal Relaxations at 50°C	p. 86
FIGURE 110	PU4 SHG Signal Relaxations	p. 86
FIGURE 111	PU1 SHG Signal Relaxations	p. 86
FIGURE 112	All of the PU SHG Signal Relaxations	p. 87
FIGURE 113	Effect of PU1C5 Film Thickness on Its SHG	p. 88

FIGURE 114	Alignment and Polarization of the Dinitroanilines Covalently Bonded to Stiff Polyurethane Chains	p. 94
FIGURE 115	Alignment and Polarization of the Dinitroanilines Covalently Bonded to Flexible Polyurethane Chains	p. 94
FIGURE 116	PU4 Polarization, Unavailable for PU3	p. 98
FIGURE 117	Effect of the SHG Active Group Density in the Polymer Chain on SHG	p. 99
FIGURE 118	Synthetic Route to a NLO Diisocyanate	p.102
FIGURE 119	Synthetic Route to a NLO Diamine	p.103
FIGURE 120	SHG from Repoled DU1C15	Appdx

LIST OF TABLES

TABLE #	DESCRIPTION	PAGE#
TABLE 1	UV Spectroscopy for Type I Molecules, Z=Se	p. 31
TABLE 2	UV Spectroscopy for Type I Molecules	p. 32
TABLE 3	Activation Energies for NAS for Type I Molecules	p. 33
TABLE 4	Dipole Moments of "Half Molecules"	p. 35
TABLE 5	Dipole Moments of Type I Molecules	p. 35
TABLE 6	Shifts of NMR Quartets in Type I Molecules	p. 37
TABLE 7	Elemental Analysis Results for the Type I Molecules	p. 40
TABLE 8	NMR Peak Assignments for the Type I Molecules	p. 41
TABLE 9	Powder SHG Results for Type I Molecules	p. 42
TABLE 10	$\Delta\nu$ vs CHCl_3 for Type I Molecules	p. 43
TABLE 11	Diphenyl derivatives	p. 46
TABLE 12	NMR Assignments for Sulfur Bridged Compounds	p. 47
TABLE 13	UV Maxima of Type I Molecules, A=NO ₂ , Z=S	p. 47
TABLE 14	Solvatochromism of Type I Molecules, A=NO ₂ , Z=S	p. 48
TABLE 15	Elemental Analysis of I-V Alcohols	p. 53
TABLE 16	NMR Peak Assignments for the I-V Alcohols	p. 54
TABLE 17	NMR Peak Assignments for the Diallyl Compounds	p. 56
TABLE 18	NMR Assignments for the Dichlorodinitrobenzenes	p. 64
TABLE 19	Elemental Analysis Fit For Poly(DNDS)	p. 68
TABLE 20	NMR Peak Assignments for Poly(DNDS)	p. 69
TABLE 21	NMR Assignments for the PU Series	p. 72
TABLE 22	NMR Assignments for the HU Series	p. 83
TABLE 23	NMR Assignments for the DU Series	p. 84
TABLE 24	Synopsis of the Elemental Analysis Results for PU's	p. 85
TABLE 25	Transmission of PU's at the Harmonic Frequency	p. 86
TABLE 26	Peak Assignments for PU IR Absorbtion	p. 86
TABLE 27	Diisocyanates Reactivities	p. 92
TABLE 28	Mechanical Properties of the HUPEG Series	p. 80
TABLE 29	Effect of Polyurethane Structure on Its SHG	p. 95
TABLE 30	Reference SHG Materials	p. 96
TABLE 31	SHG Relaxation of PU's at Elevated Temperatures	p. 97

TABLE 32	Effect of the Poling Field Strength on SHG of PU's	p. 103
TABLE 33	Alignment Polymerization vs Conventional Poling	p. 104
TABLE 34	Polyesters vs Polyurethanes for SHG	p. 105
TABLE 35	Comparison of SHG from Mono and Dinitro Urethanes	p. 106
TABLE 36	Comparison of SHG from Anilines and Sulfides on U's	p. 109

ACKNOWLEDGEMENTS

The list of people who have contributed to the birthing of this document is rather extensive. The love, patience and support of my beautiful wife Susanna during the largely unfunded research years is saintly in light of the sacrifices she had to make. I owe a great deal to my parents who took a tremendous risk when they applied to leave Soviet Union to provide a chance for higher education to their children.

I am indebted to Dr. Donald Uhlmann without whose support, advice and guidance I would not be receiving this degree. I want to thank Dr. Gary Wnek for making me a chemist for being available from 3000 miles away to listen to my synthetic ideas.

I owe a major thanks to Dr. Ray Zanoni to who helped me build a laser facility in Materials Science. I can even understand some "Opticaleze" now. Drs. Henry Hall and Sam Yalkowski receive my gratitude for letting me use their labs, equipment and pick their brains.

A special thanks goes out to Drs. Paul "Doom" Calvert, Mike Weinberg, and Brian Zelinski for patiently listening to several versions of this presentation. Finally, I want to thank the members of my Thesis Committee: Drs. Rubner, Roylance and Chiang for their participation in this unusual defence on such a short notice.

INTRODUCTION

VLSI

Recent advances in technology have created a need for new types of materials. This has been the driving force for the so called "materials revolution." Perhaps the biggest and the most challenging demand on materials had been placed by the information processing industry.

The computer industry's drive to store as much information as possible in a minimal amount of space and to access it in a short time brought forth a new class of materials and processes. New semi-conductive materials, ceramics and polymers were synthesized to meet this challenge.

Very large scale integration, VLSI, requires sharp resolution polymer films for lithography. This type of a photoactive polymer, called a photoresist, needed to be patterned by ultra-violet light and selectively removed on a micron width scale. Currently there is a strong demand for further integration. Sub-micron lithography calls for new polymers that can be patterned by an X-ray source. A shorter wavelength exposure source is needed because the desired circuits need resolution finer than that defined by the wavelength of ultra-violet light.

However, the ultimate limit of this technology is not the wavelength of the radiation source. The problem is in the fact that two transmitting wires can lay only so close to each other before the noise level becomes intolerable. This fact turned scientists to look for a new way of transmitting information. Optical information processing looks very promising as a possible replacement for the current technology.

It offers light speed information processing via a laser beam, optimizing the computational speeds. Non-linear optics provides a tool to increase the resolution by reducing the wavelength of light to a third (third harmonic generation or THG) or a half (second harmonic generation or SHG) of the input beam. Another advantage of the NLO processes is that the memory storage capacity of the material is inversely proportional to the

square of the the wavelength of the writing beam. Thus, SHG phenomena, halving the input wavelength, quadruples the storage capacity.

NLO SYSTEMS

In recent years the interest in optically non-linear (NLO) materials has been growing rapidly. This is indicated by an increasing number of symposia held on this subject every year.^{1,2,3} While earlier research centered on the evaluation of single crystals of small organic molecules⁴ and some inorganic crystals,^{5,6} the utility of polymers in the molecular design of NLO systems was quickly recognized.^{7,8} SHG utility of various material types can be seen in Figure 1.^{9,12}

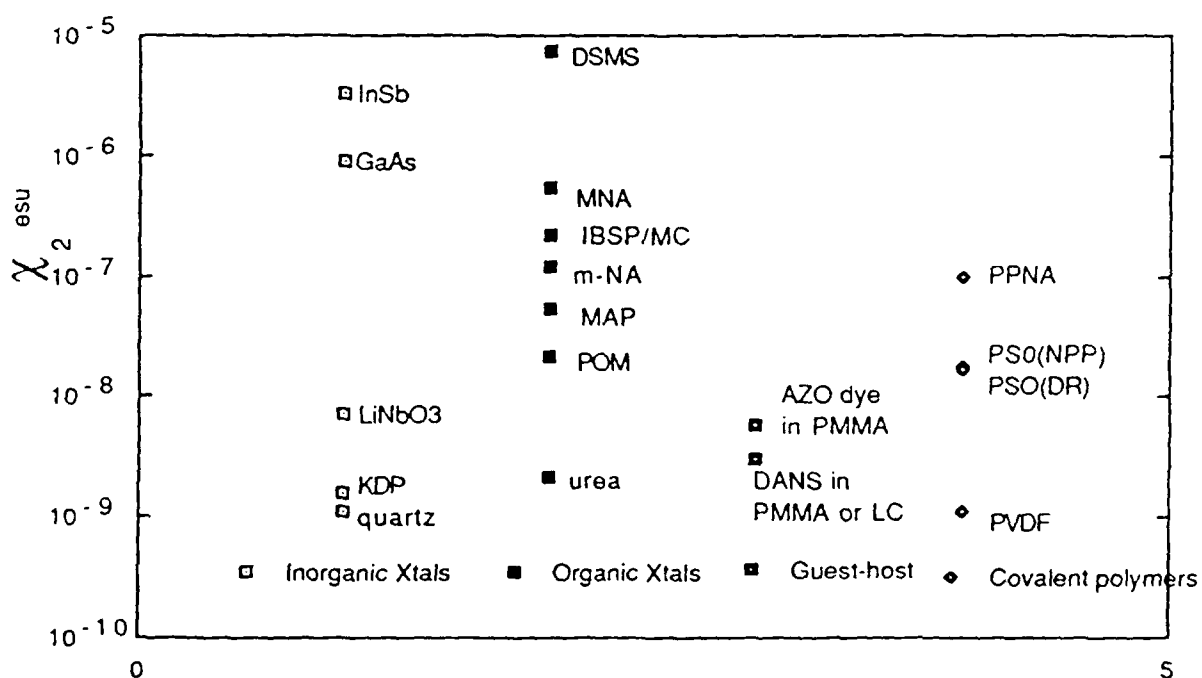


FIGURE 1: SHG COEFFICIENTS SCALE FOR SOME MATERIALS.

Some of the organic single crystals that exhibit large optical non-linearities are not useful because of their low optical damage thresholds. Typically, NLO effects take place at high laser power, which many organics cannot withstand. Processing these crystals and obtaining defect free films for device application is very difficult. It is tedious to align them precisely at the phase matching angle.

Inorganics are limited to a small subset of crystallographic classes that have no center of symmetry. Typically, the optical non-linearities from the inorganic materials are comparable to the organics, but some of the best NLO inorganics are opaque at the harmonic frequencies.⁹ Optical damage thresholds are also a major problem.⁹ Processing problems for NLO device applications are confounding.

Another class of NLO materials consists of Langmuir-Blodgett (LB) films. These are organic films carefully deposited on substrates one molecular layer at a time. LB films are designed to have a polar NLO head and a fatty acid tail. Commonly, polar substrates attract the polar head of the molecule, while the unattached nonpolar tails dangle. These systems tend to show a theoretical NLO ceiling for a particular polar group because of the carefully controlled geometry and monomolecular dimension. However, the frailty of the films limits their practical applications.

Polymers appear especially attractive as "the" materials for optical devices. They are durable and easily processed. With proper molecular engineering they can be tailored to specific optical properties. Already, polymers are employed in the optical circuits controlling airplane wing surfaces, as graded index lenses and as optical waveguide coatings. But for optical information processing, a special class of materials has yet to be developed. These substances have to act as optical switching devices, laser beam modifiers, parity checkers, and other signal processing controllers.

Two approaches to NLO polymer systems have been attempted. Earlier efforts centered on the guest/host approach, where small NLO organic molecules were imbedded in a transparent polymer matrix. These films would then be oriented and evaluated for non-linearities.^{9,10,11} Quick NLO signal relaxation and limited solid solubility plagued these systems.

The second approach involved covalent bonding of the NLO species to the polymer backbone.^{10,12,13} Larger active group

concentrations can be achieved without rapid signal relaxation. Dipole alignment longevity was a major influence in choosing amorphous polymers with covalently bonded pendant NLO groups as the system to be examined in the present work.

In the first chapter, material NLO requirements are presented, along with some NLO theory. Chapter 2 investigates the role of the "bridge" of 4-amino-4'-nitro diphenyl bridged compounds in their optical non-linearity. Chapter 3 outlines monomer preparation for NLO polyesters, described in Chapter 5, and NLO polyurethanes, detailed in Chapter 7. Chapters 4 and 6 describe attempts to synthesize polymers with more densely packed NLO groups. Chapter 8 discusses the obtained NLO results. Finally, future research directions and possible improvements are outlined in Chapter 9.

CHAPTER 1

THEORY OF SHG

NLO REQUIREMENTS

Optical non-linearity arises due to the non-vanishing χ coefficients of non-linear terms in:

$$P = P_0 + \chi_1 E + \chi_2 E^2 + \chi_3 E^3 + \dots + \quad 1$$

where P is macroscopic polarization and E is the external electric field.¹⁴ For a single molecule, **1** becomes:¹⁵

$$p = \Delta\mu = \mu_e - \mu_g = \alpha E + \beta E^2 + \gamma E^3 + \dots + \quad 2$$

Where p is the microscopic or molecular polarization, μ_e and μ_g are the excited and the ground dipole moment of a molecule, and α , β and γ are the molecular analogues of χ 's in Eqn 1.

If χ_2 , or the quadratic hyperpolarizability, is non zero, then second harmonic generation (SHG) can be observed from the material. Similarly, if χ_3 is non zero, then third harmonic generation (THG) is observed. While all materials have non-vanishing THG, three strict criteria must be met for efficient SHG:

- 1) The molecule must be easily polarizable,
- 2) Organic molecules must be conjugated.
- 3) The molecules must be non-centrosymmetric.

The third criterion must be met because when polar molecules crystallize, the oppositely charged ends tend to align. This cancels the net dipole moment of the symmetrical molecules. Non-centrosymmetric molecules have dipole moments that do not line up with the crystal axis. Therefore, there is a net dipole moment that gives rise to quadratic hyperpolarizability.¹⁶

A classic example of this point is a comparison of 2-methyl-4-nitroaniline (MNA) and 4-nitroaniline (PNA), (Figure 2).

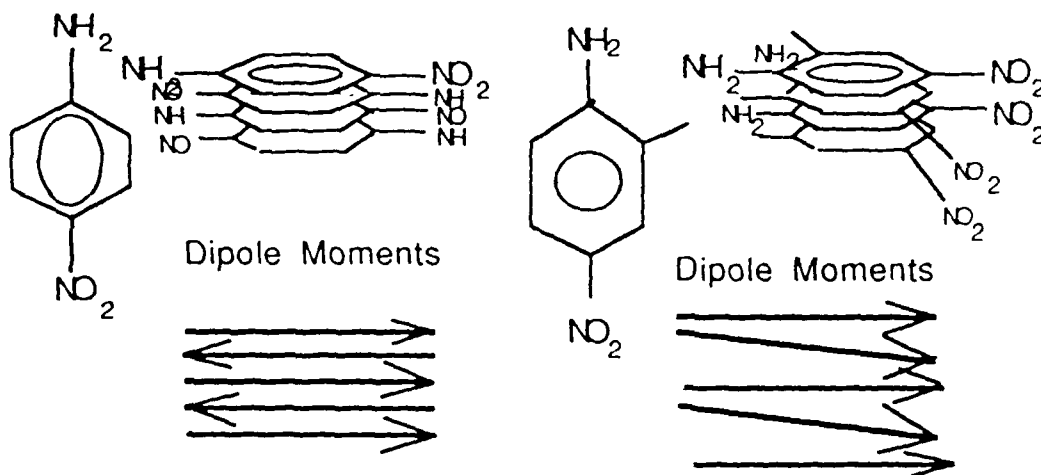


Figure 2: Centrosymmetric vs Noncentrosymmetric Crystallization

In the former, the methyl group disrupts the symmetry of the PNA and the oppositely charged molecular ends do not destructively align in the crystal as to cancel the net dipole moment. Thus, even though both molecules possess a comparably high β (42×10^{30} for MNA, 35×10^{30} for PNA),¹⁷ only MNA has a non-zero macroscopic polarizability due to its noncentrosymmetric structure.

This departure from symmetry is responsible for frequency doubling during an SHG event. Lorenz model¹⁸ describes the motion of an electron in a potential well under an applied electric field. The harmonic model for a centrosymmetric crystal :

$$\frac{d^2 r}{dt^2} + 2\gamma \frac{dr}{dt} + \omega_0^2 r = \frac{e}{m} E \quad 3$$

applies if the restoring force acting on the electron is linear and given by $f = -\omega_0^2 r$, where,

r is the displacement of the electron from its equilibrium position,

e is the electron's charge,

m is the electron's mass,

ω_0 is the electron's natural frequency,

γ is the damping factor and

E is the applied electric field.

If the electron restoring force is nonlinear and if it can be approximated by the first two terms of an infinite series: $f = \omega_o^2 r - \xi r^2$, then **Eqn.3** becomes:

$$\frac{d^2 r}{dt^2} + 2\gamma \frac{dr}{dt} + \omega_o^2 r - \xi r^2 = -\frac{e}{m} E \quad 4$$

The solution to **4** is :

$$r = - \frac{e^2 \xi E^2(\omega_i)}{m^2 (\omega_o^2 - \omega_i^2) (\omega_o^2 - (2\omega_i)^2)} \quad 5$$

Note that the electron oscillates at twice the frequency of the applied field. The second order susceptibility (quadratic hyperpolarizability) is given by :

$$\chi_2 = - \frac{e^3 \zeta N}{m^2 (\omega_o^2 - \omega_i^2) (\omega_o^2 - (2\omega_i)^2)} \quad 6$$

Note that there are resonances at $\omega_o = \omega$ and $\omega_o = 2\omega$. Thus, the produced harmonic wave will have twice the frequency of the input fundamental. The fundamental and the harmonic wave will interfere constructively and destructively. The relative power output at each frequency can be derived as a function of the phase mismatch.¹⁸

It is possible to obtain an optimal crystal orientation for maximum power output of the harmonic frequency when the destructive interference is minimized. SHG materials are birefringent. This fact makes it possible to obtain a propagation direction in a crystal where the birefringence cancels the natural dispersion.¹⁹ This process is called phase matching. In cases of poor phase matching, the harmonic signal is so weak that it is undetectable.

The present work deals with the effect of various bridging entities between an electron donor and an electron acceptor on the molecular polarizability. A series of model compounds has been designed and prepared. Later, this work was expanded to include several types of polymers which were evaluated for SHG.

There are several techniques available for the measurement of the quadratic hyperpolarizability of materials. Among them are powder SHG,⁵ the Maker-fringe method,⁶ DC induced SHG,⁴ solvatochromism²⁰ and the Kerr effect.²¹ The powder SHG method has been used as an efficient way to screen potential SHG materials obtainable in a crystalline powder form.¹⁵

In the case of powder SHG technique, the phase matching is not necessary. The crystalline samples are ground to form a powder of uniform particle size. The individual particles are assumed to be single crystals. A pulsed Nd/YAG beam is split so that one arm is directed onto the sample, and the second arm illuminates the reference. The sample SHG signal is compared to that of the reference material, which is usually urea. Unfortunately, this method cannot be used to evaluate amorphous materials.

The Pockel's effect can be used to measure χ_2 according to:
21

$$\gamma = \Delta n / n_0^3 E_0 \quad 7$$

where, γ is the Pockel's constant

$\Delta n = n_L - n_{||}$, the directional birefringence

n_0 is the refractive index of unoriented material

E_0 is the applied electric field

After the light passes the electro-optic cell, consisting of the examined material under applied voltage, it is polarized. If the electro-optic cell is placed between two polarizers, the output beam is in the form:

$$P_{\text{output}} = P_{\text{input}} \cdot \sin^2 (-\pi L \gamma n_0^3 E_0 / \lambda) \quad 8$$

where L is the length of the electro-optic cell, and

$$\chi_2 = -\gamma n_0^4 / 8\pi \quad 9$$

DC induced SHG has been used to measure the microscopic hyperpolarizability, or β , of the centrosymmetric materials in solution.²² Here, a DC electric field is applied to a solution, removing the natural center of inversion. β can be calculated from the induced polarization.

Solvatochromism has been applied to estimate β of the potential SHG materials.²⁰ This technique measures the shift of the maximum of the UV-vis absorption peak of the molecule under study. Such absorption shifts, $\Delta\nu$, are observed when the sample is dissolved in a series of solvents with varying polarity:

$$\Delta\nu = \Delta f / (\mu_e - \mu_g)^2 \quad 10$$

where

$$\Delta f = (\epsilon - 1) / (2\epsilon + 1) - (n^2 - 1) / (2n^2 + 1) \quad 11$$

and where ϵ and n are respectively the dielectric constant and the refractive index of the solvent, μ_e and μ_g are respectively the excited and ground dipole moments and f is the area under the absorption peak, related to the transition dipole moment by:

$$f \approx |\mu_{ge}|^2 \quad 12$$

Thus, β , given by

$$\beta = |\mu_{ge}|^2 (\mu_e - \mu_g) / (\omega_0^2 - \omega^2)(\omega_0^2 - 4\omega^2) \quad 13$$

can be easily measured

Finally, the Maker fringe technique⁶ measures the intensity of the harmonic beam as the noncentrosymmetric sample rotates. The SHG intensity varies with angle due to the varying beam path length through the sample and due to the interferometry of the harmonic and the fundamental wave (See Figure 3). The Maker fringe method has been used to measure the SHG from single crystals as well as from polymeric films. It has been further applied to the measurement of SHG from the molecular monolayers

in Langmuir-Blodgett films and from the surface monolayers of centrosymmetric solutions. Because this was the technique used for the measurement of the SHG from the corona poled polymers, in the present work, a detailed description of this method is appropriate.

In a uniaxial material, the power of the harmonic beam, $P_{2\omega}$ is given by:

$$P_{2\omega} = \frac{512\pi^3}{A} t_{\omega}^4 T_{2\omega}^2 d_{xx}^2 p^2 P_{\omega}^2 \frac{\sin^2 \Psi(\theta)}{n_{\omega}^2 - n_{2\omega}^2} \quad 14$$

where,

A is the area of the laser beam

P_{ω} is the power of the fundamental beam

n_{ω} and $n_{2\omega}$ are the refractive indexes of the material at the corresponding wavelengths

θ is the angle of incidence of the beam

t_{ω} and $T_{2\omega}$ are Fresnel-like transmission factors⁶

d_{xx} are the vector components of χ_2

p is the projection factor which depends on the form of the nonlinear tensor d_{xx} and the direction of $P_{2\omega}$ compared with the plane of incidence

and

$$\sin^2 \Psi(\theta) = \left(\frac{\pi L}{\lambda} \right)^2 \frac{(n_{\omega}^2 - n_{2\omega}^2)^2}{n_{\omega}^2 + n_{2\omega}^2 - 2 \sin^2 \theta} \quad 15$$

where,

L is the film thickness

$\lambda = 1.064 \mu\text{m}$, the wavelength of the Nd/YAG laser,

for a coherence length larger than the film thickness. Simplified, the harmonic power becomes:

$$P_{2\omega} = \frac{1024\pi^5 L^2 p^2 t^4 T_{2\omega}}{A\lambda^2 (n_{\omega}^2 + n_{2\omega}^2 - 2\sin^2 \theta)} d^2 P_{\omega}^2 \quad 16$$

When a quartz reference is used in this experiment, the beam diameter and the transmission factors can be assumed to be constant for the sample and the reference. Thus, in a comparison of $P_{2\omega \text{ quartz}}$ and $P_{2\omega \text{ sample}}$ these factors drop out. Furthermore, for the special symmetry case of a uniaxially poled film,

$$p = (\cos^2 \theta_{\omega}/3 + \sin^2 \theta_{\omega}) \sin \theta_{2\omega} + \cos \theta_{\omega} \sin \theta_{\omega} \cos \theta_{2\omega} \quad 17$$

Therefore, d values can be obtained from the experiment if the refractive indices are known for the sample at the harmonic and the fundamental wavelength.

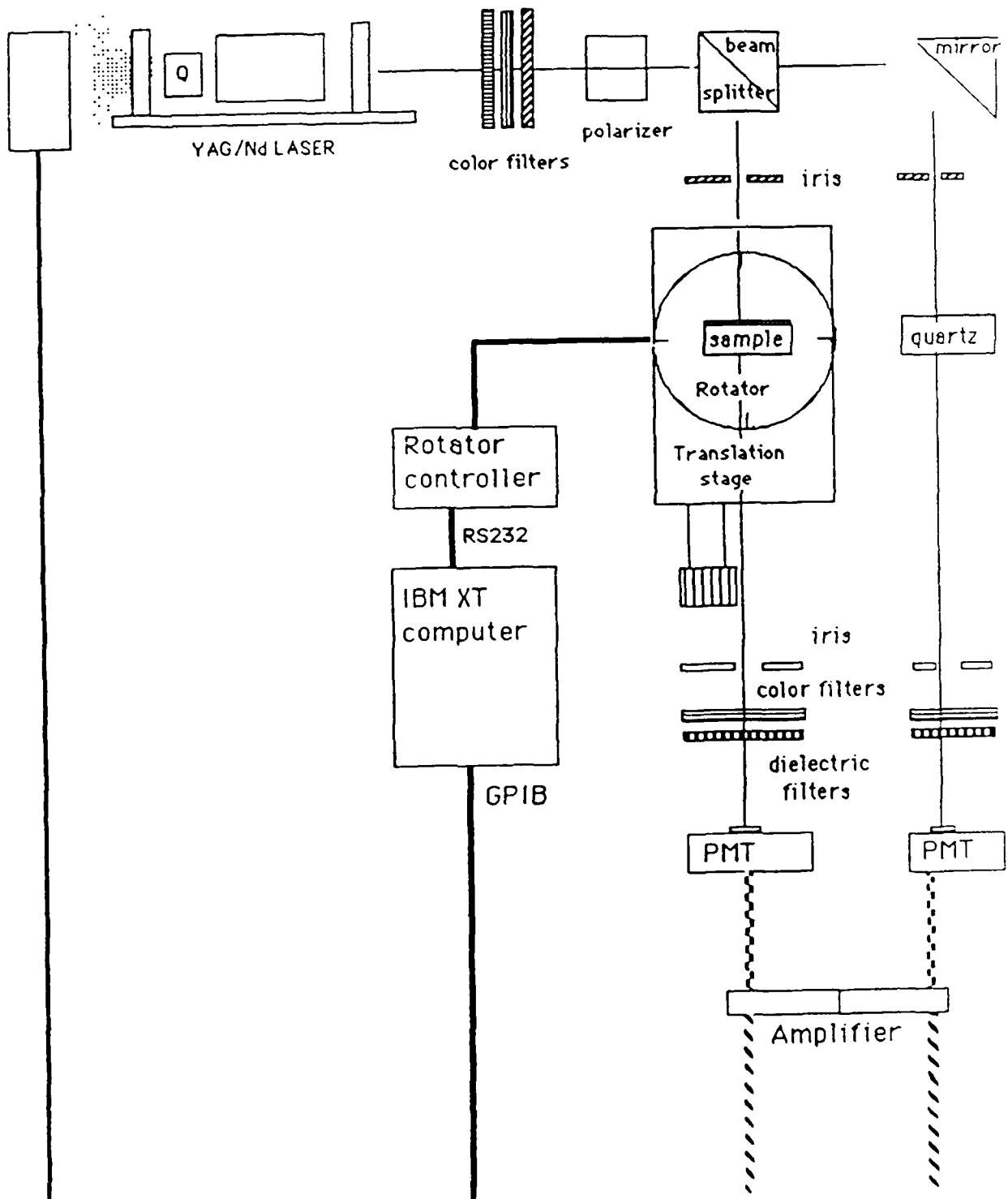
$$d_{2\omega}^2 = \frac{P_{2\omega}^{\text{sample}} \left(n_{\omega \text{ quartz}}^2 - n_{2\omega \text{ quartz}}^2 \right)^2 \left(n_{\omega \text{ sample}}^2 + n_{2\omega \text{ sample}}^2 - 2\sin^2 \theta \right)}{P_{2\omega}^{\text{quartz}} d_{\text{quartz}}^2 \sin^2 \left(\frac{2\pi L_{\text{quartz}}}{\lambda l_c(\theta)} \right) 2\pi^2 L_{\text{sample}}} \quad 18$$

$$\text{where } l_c = \lambda / 4 (n_{\omega} - n_{2\omega}) \quad 19$$

A typical experimental Maker fringe set up, such as the one used in the present work, is shown schematically in **Figure 3**.

FIGURE 3

SCHEMATIC OF THE MAKER FRINGE SHG EXPERIMENT



The Nd/YAG laser is Q-switched and the pulse repetition rate is controllable. The beam is passed through a series of filters, screening out any frequencies above and below the fundamental. The beam is subsequently polarized as it travels through the Glen laser polarizer. Then, the fundamental is divided by a beam splitter, where the first part of the beam is directed at the sample, while the second part of the beam passes through the reference material.

Before hitting the sample, the beam goes through an iris and a lens. The lens is mounted on a translation stage for precision focusing. The sample is mounted on an Oriel rotation stage, capable of x-y adjustments. The rotation is managed by the Oriel rotator controller, which in turn, is computer operated. After the beam passes the sample, possibly generating a harmonic beam, both beams pass through the second iris. The fundamental frequency is then screened out by a color filter. Interferometric filter, admitting only the green light with 530-540 nm wavelengths, is the final optical device prior to the photomultiplier tube.

The photomultiplier tube (Hamamatsu 1P28A) is powered by 1000 volts D.C., provided by the Pacific Instruments 310 power supply. The reference beam is similarly processed, except that the reference is rigidly mounted and not rotated. The photomultiplier tubes proportionately convert the harmonic light from the reference and the sample to direct current. The currents are fed into the corresponding Stanford Instruments amplifier channels, where they are converted into D.C. voltage. The signals from the amplifier are passed to the EG&G 4100 boxcar integrator.

The boxcar integrator is triggered by the photodetector that picks up the laser pulses from the back mirror. Each trigger sets up a gate in the boxcar integrator which is aligned so that the harmonic signals from the amplifier are properly positioned inside the gate. This alignment is insured by monitoring the gate and the signals on an oscilloscope.

The boxcar integrator sends the SHG information to a computer, which is also controlling the rotation of the sample. A software program plots the angle of incidence vs the magnitude of SHG.

These plots are the typical output of a Maker fringe experiment. The $\sin^2\theta$ angular dependence (equation 14) of the harmonic signal is seen in the plots. If the samples are

sufficiently thick (more than a coherence length), actual fringes can be observed. Since the polymeric films are thinner than the coherence length of the light employed, the SHG plots do not show fringes.⁶ A typical θ -plot can be seen on Figure 4.

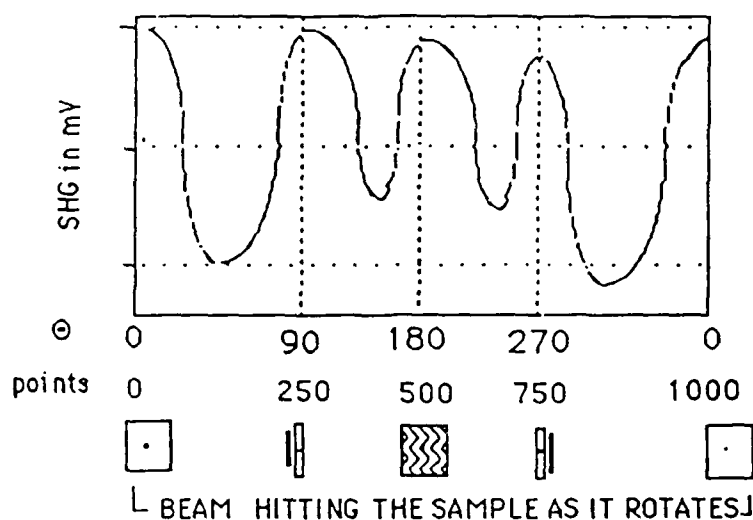


FIGURE 4: A TYPICAL MAKER FRINGE RESULT FROM A THIN POLED POLYMER

The SHG signal is maximum near 65° and not 90° as predicted by 14. This is due to the increasing reflection of the fundamental beam from the glass substrate as the angle of incidence becomes more obtuse. During a typical sample scan, depicted in Figure 4, the sample starts perpendicular to the beam, with the dipoles aligned parallel to the beam. The sample rotates 360° during the run. At $\theta = 90^\circ$, the sample is parallel to the beam and the dipoles are perpendicular to the beam. At $\theta = 180^\circ$, the back of the sample or the glass substrate is orthogonally facing the beam.

The reflection of the fundamental beam from the glass substrate at the high angles of incidence is also responsible for the asymmetry of the periodic sinusoidal response. Thus, because of the reflection, the harmonic signal from the incidence angles between 90° and 180° , is less than that from the 0° to 90° range.

The SHG maximum is normalized by the sample thickness when the harmonic data are compared for various samples. Ideally, d_{33} components of χ_2 should be compared. However, the d_{33} calculations require knowledge of the indices of refraction at the

fundamental and harmonic frequencies. For path lengths larger than the coherence length, this information can be obtained directly from the Maker fringe plot. The coherence length is the distance between the two adjacent extrema. Since the angle of incidence, θ , and λ are

known, the birefringence is readily obtained from $l_c = \lambda/4(n_\omega - n_{2\omega})$, Equation 19.

Since the beam path length in the thin polymeric films used for SHG is typically less than the coherence length, the sample birefringence between the fundamental and the harmonic frequency must be experimentally obtained.^{12,23} Unfortunately, such equipment was unavailable, and the thickness normalized data were used.

CHAPTER 2

STUDY OF THE BRIDGED DIPHENYL COMPOUNDS

In the last thirty years there has been a significant number of studies of the "bridged" diphenyl compounds that are capped with an electron accepting group A on one end, and with an electron donating group D on the other (type I molecule, see Figure 5).

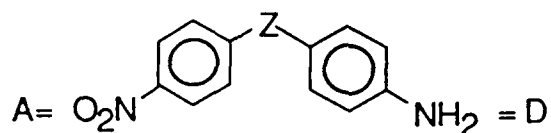


FIGURE 5 : TYPE I MOLECULE

More recently, SHG data interpretation once again has called upon a better understanding of the charge interactions in a type I molecule.^{24,25} Equation 13 describes the dependence of β on the dipole moments of the molecule.

$$\beta = |\mu_{eg}|^2 (\mu_e - \mu_g) / (\omega_0^2 - \omega^2)(\omega_0^2 - 4\omega^2) \quad 13$$

It is clear that the magnitude of the polarizability, which is dependent on the charge separation in the first excited state of the molecule, is ultimately responsible for the optical nonlinearity. So the length of the conjugated bridge separating the charges in the excited state and the dipoles in the ground state plays a vital role in SHG.

Figure 6 shows several polarizations possible for a Type I molecule. These chromophores have varying conjugation lengths, depending on the role of the bridging Z entity. Numerous attempts have been made to demonstrate the role of the "bridge," Z, in the long range electronic interactions between A and D.

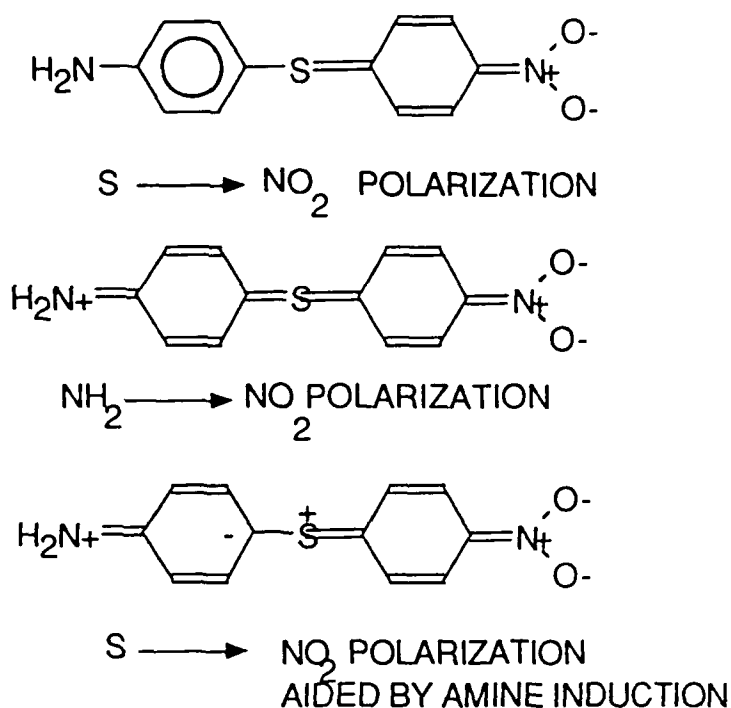


FIGURE 6: POSSIBLE POLARIZATIONS FOR A
TYPE I MOLECULE WHEN Z = S

Investigators have used ultraviolet spectroscopy,^{26,27,28,29} dipole moment measurements,^{30,31} acid-base reaction kinetics,³² and nuclear magnetic resonance³³ to characterize the different impact of heteroatoms in the Z position. It is important here to separate the studies examining the ground state interactions from those in the excited state of the molecule. The magnitude of β depends on the difference between the two dipole moments as can be seen from Eqn. 13.

In the 1950's, researchers looked at the ultraviolet spectra of these compounds in efforts to relate the role of the "bridge" to the energetic ease of the excited state formation. This energy is quantized and given by:

$$\Delta E_{1 \rightarrow 2} = h\nu = hc/\lambda \quad 20$$

where h is Plank's constant, c is the speed of light and $\Delta E_{1 \rightarrow 2}$ gives the energy required for electronic transition from state 1 to

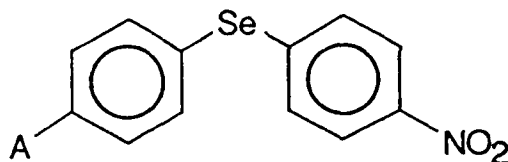
state 2.³⁴ Clearly, from Eqn. 20, transitions that occur at higher wavelengths λ , or lower frequencies ν , require less energy ΔE .

Typically, $n \rightarrow \pi^*$ and $\pi \rightarrow \pi^*$ transitions of conjugated molecules are studied in UV spectroscopy. Both are the transitions from the ground state to the first excited state. Modena²⁸ studied the 4-amino-4'-nitro-diphenyl selenide UV absorption spectrum and compared it to those of 3-amino-4'-nitro-diphenyl selenide and 4-amino-4'-nitro-phenyl benzyl selenides. He found that methylene linkage next to a selenide shifts $n \rightarrow \pi^*$ transition by increasing the wavelength at which it occurs from 343 nm to 346-348 nm. Moving the amine from para to meta renders the excitation more difficult by shifting the wavelength from 343 nm to 339 nm.

Modena also looked at the acceptor A in the 4' position in a capped series of 4-nitro-diphenyl selenides. The summary of the UV spectra is shown in Table 1.

TABLE 1

UV spectroscopy data for



increasing e- donor ability

A	H	OH	OMe	NH ₂	NMe ₂	O-
λ_{\max} (nm)	337	338	338	343	341-348	360-364

maxima for $n \rightarrow \pi^*$ in nm

Modena's conclusion that "the excitation of the chromophore (XI) [Figure 7] is not significantly modified by the substituent A" is in direct opposition to his own data.

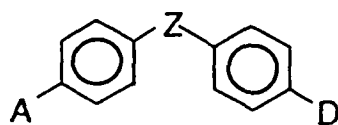


FIGURE 7: MODENA'S CHROMOPHORE XI

The wavelength of transition increases/energy decreases with increasing electron donating ability of A. According to March,⁴³ this electron donating ability can be arranged as follows: $-O > NMe_2 > NH_2 > OCH_3 > OH > H$

When Modena's data are put together with Szmant and McIntosh's,³⁵ who examined the series of diphenyl compounds appearing in **Table 2**, a definite pattern emerges.

Table 2: UV spectroscopy for



Z	D = A =	NH ₂ NO ₂	H NO ₂	NH ₂ H
SO ₂		267nm	261-262nm	292nm
SO		276nm	265-267nm	276nm
O		300nm	300-301nm	243nm
S		343nm	338 nm	255nm
Se		343nm	337 nm	273*nm

Maxima locations are listed in nm. *Here, D=N(Me)₂. No data were available for D=NH₂. Since data for the Se bridge were in good agreement for NH₂ and NMe₂ for various A's, the value of 273 nm was used.

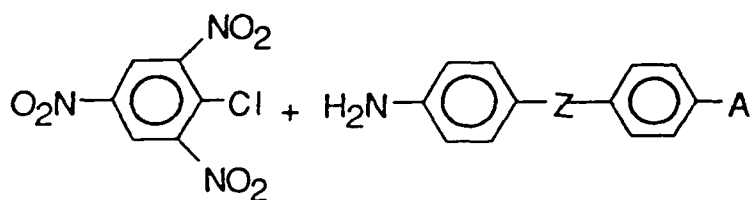
The Z entities, which have been categorized as electron acceptors, such as SO and SO₂, the **Series I** molecules undergo excitation the easiest (at the longest wavelength) when diphenyl molecules are solely capped by an electron donor such as an amine. When this donor is replaced by an acceptor (4-nitro-diphenyls) the excitation becomes much more difficult energetically. If the acceptor bridge is placed between a donor and an acceptor, as in amino-nitro-diphenyls, then the nitro group hinders the interactions between the bridge and the donor, increasing the excitation energy.

When the bridge is a donor, such as oxygen, the exact opposite is observed. Amino-diphenyl-ether shows a maximum in the UV absorption spectrum at 243 nm. Nitro-diphenyl ether undergoes $n \rightarrow \pi^*$ at 300-1 nm. In the cases of sulfur and selenium bridged molecules, the Z atoms interact with both donors and acceptors because the 4-amino-4'-nitro diphenyl sulfides and selenides have maxima at 343 nm, while the diphenyl sulfides and selenides with only one para substituent absorb farther in the ultraviolet.


Hence, UV spectra show that all bridges examined "feel" the presence of both amine and nitro groups. But only in the cases of sulfur and selenium is the $n \rightarrow \pi^*$ transition eased when both electron donor and acceptor are present simultaneously.

In the early 1960's, Litvinenko's group attempted to monitor the role of the bridging Z entity by examining the nucleophilicity of the amine in the series of 4-amino-4'-nitro diphenyl compounds and in the 4-amino-diphenyl series.³² To this end, they monitored the kinetics of the reaction of these amines with picryl chloride and with nitrobenzoyl chloride. Activation energies and speeds of the reactions were measured and are listed in **Table 3** for a series of ethers, sulfides, selenides, amines, methanes, ethanes, vinyls, acetylenes and biphenyls.

TABLE 3
ACTIVATION ENERGIES FOR NUCLEOPHILIC
AROMATIC SUBSTITUTION REACTIONS OF



(in cal/mol)

A, Z	CH ₂	(CH ₂) ₂	NH ₂	O	C=C		Ø	C≡C	Se	S
NO ₂	7650	8000	8700	9100	9700	9700	1000	10600	12100	12400
H	7000	7900	7300	8400	9800	8400	8800	10300	9300	10100

As expected from the UV data, the nitro- substituted diphenyl sulfides reacted the slowest, requiring the largest

activation energies and producing the slowest rate constants. Selenides were a close second worst. The rest of the bridges are arranged below in increasing nucleophilicity of the amine/decreasing transmission through the bridge:

→ increasing nucleophilicity →

-S- < -Se- < -C=C- < - < -Ph- < -C≡C- < -O- < -NH- < -CH₂CH₂- < -CH₂-

← increasing bridge interaction ←

Note here that both UV spectroscopy and amine nucleophilicity studies agree on the simultaneous donor and acceptor interaction ability of the bridge in order of S>Se>O heteroatoms in the Z position.

Litvinenko's group³⁰ also examined the role of the Z moiety by the difference between the calculated and the observed dipole moment of type I molecules. Another work, also approached the "Z question" via dipole moment studies but with a slightly different twist. Baliah³¹ looked at amino diphenyl ether and found that the dipole moment predicted by the vector sum of the freely rotating, non-interacting functional component dipole moments agreed well with experimental measurements.

However, when the 4'-nitro group was added to form 4-amino-4'-nitro diphenyl ether (ANDE), the experimentally measured dipole moment deviated a bit more from that predicted from the non-interacting theoretical model. The experimental dipole moment was greater than the sum of its parts, indicating interaction by the nitro group through the oxygen's p orbitals.

This interaction is much more pronounced in case of aminodiphenyl sulfide. The observed dipole moment exceeded the non-interacting theoretical model by 0.42 Debye units. It deviated even further (0.67 D) in the case of ANDS. This shows resonance interaction with the sulfur, not only by the amine, but also by the nitro group.

Litvinenko et al³⁰ give more detailed data for the dipole moments of 4-amino-4'-nitro diphenyl methane (ANDM) and ANDE, and

calculated the dipole moments for the corresponding "half-molecules." They chose p-aminothiophenol and methyl 4-nitrophenyl sulfide for ANDS and p-nitrotoluene and p-methyl aniline for ANDM. The deviations between the model and experiment are shown in Table 4.

TABLE 4

CALCULATED AND EXPERIMENTAL DIPOLE MOMENTS (in Debye units)

OF  HALF MOLECULES (X=A OR D)

X	Z	$\mu_{\text{calculated}}$	μ_{measured}	Δm
NO ₂	CH ₂	4.38	4.44	0.06
NH ₂	CH ₂	1.26	1.32	0.06
NO ₂	S	3.25	3.77	0.52
NH ₂	SCH ₂	1.76	2.50	0.74

The deviations were small for the ANDM components and appreciable for ANDS. When the dipole moments of the ANDS and ANDM were measured, they were compared to the sum of the two half-molecules' measured dipole moments. In other words, the noninteracting functional group model was applied to the two half molecules; interactions were allowed within each half, but not between the halves. The positive deviation in Table 5 for the whole molecule from the sum of the halves indicates interactions through the bridge between the donor and the acceptor.

TABLE 5

CALCULATED AND EXPERIMENTAL DIPOLE MOMENTS (in Debye units)

OF  AND COMPARISON WITH THE "HALF

MOLECULES DEVIATION SUM"

Z	$\mu_{\text{calculated}}$	μ_{measured}	$\Delta \mu$	$\Sigma \Delta_{1/2}$
CH ₂	4.52	4.91	0.39	0.12
S	4.08	5.82	1.74	1.26

Moreover, the $\Delta \mu = \mu_e - \mu_{(1/2+1/2)}$ significantly exceeded the sum of deviations of the two halves from the theory. This means that the donor-acceptor interactions through the bridge are significantly higher than the sum of the bridge to donor and bridge to acceptor

interactions. The authors rated the bridge efficiency for such interactions as $S>O>CH_2$.

Nuclear magnetic resonance (NMR) is another useful tool for examining the series I type of molecules. Each para di-substituted phenyl ring has two pairs of NMR non-equivalent protons that produce a quartet of peaks. Paranitrobenzenes yield a quartet with very different NMR chemical shifts and coupling constants from the paraaniline ring quartets (See Figure 8).

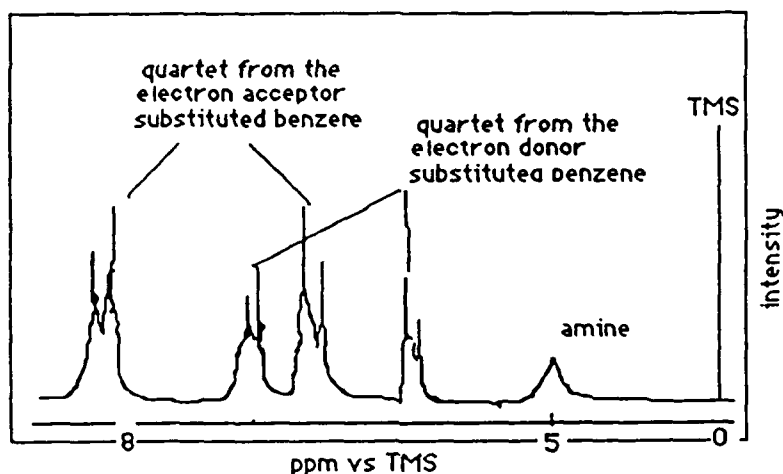


FIGURE 8: TYPICAL NMR SPECTRUM OF A SERIES I MOLECULE

This reflects the fact that NMR is extremely sensitive to the electron density around the proton. Electron withdrawing groups effectively reduce the electron density on the phenyl ring and "move" the signal downfield. Electron acceptors have the opposite impact.

Hyne and Greidanus³³ analyzed NMR spectra of series I molecules and compared them to the component "half molecule" spectra. These "half molecules" were very similar to those in the dipole moment study: $X-Ph-Z-CH_3$. Here X is either A or D in our notation, and Z is the familiar bridging entity. The authors measured the centers of quartets in all of these molecules. If the Z in is an electron insulator, then the quartets for the phenyl rings should appear at the same frequency as those in the parent "half molecules." This is because the "half molecules" have only one "cap," either A or D, and cannot "feel" the electron push or pull of the other "cap." If the full Series I molecule behaves the same

way, then Z is an insulator and the nitro group does not "feel" the amine and visa versa.

Hyne and Greidanus looked at methyl, sulfone, sulfoxide, oxygen and sulfur bridged compounds. Their findings are summarized in Table 6.

TABLE 6

NMR SHIFTS (in c.p.s.) IN CENTERS OF A AND D NMR QUARTETS OF



RING ↓	Z →	CH ₂	SO	SO ₂	O	S
A		1.2	2.4	-0.6	-7.3	-8.0
D		2.1	5.5	7.5	2.2	7.6

Clearly, the trend is -S- > -O- > -OSO- ≈ -SO- > -HCH-. The authors discounted all shifts less than 2 c.p.s. because these are attributable to the phenyl-bridge inductive interactions.

Very recently, ANDS has been examined for its NLO properties.^{24,36} Cowan²⁵ and coworkers measured SHG signal from ANDS powder and compared the magnitude of the harmonic signal to that of urea. The results showed an SHG signal comparable to that MNA, one of the best SHG materials known. This prompted the authors to examine closely the crystalline structure of ANDS by X-ray diffraction. It was found that the two phenyl rings are orthogonal to one another and that the sulfur bond angle is 104 degrees. There was also an intermolecular contact between the amine of one molecule and the nitro group of another, suggesting hydrogen bonding.

According to the paper it is this hydrogen bonding that forces achiral molecules of ANDS to crystallize in a noncentrosymmetric fashion. The authors use the orthogonality of the phenyl ring to rule out any intramolecular charge transfer between the amine and the nitro ends. They conclude that electron transfer from the sulfur donor through the phenyl to the nitro acceptor is responsible for the SHG.

This is in sharp contrast to the previous studies that utilized NMR, UV, dipole moment and basicity of the amine to demonstrate significant "through sulfur" interaction between the amine and the nitro group in ANDS. If interaction is possible between the orthogonal phenyl rings, then the apparent discrepancy between Cowan's study and prior art can be resolved, since Cowan's argument is solely based on the assumption that the electron transfer is not possible between the mutually orthogonal benzene rings.

Interestingly, this point has been addressed by Mangini as an "apropos" comment in his 1963 paper.³⁷ "It is noteworthy that the twisting of the two rings in the former compound [ANDS] ought not to matter for structures (2) [$\text{NH}_2 \rightarrow \text{S}$ transmission] and (3) [$\text{NH}_2 \rightarrow \text{NO}_2$ transmission] since an appropriate combination of d orbitals, which can interact with the π -system of benzene, always exists. In fact an investigation on the dibenzothiophene series - where the planarity of the aromatic system insured - shows that the situation appears to be identical with the previous one [that of ANDS]".

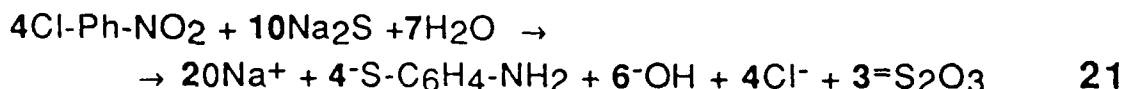
Poly(phenylene sulfide) has sulfur connected phenyl rings that are almost orthogonal. Recent work³⁸ with PPS implies "that the sulfur atoms play an important role in connecting the conjugated systems of consecutive phenyl rings." Moreover, CNDO/S3 calculations on poly(phenylene oxide) suggest that oxygen provides electronic "connectivity" between adjacent phenyls.³⁹

In summary, the literature shows that sulfur plays an important role in donor/acceptor interactions in ANDS. Electron donors and acceptors are able to "feel" each other's presence in diphenyl compounds with judicious choice of the bridge. Cowan's conclusions seem to diverge from the body of the earlier work and a more detailed study involving SHG is in order.

EXPERIMENTAL

ANDS

The 4-amino-4'-nitro-diphenyl ethers⁴⁰, sulfides,^{41,42} methanes,^{43,44} sulfoxides,⁴⁵ and sulfones⁴⁶ were synthesized as described earlier.³³ The synthesis of ANDS is as follows: 15.716g (0.1m) of p-chloronitrobenzene (Aldrich) and 60.045g (0.25m) of sodium disulfide ($\text{Na}_2\text{S} \cdot 9\text{H}_2\text{O}$, Aldrich) were refluxed in 200 ml of water for 8 hours. An additional 15.716g (0.1m) of p-chloronitrobenzene was added and refluxed for 8 more hours. The reaction flask was steam distilled with 100 ml of water and the red reaction precipitate, $T_m = 145^\circ\text{C}$, was recrystallized from ethanol. This reaction proceeds according to:



The p-amino-thiophenoxide anion formed in Eqn. 21 nucleophilically attacks the second equivalent of p-chloronitrobenzene that is added during the second stage of the reaction to give the desired ANDS.

This synthetic route was originally used by Lantz,⁴² U.S. Patent #1,965,776, and combines nucleophilic aromatic substitution (NAS) with Zinin reduction⁴⁷ in a single stage reaction. Sulfur nucleophilically displaces the chlorine, which is activated by the nitro group in the para- position, and then the slower sulfur reduction of the nitro group proceeds. Water acts as the proton source for the reduction.

Immediately upon introducing of the reactants, the mixture starts turning bright red, indicating the onset of NAS. P-nitro-thiophenoxide ion is bright yellow; sulfur acts as an electron donor and the nitro group is the acceptor. This chromophore absorbs in the yellow region near 350 nm. As the reduction progresses, the solution becomes aminothiophenoxide (colorless)-rich and the solution color fades. After eight hours the conversion is essentially complete; and another mole of p-chloronitrobenzene is added. ANDS begins precipitating almost immediately; and after an additional eight hours refluxing in water, the reaction is complete. The reaction products are steam distilled then and allowed to cool. The precipitate is recrystallized from ethanol. Almost theoretical yields can be attained.

The 4-amino-4'-nitro-diphenyl sulfone, 4-amino-4'-nitro-diphenyl sulfoxide, 4-amino-4'-nitro-diphenyl ether, 4-amino-4'-nitro-diphenyl methane were also prepared according to the procedures described elsewhere.^{33,40-46}

RESULTS

The structures of the bridged compounds was confirmed by elemental analysis, NMR and comparison of the melting points with those found in literature. Table 7 summarizes the elemental analysis results:

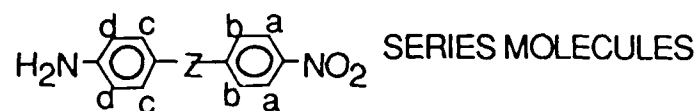
TABLE 7
ELEMENTAL ANALYSIS RESULTS FOR THE
 $\text{H}_2\text{N}-\text{C}_6\text{H}_4-\text{Z}-\text{C}_6\text{H}_4-\text{NO}_2$ SERIES MOLECULES

Z=	S		SO		OSO		O		HCH	
Tm =	145°C		130-131°C		170-171°C		133°C		98°C	
Elem.	theor	found	theor	found	theor	found	theor	found	theor	found
%C	58.52	58.24	54.95	53.29	51.79	51.48	62.61	62.70	68.41	68.10
%H	4.09	4.08	3.84	3.71	3.62	3.45	4.38	4.26	5.30	5.15
%N	11.37	11.17	19.68	10.17	10.07	9.97	12.17	12.15	12.27	12.30
%O	13.12	12.99	18.30	19.47	23.00	23.92	20.85	20.89	14.02	14.45
%S	13.27	13.02	12.22	12.05	11.52	11.18	-	-	-	-

Table 8 lists the assignments for the nuclear magnetic resonance peaks of the bridged compounds, obtained on a 270 MHz machine. CDCl_3 was used as a solvent and TMS as a reference in all cases. For the doublet peaks, the center value is listed.

TABLE 8

NMR PEAK ASSIGNMENTS FOR THE



Peak locations in ppm.

Assign Z=	S	O	SO	SO ₂	CH ₂
a	8.026	8.164	8.239	8.298	8.105
b	7.084	6.951	7.760	8.060	6.943
c	7.333	6.895	7.400	7.709	7.299
d	6.632	6.742	6.722	6.683	6.683
NH ₂	3.959	3.705	4.147	4.321	3.565

Another interesting way to analyze the NMR data was recently outlined.⁴⁸ Here, the author plotted the Hammett Constants for the CH₃-Z-Ph-NO₂ series molecules vs the location of the d peak, which is ortho to the amine, in the p-amino-p'-nitro diphenyl compounds (see Figure 9).

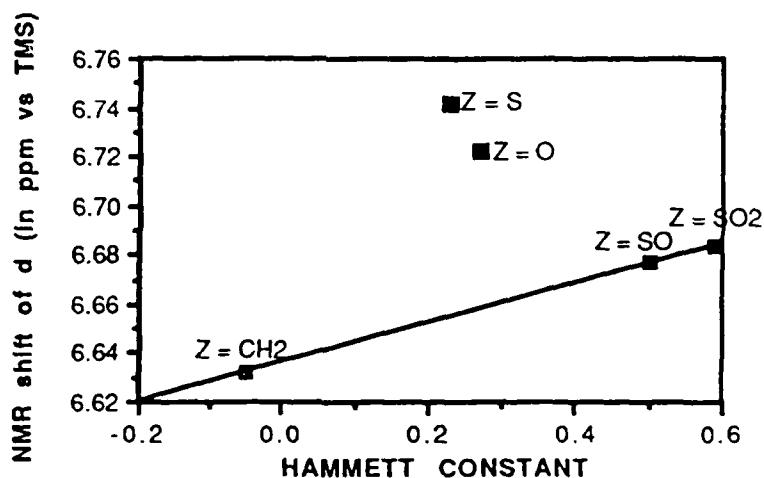


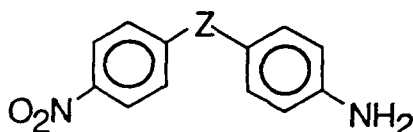
FIGURE 9: NMR SHIFTS FOR THE PROTON ORTHO TO THE AMINE

For $Z = \text{CH}_2$, SO , or SO_2 the chemical shifts of d proton vs the Hammett Constants form a straight line, defining the minimal electronic interaction across the bridge. However, for $Z = \text{O}$ or $Z = \text{S}$, a significant deviation from the "zero interaction line" is seen.

This suggests bridge participation between the amine and the nitro in the sulfide and in the ether .

SHG of the bridged compounds was evaluated by powder SHG and also by solvatochromism. Powder SHG measurements were performed at RPI by Wnek,⁴⁹ using the powder method outlined in Chapter 1. Solvatochromic measurements were obtained from dilute solutions of the ANDS, ANDE and ANDM.⁵⁰ The powder SHG results are listed below.

TABLE 9
POWDER SHG RESULTS FOR



Z =	SHG EFFICIENCY (x UREA SHG)
S	10-20
CH ₂	0-9, depending on structure
SO	2.1
SO ₂	0.00064
O	0.0023

As Cowan²⁵ observed, the high SHG efficiency of ANDS can be attributed to the preferentially-directed stacking of the dipoles which is insured by hydrogen bonding. Crystal structures of the ANDM and of the ANDS are somewhat similar.⁴⁹ Crystal structures of the ether, of the sulfone and of the sulfoxide have not been investigated.

To show conclusively what gives rise to SHG in ANDS is more difficult than analyzing the "half molecules" for SHG. Molecules must crystallize in a noncentrosymmetric pattern and that is not trivial to insure. Powder SHG is a macromolecular optical nonlinearity measurement, where the crystalline arrangement of the molecules plays a vital role in the magnitude of the harmonic signal from the powder aggregate. This added complication hampers the quantitative evaluation of SHG from the Type I molecules via the powder method.

Microscopic polarizability (β) is not dependent on the centrosymmetry. β comparisons for a series of molecules can be

modeled with the aid of solvatochromism of these molecules in the ultraviolet range. Equation 13 shows that the solvent dependence of the $n \rightarrow \pi^*$ transition is closely related to β . Table 10 shows the absorption maxima of the Type I molecules in various solvents. The magnitude of the $\Delta\nu$ for solvents of different polarity gives a quantitative "feel" for the hyperpolarizability of each molecule.

TABLE 10
Relationship between $\Delta\nu$ vs CHCl_3 (in nm)
and β for Some Molecules

SOLVENT Z =	-S-	-O-	-CH ₂ -	PNA
CH ₃ OH	-7.5	-1.5	-1.0	24
EtOH	-9.0	-6.0	-2.0	32.5
EtOH*HCl	-21	-2.0	-2.0	32.5
$\beta \cdot 10^{30}$ esu	27	15		35

Clearly, the largest solvatochromism is exhibited by PNA and ANDS. Unlike in powder SHG, hydrogen bonding and preferential crystalline orientation are not relevant in solvatochromism. Therefore, ANDS' largest β among the Series I molecules shows the significance of the sulfur link in the bridged compounds for SHG. Regardless of whether $\text{S} \rightarrow \text{NO}_2$ or $\text{NH}_2 \rightarrow \text{NO}_2$ excitation takes place in ANDS during the NLO event, these data show the utility of an ANDS type pendant group in the polymers that were prepared in Chapters 5 and 7 for second harmonic generation.

Recent low temperature fluorescence work with ANDS at JPL⁵⁰ shows that the excited state is dominated by the amino \rightarrow nitro transition, while in the ground state, the $\text{NH}_2 \rightarrow \text{NO}_2$ effect is virtually absent. This was concluded because the transition peak was only slightly affected when hydrochloric acid was added to the ANDS solution. It was concluded that the excited state probably does not get populated fast enough in a "picosecond NLO event", so the SHG response must be dominated by the $\text{S} \rightarrow \text{NO}_2$ polarization in ANDS.

Several additional compounds have been synthesized to elucidate further the role of sulfur in the second harmonic response of ANDS. They are:

A, N,N dimethyl-4-amino-4'-nitro diphenyl sulfide, prepared by Kitipichi at RPI by the electrophilic attack of 4-nitrobenzenesulfenyl chloride on the para position in N,N dimethyl aniline.⁵⁰ The structure of **A** appears in Table 11.

B, 2,2' dimethyl-4-amino-4'-nitro diphenyl sulfide was synthesized by adding 5 grams (0.03223 moles) of 2-flouro-5-nitro-toluene (Aldrich) to an aqueous solution of 19.353 grams (0.0805 moles) of $\text{Na}_2\text{S}\cdot 9\text{H}_2\text{O}$ and refluxing the mixture for 24 hours. Then, an additional 5 grams (0.03223 moles) of 2-flouro-5-nitro-toluene (Aldrich) were added and refluxing was continued for another 20 hours. The solution was steam distilled and cooled. Red precipitate was recrystallized from ethanol to obtain the pure product melting at 126 - 127°C in 90% yield. 100 MHz NMR spectrum of **B** dissolved in deuterated DMSO, with TMS added as a reference, appears in Figure 10. The structure of **B** appears in Table 11. The NMR peak assignments are shown in Table 12.

C, 2-methyl-4-amino-4'-nitro diphenyl sulfide was prepared by adding 1.551 grams (0.01 mole) of 2-flouro-5-nitro-toluene (Aldrich) to aqueous solution of 6.005 grams (0.025moles) of $\text{Na}_2\text{S}\cdot 9\text{H}_2\text{O}$ and refluxing the mixture for 24 hours. Then, an additional 1.576 grams (0.01 mole) of p-chloronitrobenzene (Aldrich) were added and refluxing was continued for another 20 hours. The solution was steam distilled and cooled. Red precipitate was recrystallized from ethanol to obtain the pure product melting at 124.5 - 125°C in 70% yield. 100 MHz NMR spectrum of **C** dissolved in deuterated DMSO, with TMS added as a reference, appears in Figure 11. The structure of **C** appears in Table 11. The NMR peak assignments are shown in Table 12.

D, 2'-methyl-4-amino-4'-nitro diphenyl sulfide was prepared by adding 1.576 grams (0.01 mole) of p-chloronitrobenzene (Aldrich) to an aqueous solution of 6.005 grams (0.025moles) of $\text{Na}_2\text{S}\cdot 9\text{H}_2\text{O}$ and refluxing the mixture for 24 hours. Then, an additional 1.551 grams (0.01 mole) of 2-flouro-5-nitro-toluene (Aldrich) were added and refluxing was continued for another 20 hours. The solution was steam distilled and cooled. Red precipitate was recrystallized from ethanol to obtain the pure product melting at 123°C in 89% yield. 100 MHz NMR spectrum of **D** dissolved in deuterated DMSO, with TMS added as a reference, appears in Figure 12. The structure of **D** appears in Table 11. The NMR peak assignments are shown in Table 12.

E, 2-amino-7-nitro-dibenzothiophene was prepared according to a procedure described elsewhere^{51,52}. However, the recrystallization from ethanol afforded the product melting at

205 - 206°C, which is 24°C higher than the previously reported melting point. Elemental analysis results are: calculated: C 59.01%, H 3.30%, N 11.47%, O 13.10%, S 13.13; found: C 58.52%, H 3.17%, N 11.37%, O (by difference) 13.48, S 13.46%. Elemental analysis and NMR, shown in **Figure 13** confirm the proposed structure. The structure of **E** appears in **Table 11**. NMR peak assignments can be found in **Table 12**.

F, 4-hydroxy-4'-nitro diphenyl sulfide was prepared by the dissolution of 1.262 grams (0.01 mole) of p-hydroxythiophenol (Aldrich) with 1.122 grams (0.02 moles) of KOH (Aldrich) in water. 1.576 grams (0.01 mole) of p-chloronitrobenzene were added to the solution and the reaction was allowed to take place at room temperature for 7 hours. The cherry red solution colored bright yellow - orange when it was acidified with dilute HCl and precipitate began forming. Methylene chloride was added and the mixture was stirred and allowed to separate overnight. Red oil gathered in the bottom organic layer, while the aqueous layer afforded brownish-yellow needles, which were filtered hot in CHCl₃ and recrystallized from the benzene to yield the product melting at 154°C. 100 MHz NMR spectrum of **F** dissolved in deuterated DMSO, with TMS added as a reference appears in **Figure 14**. The structure of **F** appears in **Table 11**. The NMR peak assignments are shown in **Table 12**.

G, 4-chloro-4'-nitro diphenyl sulfide was prepared according to a procedure described elsewhere^{31,33}. 100 MHz NMR spectrum of **G**, dissolved in deuterated DMSO, with TMS added as a reference, appears in **Figure 15**. The structure of **G** appears in **Table 11**. Assignments are listed in **Table 12**.

A, **F**, and **G** were prepared to see the effect of various electron donors in nitro diphenyl sulfides on b. **B**, **C**, **D**, and **E** were prepared to illustrate various steric effects on SHG in amino nitro diphenyl sulfides. In planar **E**, the planarity of the rings is insured, while in **C**, **D**, and **B**, various degrees of steric hindrance is provided to keep the phenyl rings staggered.

TABLE 11: DIPHENYL DERIVATIVES

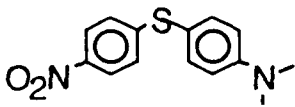
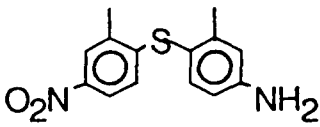
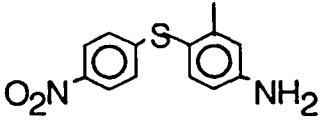
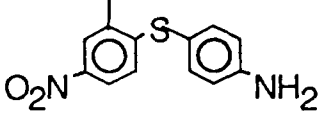
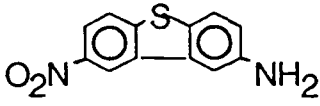
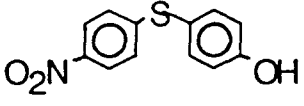
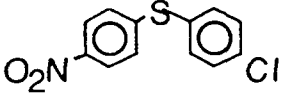
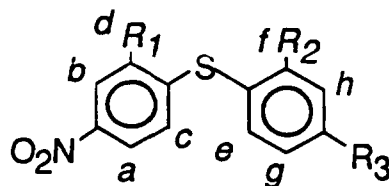
COMPOUND	STRUCTURE	NAME
A		N,N dimethyl-4-amino-4'-nitro diphenyl sulfide
B		2,2' dimethyl-4-amino-4'-nitro diphenyl sulfide
C		2-methyl-4-amino-4'-nitro diphenyl sulfide
D		2'-methyl-4-amino-4'-nitro diphenyl sulfide
E		2-amino-7-nitro-dibenzothiophene
F		4-hydroxy-4'-nitro-diphenyl sulfide
G		4-chloro-4'-nitro diphenyl sulfide

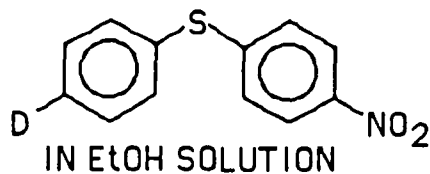
TABLE 12
NMR PEAK ASSIGNMENTS FOR



ASSIGN	B	C	D	E	F	G
R1	CH ₃	H	CH ₃	R1=R2=H	H	H
R2	CH ₃	CH ₃	H	R1=R2=H	H	H
R3	NH ₂	NH ₂	NH ₂	NH ₂	OH	Cl
a	8.04-8.05	8.08-8.11	8.03-8.04	8.18-8.28	8.02-8.07	8.13-8.19
b	7.87-7.92	8.08-8.11	7.89-7.91	8.91-8.92	8.02-8.07	8.13-8.19
c	7.19-7.22	7.08-7.11	under g, h	-	7.07-7.12	7.33-7.39
d	Me@2.425	7.08-7.11	Me@3.41	under a	7.07-7.12	7.33-7.39
e	6.70-6.71	7.20-7.23	7.20-7.22	-	7.42-7.48	7.54-7.64
f	Me@2.155	Me@2.164	7.20-7.22	7.71-7.74	7.42-7.48	7.54-7.64
g	6.60-6.62	6.6529	6.72-6.74	6.94-6.98	6.92-6.98	7.54-7.64
h	6.57-6.59	6.6428	6.72-6.74	7.61-7.62	6.92-6.98	7.54-7.64
R3	5.6688	5.6540	5.7172	5.4081	5.4829	-
solvent	2.58	2.58	2.35-2.39	2.51-2.52	7.2628	2.0582

The UV spectroscopy study^{26,27} for a series of electron donors in the 4 position of the 4-donor-4'-nitro diphenyl sulfides appears in the **Table 13** below. This table mirrors Modena's study of selenides, summarized in **Table 1**.

TABLE 13
LOCATION (nm) OF THE UV MAXIMA OF



N(Me) ₂	NH ₂	NHAc	Me	H	Cl	I	Br
342	341.5	339	339	337	336	336	334

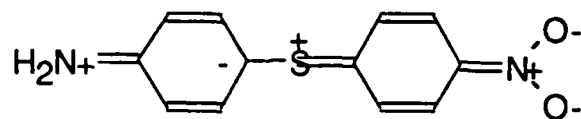
Since the position 4 substituents are listed in the order of increasing electron donor ability from right to left, the trend is clearly visible. It is to ease the electronic $S \rightarrow NO_2$ transition, with increasingly electron rich substituents, as indicated by higher λ_{max} locations.

Similar results are seen in the solvatochromic data. Table 14 lists the solvatochromic effects for **ANDS**, **B**, **D** and **E**. If Cowan's orthogonality argument is true, then solvatochromic effects should be the largest for the planar **E**, and the smallest for sterically staggered **B**. In reality, the opposite is observed.

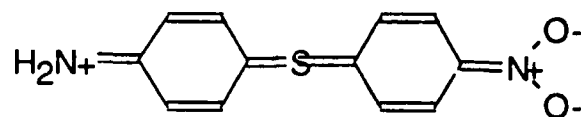
TABLE 14
SOLVATOCHROMISM (in nm vs $CHCl_3$) OF
4-DONOR-4'-NITRO DIPHENYL SULFIDES

solvent cmd	ANDS	B dimethyl	D methyl	E planar
$CHCl_3$	350.5	354	332.75	326
MeOH	-7.5	-9.0	11.25	-3.75
EtOH	-9.0	-9.0	-0.5	-2.25
EtOH*HCl	-21.0	-23.0	n/a	+2.5

In summary, it is interesting to point out that all of the studies of the excited state of **ANDS** indicate the amine \rightarrow nitro electronic transition. Of the ground state studies, the amine nucleophilicity, NMR, and ground state dipole moment phenomena dictate "through the bridge" interactions, while the low temperature fluorescence data shows only weak amino effect. Finally, among the NLO data, solvatochromic data indicate a weak amine effect, while Cowan's conclusion of $S \rightarrow NO_2$ can be dismissed because it was solely based on the orthogonality of the rings and tetrahedral geometry at sulfur argument. A reasonable conclusion is that amine does contribute somewhat to the SHG of **ANDS** and its contribution is best represented by the inductive effect:



A full $\text{NH}_2 \rightarrow \text{NO}_2$



intramolecular electronic transition most likely does not occur during an SHG event. Nonetheless, a limited amine participation in the sulfur to nitro polarization is indicated by all ground and excited state of ANDS investigations.

CHAPTER 3 ALCOHOL MONOMERS

Diols I - IV and tetrol V (Figure 16, below) were designed to covalently incorporate either a nitroaniline derivative or a aminonitrodiphenyl sulfide group into a polymer chain. The nitroaniline entity in I and II was chosen to mimic MNA SHG response.^{4,10,15} Molecular design of the sulfides III and IV was based on the ANDS structure. These functionalities were chosen for their excellent SHG characteristics.^{24,25,36}

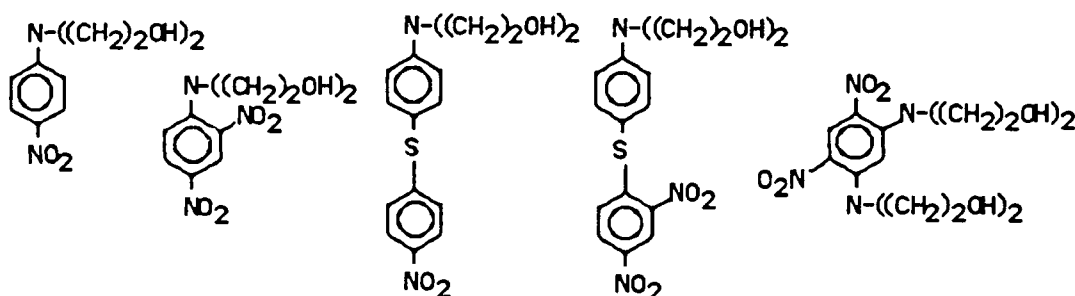


FIGURE 16: VARIOUS ALCOHOLS FOR POLYMERIZATION

EXPERIMENTAL

Diol I was prepared according to a modified procedure described elsewhere.¹³ 31.51 grams (0.2 moles) of p-chloronitrobenzene (CNB, Aldrich) and 42.06 grams (0.4 moles) of N,N diethanol amine (Aldrich) were heated at 115°C for 24 hours. The mixture was then steam distilled to remove the unreacted CNB. When removal of CNB was complete, the reaction mixture in water was allowed to cool to room temperature, recrystallizing crude I. Crude product was dried overnight at room temperature and recrystallized from $CHCl_3$. Yield=33%; $T_m = 106^\circ C$. A dilute chloroform solution of I was passed through a silica gel permeation column. Only one peak, corresponding to I, was detected during a 15 minute elution time.

NMR (Figure 18) and elemental analysis confirmed the diol I structure. Its summary is listed in Table 15. A detailed discussion of the structure proof appeared earlier.¹³

Diol II was prepared similarly to I. 20.26 grams (0.1 moles) of 1-chloro-2,4-dinitrobenzene (Aldrich) and 21.03 grams (0.2 moles) of N,N diethanol amine (Aldrich) were heated at 70°C - 80°C for 17 hours. The mixture was recrystallized from ca. 400

ml of water. For optimal yield, the solution was refrigerated. 22 grams (81% yield) of the dry yellow product, melting at 93°C, were collected by filtration. Subsequent recrystallization from chloroform raised T_m to 99 -100°C. Dilute chloroform solution of **II** was passed through a silica gel permeation column. Only one peak, corresponding to **II**, was detected during a 15 minute elution time.

100 MHz NMR was performed on a deuterated (d_6) dimethyl sulfoxide solution of the yellow product, with tetramethyl silane as a reference. The spectrum appears on **Figure 19**, and the peaks are assigned in **Table 16**. The diol was submitted to Desert Analytics for the elemental analysis.

Diol **III** was prepared by stirring 4.741 grams (0.025 moles) of 4-nitrobenzenesulfonyl chloride (Aldrich) with 4.531 grams (0.025 moles) of N-phenyldiethanolamine (Aldrich) in 100 ml of methylene chloride for 24 hours in the darkened container at room temperature. 7.856 grams of greyish green precipitate (85% yield) were collected. This hydrochloride salt precipitate was washed for 24 hours in concentrated aqueous NaOH solution at room temperature. A crude yellow free amine was recrystallized from $CHCl_3$ to afford clean **III**, melting at 103 -104°C.

Dilute chloroform solution of **III** was passed through a silica gel permeation column. Only one peak, corresponding to **III**, was detected during a 15 minute elution time.

A 100 MHz NMR was performed on a deuterated (d_6) dimethyl sulfoxide solution of the yellow product, with tetramethyl silane as a reference. The spectrum appears on **Figure 20**, and the peaks are assigned in **Table 16**. The diol was submitted to Desert Analytics for the elemental analysis.

Diol **IV** was synthesized similarly to **III**. 5.866 grams (0.025 moles) of 2,4 dinitrobenzenesulfonyl chloride (Aldrich) and 4.531 grams (0.025 moles) of N-phenyldiethanolamine (Aldrich) were stirred in 100 ml of $CHCl_3$ in a darkened container at room temperature for 19 hours. 9.0 grams of crude greyish-beige hydrochloride salt precipitate (yield = 95%) were stirred in a concentrated aqueous KOH solution for 12 hours. Blood red precipitate was collected. Clean **IV** was obtained by recrystallization of the precipitate from $CHCl_3$. T_m = 152°C.

Dilute chloroform solution of **IV** was passed through a silica gel permeation column. Only one peak, corresponding to **IV**, was detected during a 15 minute elution time .

A 100 MHz NMR was performed on a deuterated (d_6) dimethyl sulfoxide solution of the red product, with tetramethyl silane as a reference. The spectrum appears on **Figure 21**, and the peaks are assigned in **Table 16**. The diol was submitted to Desert Analytics for the elemental analysis.

Tetrol **V** was obtained from refluxing a mixture of 3.723 grams (0.0157 moles) of 1,3-dichloro-4,6-dinitrobenzene (Chapter 6) and 3.3 grams (0.0314 moles) of diethanol amine (Aldrich) in triethyl amine for 40 hours. The mixture separated into a red oil bottom layer and a yellow solution. The yellow solution was decanted and allowed to cool to room temperature with virtually no precipitate.

The red oil was repeatedly recrystallized from $CHCl_3$ until the melting point reached $123^\circ C$. The dilute chloroform solution of **V** was passed through a silica gel permeation column. Only one peak, corresponding to **V**, was detected during a 15 minute elution time.

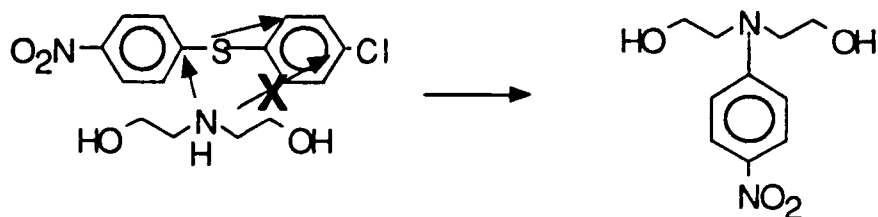
100 MHz NMR was performed on a deuterated (d_6) dimethyl sulfoxide solution of the red product, with tetramethyl silane as a reference. The spectrum appears on **Figure 22**, and the peaks are assigned in **Table 15**. The tetrol was submitted to Desert Analytics for the elemental analysis.

DISCUSSION

Steam distillation, used to purify **I**, is a well established procedure in organic chemistry. It is used to remove water insoluble solids with fairly high vapor pressures.⁵³ It dramatically improves the yield (up to 284% !). This procedure is certainly less tedious and safer than the one used earlier.¹³

Several other routes to synthesizing **III** and **IV** have been proposed. The first involved nucleophilic aromatic substitution of the chlorine in the 4-chloro-4'-nitro diphenyl sulfide by the diethanol amine. It was presumed that the nitro group is able to activate the chlorine through the sulfur. However, as predicted by Hyne and Greidanus³³ for such interaction, both a good electron donor and a good electron acceptor are needed. Chlorine is not good enough of an electron donor to be activated for NAS. As a result, in this reaction, p-chlorothiophenol was the leaving group and the main product was **I**, see **Figure 17**, below:

FIGURE 17



REACTION OF p-CHLORONITRODIPHENYL SULFIDE
WITH DIETHANOL AMINE

N-alkylation of the 4-amino-4'-nitro diphenyl sulfide with 2 equivalents of 2-bromoethanol was not attempted. As discussed in chapter 2, a great body of evidence exists that suggests delocalization of the amine lone pair electrons either by induction or by the remote nitro group. This would greatly deactivate the nucleophilicity of the amine, as seen from Litvinenko's work.³² Thus, electrophilic aromatic substitution routes were chosen.

Elemental analysis results are summarized in **Table 15** below.

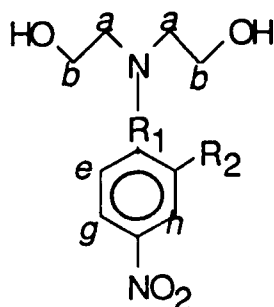
TABLE 15
SYNOPSIS OF THE ELEMENTAL ANALYSIS
RESULTS FOR ALCOHOLS

Alcohol	I		II		III		IV		V	
Element	theo.	expt.	theo.	expt.	theo.	expt.	theo.	expt.	theo.	expt.
C	53.08	52.07	44.28	44.14	57.50	57.30	50.65	50.80	44.92	44.27
H	6.25	6.50	4.83	4.74	5.40	5.37	4.52	4.50	5.92	5.76
N	12.38	12.16	15.49	15.40	8.40	8.27	11.08	10.93	14.97	14.83
O	28.29	28.63	35.39	35.72	19.10	19.81	25.30	25.40	34.19	35.14
S	-	-	-	-	9.60	9.25	8.45	8.37	-	-

These elemental analysis results are in excellent agreement with the supposed structure.

Nuclear magnetic resonance spectra, shown in **Figures 17 - 20**, further confirm the diol structures I - IV. The peak assignments are listed in **Table 16**, below.

TABLE 16
NMR PEAK ASSIGNMENTS FOR THE I - IV ALCOHOLS



DIOL#	1	2	3	4	5
R ₁ Peak asgn.	-	-			g= N(EtOH) ₂
R ₂ →	H _F	NO ₂	H _F	NO ₂	NO ₂
h	8.02-8.07	8.54,8.53	8.01-8.04	8.86,8.87	8.4009
g	8.02-8.07	8.18-8.23	8.01-8.04	8.31,8.40	-
f	6.83-6.90	-	7.07-7.11	-	-
e	6.83-6.90	7.46,7.50	7.07-7.11	7.10, 7.07	7.0024
d	-	-	7.37-7.40	7.38,7.34	-
OH	4.2733	4.82-4.86	3.63	4.83,4.87	4.5-4.76
H ₂ O	2.96	under a	-	3.36,3.38	3.2479
c	-	-	6.72-6.76	6.86,6.89	-
solv.	2.05-2.07	2.5182	7.27	2.50-2.52	7.75,2.6
b	3.81-3.90	3.57-3.69	3.89-3.93	3.57-3.61	3.67-3.7
a	3.70-3.78	3.33-3.46	3.64-3.68	3.50-3.52	3.4-3.47

The peak integration is in excellent agreement with the assigned diol structures. This data, combined with elemental analysis conclusively proves the I - V structures.

Diols were checked for SHG via the powder technique. None of the five diols showed any second order optical nonlinearity.

CHAPTER 4 DIALLYL COMPOUNDS AND CYCLOPOLYMERIZATION

The diallyl compounds, shown in **Figure 23**, below, were synthesized as monomers for cyclopolymerization. Cyclopolymerization of unsaturated quaternary ammonium salts⁵⁴ was discovered by Butler in 1951.

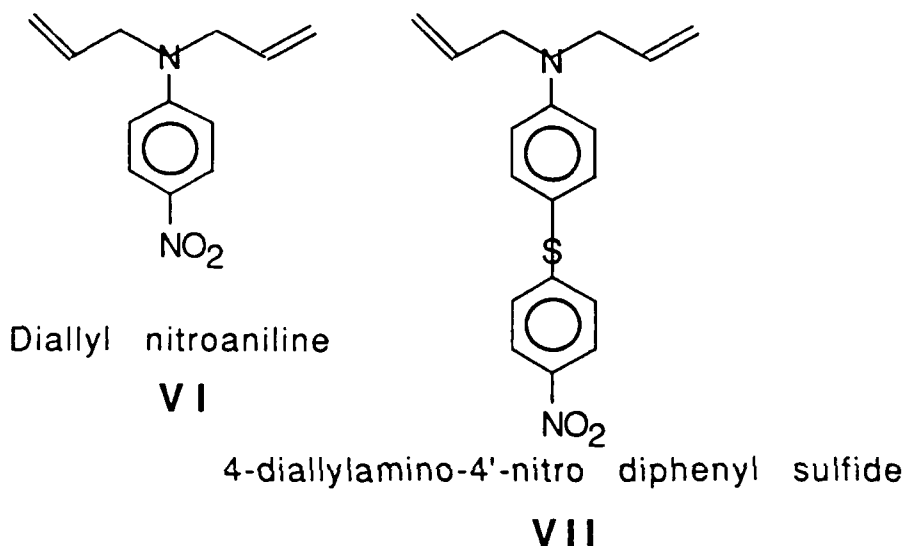


**FIGURE 23: POTENTIAL SHG COMPOUNDS FOR
CYCLOPOLYMERIZATION**

Free unsaturated tertiary amines have been cyclopolymerized as well.⁵⁵ The polymerization mechanism is free radical chain growth and it has been discussed in detail elsewhere.⁵⁶

EXPERIMENTAL

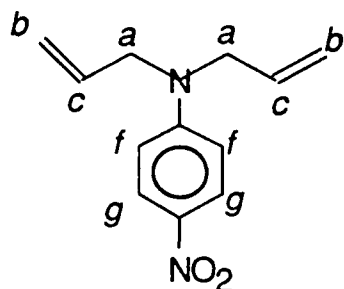
Synthesis of diallyl nitroaniline

15.756 grams (0.1 moles) of p-chloronitrobenzene (Aldrich) and ca. 25 ml (0.2 moles) of diallyl amine (Aldrich) were refluxed at 115°C for 18 hours. Resulting brown grease was washed with water to remove the hydrochloride salt and dried in vacuo at 115°C. Brown liquid was dissolved in CDCl₃ and 100 MHz NMR revealed the desired structure. Peak assignments are summarized in **Table 17**, below. **Figure 24** displays the NMR spectrum.

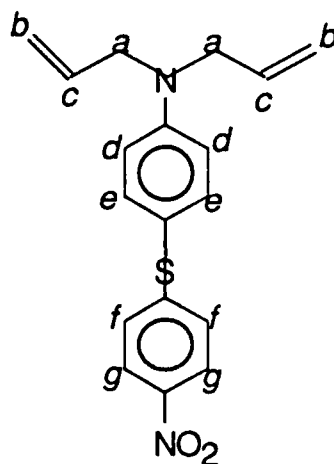
Synthesis of 4-diallylamino-4'-nitro diphenyl sulfide

1 gram (0.00577 moles) of N,N diallyl aniline (Monomer, Polymer and Dujac Labs) was added to 1.094 grams (0.00577 moles) of 4-nitrobenzenesulfonyl chloride (Aldrich), dissolved in 25 ml of methylene chloride. The reaction was allowed to proceed in the dark at room temperature for 24 hours. The solvent was then allowed to evaporate and the remaining red solid was washed in dilute aqueous sodium hydroxide. The resulting red precipitate was dried at 130°C in vacuo for two hours. It was dissolved in CDCl₃ and submitted for 100 MHz NMR with TMS as a reference. Peak assignments are given in **Table 16** and the spectrum appears in **Figure 25**.

TABLE 17
NMR PEAK ASSIGNMENTS FOR



Diallyl nitroaniline
VI



4-diallylamino-4'-nitro diphenyl sulfide
VII

Peak assignments	VI	VII
<i>g</i>	8.0624 - 8.0246	7.9996 - 8.0359
<i>f</i>	6.5889 - 6.6267	7.0515 - 7.0722
<i>e</i>	-	7.3264 - 7.3741
<i>d</i>	-	6.7141 - 6.7781
<i>c</i>	5.7701 - 5.9169	5.8148 - 5.9248
<i>chloroform</i>	7.3	7.2558
<i>b</i>	5.1130 - 5.2381	5.1285 - 5.2348
<i>a</i>	4.0148 - 4.0329	3.9061 - 3.9914

Attempts to cyclopolymerize VI and VII as free amines and as quaternary ammonium hydrochloride salts failed. Various free radical initiators were tried, including AIBN, t-butyl hydroperoxide, di-t-butyl peroxide and benzoyl peroxide. Yellow crosslinked polymer was obtained inadvertently as a product when VI was dried at temperatures above 115°C during the monomer purification procedure. Such side reactions with the quaternary diallyl amine salts are well documented in the literature.⁵⁶

Thermally initiated crosslinking demonstrates that VI and VII can be polymerized under extreme conditions. However, the failure to produce *linear cyclopolymerized* polymers at 60 - 70 °C indicates that free radical transfer takes place. The transfer phenomenon can be linked to two causes.

The growing radical can transfer an electron to the nitro group, which has been documented to be responsible for two transfer routes. If the electron is taken by a monomer's or by another growing polymeric radical's nitro group, then the *transfer to monomer* or *transfer to polymer*⁵⁷ occurs. The nitrobenzene group, which is a substituent of both VI and VII, has been also documented to act a *retarder* and a *weak chain transfer agent*.⁵⁸ Regardless of the exact role that the nitro group plays in this cyclopolymerization, the net effect is the same: the inability to produce a linear polymer.

It is not apparent at present how to combat the premature free radical termination. The nitro group is a necessary substituent, placed by the molecular design requirements of the SHG process. Other strong electron withdrawing groups, such as the cyano moiety, are also known for their transfer ability. Perhaps other solvent/initiator systems can be tried where the transfer effect is minimized.

CHAPTER 5 POLYESTERS

Diol I from Chapter 3 has been polymerized with several diacid chlorides in the previous work.¹³ There, condensation was carried out in dioxane solution with triethyl amine as an HCl acceptor. In the case of terephthaloyl chloride the polymerization was also carried out in a melt. Details of the polymer synthesis, structure confirmation, and characterization can be found in that work.

In an effort to increase the molecular weight of these polyesters, another approach has been attempted. Side reaction resulting in ketene formation⁵⁹ reduced the molecular weight attained by the polyester.

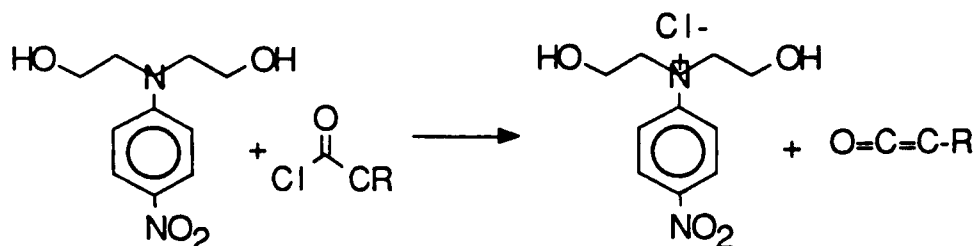


FIGURE 26: KETENE SIDE REACTION DURING A TERTIARY AMINE AND ACID CHLORIDE POLYMERIZATION

Similar polyesters, containing tertiary amines, have been reported in literature.^{60,61} Sulzberg and Cotter⁶¹ carried out these polymerizations in 1,2 dichloroethane at 70°C. Several factors indicate that these polymers were of low molecular weight. Firstly, the polyesters were soluble in 1,2 dichloroethane and in chloroform. The polyesters prepared in Reference 13 were thought to suffer from low molecular weight because their films were somewhat brittle. However, they were insoluble in dioxane, chloroform, and acetone. Intrinsic viscosities were measured in Reference 13, but in Sulzberg and Cotter's work only reduced viscosity for one concentration was reported. It was lower than the corresponding viscosity in the Reference 13 at that temperature and concentration.

To avoid this problem condensation with the diphenyl esters of corresponding diacids was attempted. This reaction is an ester

interchange polyesterification. There are two basic issues involved in these reactions.

Firstly, the polyesterification is improved with the increasing acidity of the leaving group. Here, diphenyl esters of the diacids are advantageous because phenol is more acidic than aliphatic alcohols from the dialkyl esters. Conversely, the alcoholic byproduct of the polymerization must be removed for the polyesterification to proceed according to the LeChatelier's Principle. Here, the poor volatility of phenol is detrimental to the high molecular weight attainment.

Because a large number of commercial polymerizations successfully utilize the melt ester interchange,^{62,63,64,65} this was the route chosen in the present work.

EXPERIMENTAL

Diphenyl malonate synthesis

Diphenyl malonate was prepared by heating 14.18 grams (0.1 moles) of malonyl chloride (Aldrich) with 18.367 (0.2 moles) of phenol (Aldrich) in a water bath at 60°C for 19 hours. The mixture was then dumped into ice water. Brown grease separated immediately, and solidified in 10 minutes. The precipitate was repeatedly recrystallized from ethanol until the melting temperature leveled off at 48.5°C. Previously reported melting temperature of 50°C⁶⁶ could not be reproduced.

Diphenyl malonate, melting at 48.5°C, was dissolved in CDCl₃ and 100MHz NMR was performed. The spectrum appears in **Figure 27**. Because in it no impurities can be detected, this material was subsequently used for the polymerizations.

Polymer synthesis

Attempts to polymerize the diol **I** with the diphenyl terephthalate or with diphenyl isophthalate failed, because these diphenyl esters melt at temperatures at which the diol decomposes. Melt polymerization, therefore, was attempted with **I** and the diphenyl malonate.

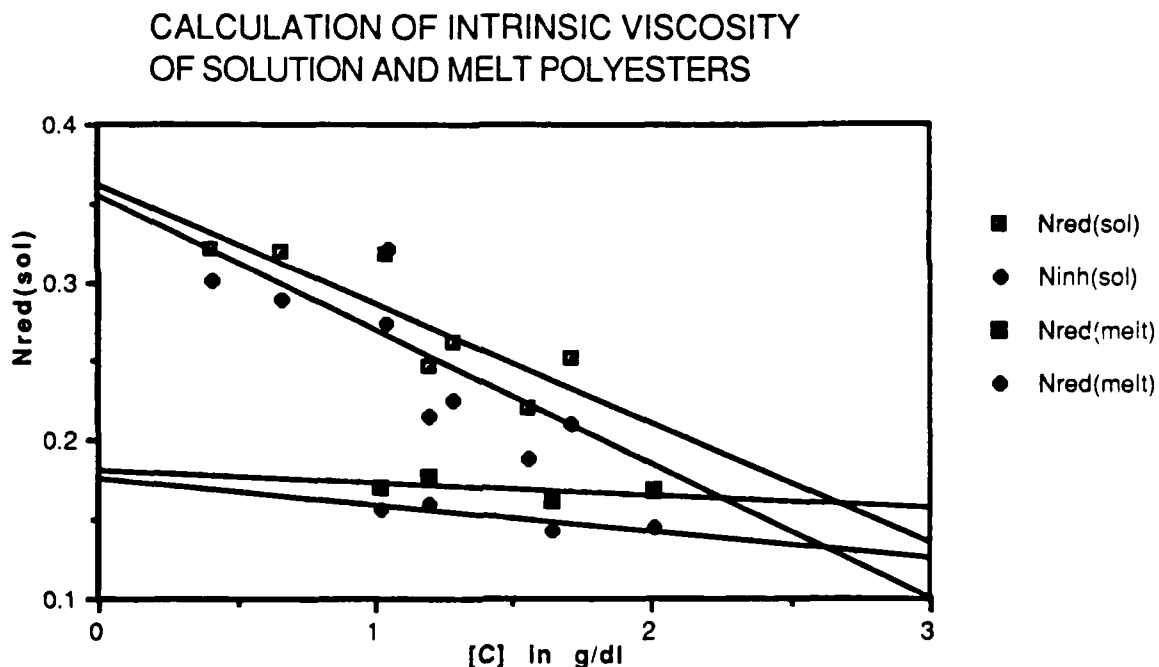
1.281 grams (0.005 moles) of diphenyl malonate and 1.131 grams (0.005 moles) of **I** were sealed in a test tube under nitrogen. The reaction was then heated to 110°C with the gas bubbling through the molten reactants. The tube was then evacuated while the temperature was ramped slowly to 170°C.

After 2 hours at 170°C the mixture was heated to 210°C where it remained for 24 hours.

POLYESTER DISCUSSION

Dilute solution viscometry was performed on dilute DMSO solutions of the melt condensation polymer. Reduced and specific viscosities were extrapolated to zero concentration to obtain the intrinsic viscosity. The data appears in Figure 28 together with the dioxane solution synthesized polyesters.

FIGURE 28:



It is clear that the molecular weight of this polyester is even lower than that of the solution polymer. This is due to the inability to effectively remove the phenol biproduct of the melt condensation.

The viscosity of the growing oligomers increases with the increasing molecular weight. This hampers the efficient phenol vacuum removal from the reaction site. Bubbling nitrogen through the mixture and increasing the reaction temperature with time helps to remove phenol but apparently not enough. Usually in nylon synthesis, where this technique is sometimes employed, viscosity

is not an issue. Because of the partial crystallinity of the polyamides, this reaction is carried out above the melting point. Crystallinity in polyesters would be detrimental to the optical properties for which these polymers are being synthesized.

In summary, it appears that the melt diphenyl ester interchange polymerization is not an acceptable route to high molecular weight polyesters from these diols. Perhaps, the dialkoxy malonates could achieve higher molecular weights. Finally, the best results can be attained by going to a higher temperature reaction in a better solvent. In reference 13, the polyesters precipitated out of room temperature and hot dioxane. It is possible that the reaction depicted in **Figure 26** is not a problem at all here, just that dioxane can not support the high molecular weight polyester. Solvents like DMSO and DMF should be tried for higher molecular weight polyesters.

SHG EVALUATION

Thin films of the solution polymerized terephthaloyl polyester were spun from the dimethyl sulfoxide solution on microscope slide and dried in vacuo at 140°C. They were then corona poled at 150°C for 15 minutes at 15000 volts as described in more detail in Chapter 8. This sample was labeled PE1C15.

A beam from a pulsed Nd/YAG laser was focused on the sample, as the film was rotated 360°. The resulting SHG was detected as described in Chapter 2 and the resulting SHG intensity plot vs the angle of incidence appears in **Figure 84**.

Discussion of the SHG results from the terephthaloyl polyester from **1** appears in Chapter 9 along with the SHG results from other polymers.

CHAPTER 6

POLYMERS WITH INCREASED CONCENTRATION OF NLO GROUPS

Polyesters prepared in Reference 13 had at best (malonyl polyester) an SHG active group covalently attached to one backbone atom in every 13. Unless the free radical cyclopolymerization route, mentioned in Chapter 4, is able to produce high polymers, present condensation systems have this "built in" density limitation.

Eich and coworkers¹² were able to covalently introduce a nitroaniline group on every other atom in poly(allylamine hydrochloride). They named this polymer poly(nitroaniline). The authors took a different approach here by avoiding a free radical polymerization of a monomer with "built in" transfer agent groups that are necessary for SHG.

Yet another approach of increasing the concentration of the NLO active groups in the polymer backbone was attempted in the present work. The underlying idea was to create a polymer with ANDS as a repeat unit. This way, not only high NLO group concentration is achieved by maximizing the number of active pendant groups, but the entire polymer chain participates in the SHG. Several ways of preparing poly(ANDS) have been pursued.

The first, and perhaps, the most naive route, was an effort to extend Lantz's strategy of ANDS preparation to dinitrodichlorobenzenes. The second idea was the application of Wolfe's monomer synthesis for PBT and PBO polymers⁶⁷ to fit the poly(ANDS) scheme. The second route is still very promising. However, time and equipment limitations prevented the completion of this work.

Another system, extending the poly(phenylene vinylene) synthesis to prepare poly(ANDS) analogue, had to be suspended for the same reasons. Ultimately, a compromise approach was chosen, and instead of poly(ANDS), a poly(dinitrophenyl sulfide) or poly(DNPS) was prepared.

EXPERIMENTAL

Monomer synthesis

1,4-dichloro-2,5-dinitrobenzene, VIII, and 1,4-dichloro-2,6-dinitrobenzene, IX, were prepared by nitration of 15 grams

(0.0781 moles) of 1,4-dichloro-2-nitrobenzene (Aldrich) in a mixture of 50 ml of fuming (15% NO₂) nitric acid and 50 ml of fuming (20% SO₃) sulfuric acid at 110°C for 16 hours. The reaction mixture was then decanted over 1 liter of ice water and filtered. The precipitate was washed with cold water and dried. The reaction yielded ca. 14.5 grams (78%) of the product, melting at 75°C.

The product separated in boiling heptane into two layers. The top layer was white, while the bottom was brownish-yellow sludge. Top layer was carefully separated and cooled, allowing the precipitate to form. This product was recrystallized twice from dilute acetic acid, and then from methanol. The first crop, collected from MeOH, melted at 103°C. The final recrystallization from MeOH yielded clean 1,4-dichloro-2,6-dinitrobenzene, *T_m* = 105.5-106°C. The 100 MHz NMR of VIII dissolved in CDCl₃ appears in **Figure 29**.

The mother liquors from all methanol and acetic acid recrystallizations were collected and dried. The substance was recrystallized twice from dioxane, yielding long light amber needles, melting at 117.5-118°C. The 100 MHz NMR of this product in CDCl₃ revealed that 1,4-dichloro-2,5-dinitrobenzene co-crystallized with 2 equivalents of dioxane, **Figure 30**. Vacuum drying these needles at 100°C overnight left the clean dichlorodinitrobenzene. **Figure 31** shows the clean NMR.

1,3-dichloro-4,6-dinitrobenzene, **X**, was prepared by nitration of 20 grams (0.104 moles) of 2,4-dichloro-1-nitrobenzene (Aldrich) in a mixture of 50 ml of fuming nitric acid and 50 ml of concentrated (96%) sulfuric acid at 100-110°C for 44 hours. The reaction mixture was then decanted over 1 liter of ice water, forming greenish-white precipitate. The precipitate was filtered and recrystallized three times from ethanol to yield pure product melting at 102°C. The NMR of **X** in CDCl₃, shown in **Figure 32** confirmed the structure.

1,2-dichloro-4,5-dinitrobenzene, **XI**, was prepared by nitration of 100 grams (0.335 moles) of 1,2-dichlorobenzene (Aldrich) in a mixture of 220 ml of fuming nitric acid and 200 ml of fuming sulfuric acid at 100-110°C for 5 hours. The reaction mixture was then decanted over 1 liter of ice water, forming greenish-white precipitate. The precipitate was filtered and recrystallized from dilute acetic acid and ethanol to raise the melting to ca. 60° C. Upon subsequent recrystallization from

dilute acetic acid, the solution separated into a top white and a bottom yellowish layer. The top layer was carefully separated. Precipitate melted at 90°C. Three subsequent recrystallizations from the dilute acetic acid yielded the desired product, melting at 107 - 108°C. The NMR in CDCl₃, found in **Figure 33**, confirmed the structure. The peak assignments from the NMR spectra of the dichlorodinitrobenzenes appear in **Table 18**, below.

**TABLE 18: NMR PEAK ASSIGNMENTS FOR THE
DICHLORODINITROBENZENES**

benzenes → assigned ↓	1,4 dichloro 2,6 dinitro	1,4 dichloro 2,5 dinitro	1,3 dichloro 4,6 dinitro	1,2 dichloro 4,5 dinitro
2	-	-	7.8529	-
3	8.0186	8.0917	-	8.0595
5	8.0186	-	8.5844	-
6	-	8.0917	-	8.0595

Procedures for the synthesis of these compounds have been described earlier.⁶⁸⁻⁷² However, many of the results have been found irreproducible and also, erroneous melting temperatures were found to have been reported. All NMR assignments were checked with Sadtler NMR Library. Furthermore, gel permeation chromatography was done with all dinitro compounds to ascertain their purity.

Polymer synthesis

Poly(ANDS) by Lantz's method

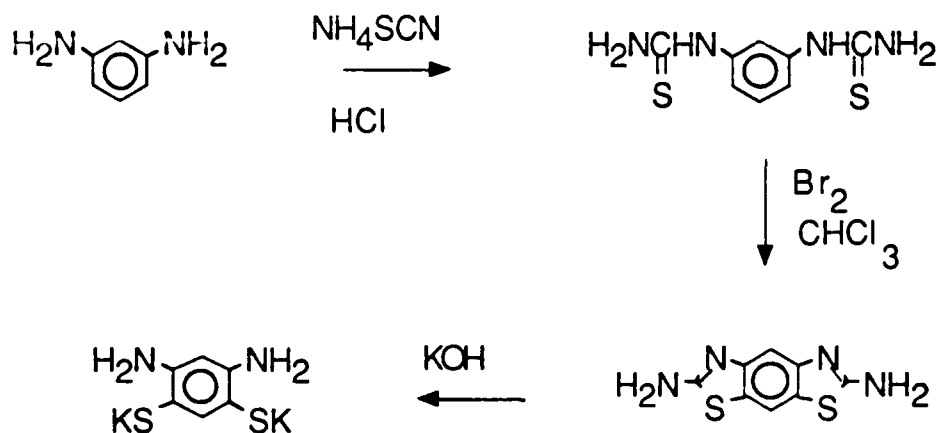
9.6 grams (0.05 moles) of 2,4 dichloronitrobenzene (Aldrich) and 42.032 grams (0.175 moles) of Na₂S*9H₂O (Aldrich) were refluxed in water for 24 hours. Another 9.6 grams (0.05 moles) of 2,4 dichloronitrobenzene was added to the reaction mixture and it was refluxed for additional 24 hours. The reaction was then steam distilled and brown fiber-forming product was isolated and cooled. The precipitate was dissolved in deuterated dimethyl sulfoxide for 100 MHz NMR. Elemental analysis was performed by the Desert Analytics.

The NMR spectrum showed peak integration corresponding to a pentamer of poly(ANDS) structure and the elemental analysis results diverged from the true polymeric composition. Similar

reactions were carried out with VIII - XI and 5 molar equivalents of $\text{Na}_2\text{S} \cdot 9\text{H}_2\text{O}$ with inferior results.

The failure of Lantz's route to poly(ANDS) lies in the instability of the intermediate product of the reaction. Lantz's first stage compound was sodium aminothiophenoxide. In the polymerization, this compound is sodium diaminodithiophenoxide (reaction with VIII - IX) or sodium aminodithiophenoxide (reaction with 2,4 dichloronitrobenzene). Wolfe⁶⁷ has shown that these salts are very unstable. They are very electron rich and therefore, quickly react with the oxygen in the air. Thus, the required exact stoichiometry is broken and the polymer never forms. In an effort to combat this oxygen sensitivity, another synthetic route to poly(ANDS) was proposed.

FIGURE 34



SYNTHETIC ROUTE TO DIAMINODITHIOPHOXIDE SALT, WOLFE'S APPROACH

27 grams (0.157 moles) of m-phenylene diamine (Aldrich) were heated to 50°C with activated carbon and 30 ml of 37% HCl dissolved in 140 ml of water. The mixture was stirred and filtered hot. 48.4 grams (0.636 moles) of NH_4SCN were added and the mixture was refluxed for 24 hours. The granular orange precipitate (50.5 grams) was washed with water. The 100 MHz NMR spectrum of the product dissolved in $\text{dms}-d_6$ confirmed the phenyl bis thiourea structure.

50 grams (0.221 moles) of m-phenyl bis thiourea was suspended in 235 ml of chloroform, and 26.26 ml (0.512 moles) of bromine, dissolved in 33 ml of chloroform were added dropwise to

the mixture. The orange slurry was refluxed for 24 hours, after which, the precipitate was washed in chloroform. When it was stirred with aqueous sodium bisulfite, the precipitate lost its orange color and turned lemon yellow. After another washing with concentrated ammonium hydroxide, the now beige product was rinsed with water and recrystallized from glacial acetic acid. It was sparingly soluble in the acid. Both, the undissolved fraction and the recrystallized portion decomposed between 260 - 270°C without melting.

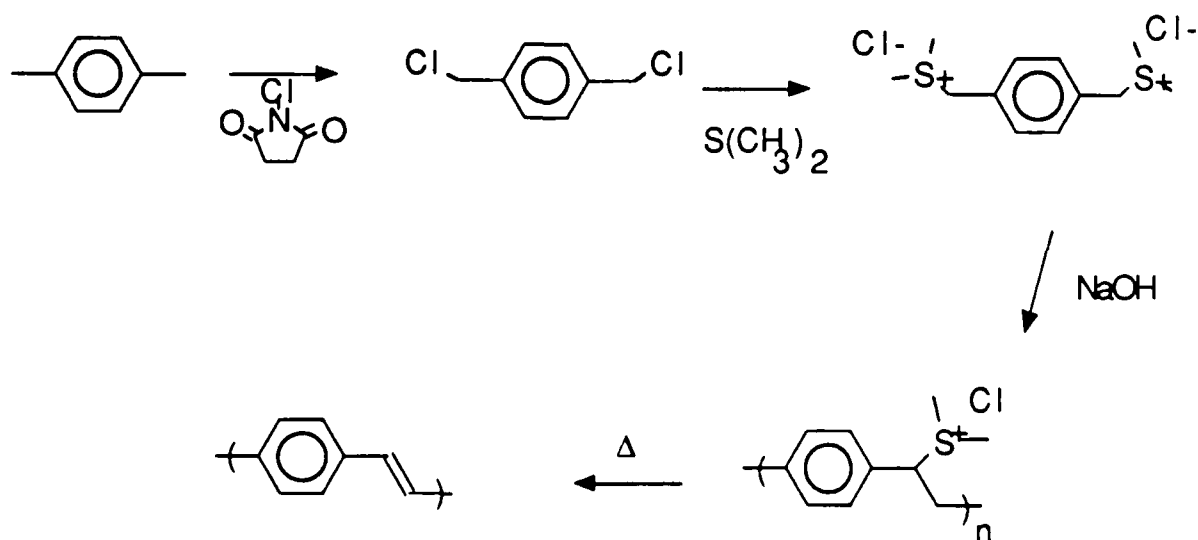
Attempts to cleave the thiazole ring with KOH in inert atmosphere failed to isolate the dipotassium salt due to inadequacy of the dry glove box. A bright yellow color, characteristic of the desired potassium diaminodithiophenoxide, was seen only briefly in the reaction mixture. The reaction then quickly turned dark green, and then black, indicating oxidation.

It is clear that this is a viable route towards poly(ANDS), but better atmospheric control is needed for this reaction to succeed.

Poly(ANDS vinylene) route

The synthetic route to poly(phenylene vinylene) first attempted by Wessling and Zimmerman⁷³ and expanded by Lenz and coworkers⁷⁴ (see the Figure 35 below) was applied to prepare poly(ANDS vinylene).

FIGURE 35: SYNTHETIC ROUTE TO POLY(PHENYLENE VINYLENE)



SYNTHETIC ROUTE TO POLY(PHENYLENE VINYLENE)

However, when 1.947 grams (0.0145 moles) of N-chlorosuccinimide (Aldrich) and 1.750 grams (0.00638 moles) of 4-amino-2,2'-dimethyl-4'-nitrodiphenyl sulfide (compound **B**, Chapter 2) were refluxed in a benzene/carbon tetrachloride solvent system, aromatic carbons on the aniline ring were chlorinated, instead of the methyl carbons. The NMR spectrum of the product, recrystallized twice from MeOH with $T_m = 168^\circ\text{C}$, that appears in **Figure 36** confirms that reaction.

Aniline ring chlorination takes place because N-chlorosuccinimide does not dissociate free radically with the polar **B**. Instead, a heterolytic cleavage of the C-Cl bond takes place and the anionic Cl⁻ species are formed. These anions are "attracted" to the electron-rich aniline ring, and the chlorination occurs there.

Because of the time limitations and the high cost of the starting materials involved, alternate halogenations of **B** were not attempted. Other agents, such as Cl₂ or Br₂ are easily available and are much less likely to generate ionic species when a homolytic cleavage is required. Clearly, additional effort in this synthetic route has a potential to bring very promising results.

Synthesis of the poly(DNDS)

0.5 grams (0.0035 moles) of *m*-benzenedithiol (Aldrich) was added to a solution of 0.861 grams (0.0035 moles) of 1,3-dichloro-4,6-dinitrobenzene, pyridine and dimethyl formamide at room temperature. An instant color change from colorless \Rightarrow purple \Rightarrow yellow was observed as the precipitate deposited. The crude yellow powder was obtained in 100% yield.

The precipitate was washed with hot water and refluxed in acetone. It was recrystallized from dimethyl sulfoxide and dried. The final weight of the polymer was 0.950 grams, indicating 85.3% yield of the high molecular weight poly(phenylene sulfide).

Discussion

The polymer had no visible glass transition range as can be seen from the differential scanning calorimetry graph, appearing in **Figure 37**. The polymer decomposed before melting, as evidenced by the irreversible color loss near 350°C. Polymer was shown to be crystalline by wide angle X-ray scattering, plot of which is shown on **Figure 38**. The polymer was submitted to Desert Analytics for elemental analysis. The results of the elemental analysis are listed in **Table 19**.

TABLE 19
ELEMENTAL ANALYSIS FIT FOR POLY(DNDS)

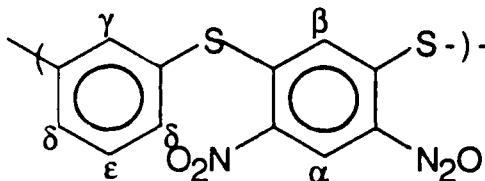
Element	Experim.	Polymer	Decamer	Trimer	Dimer
C	46.89	47.05	47.49	48.19	42.04
H	1.92	1.95	2.13	2.70	2.06
N	8.23	9.15	9.23	6.25	8.17
O	22.29	20.89	22.14	14.27	18.67
S	20.96	20.93	19.01	28.59	10.34

It can be seen from this table that the elemental analysis results indicate a polymeric, and not oligomeric, structure for the product. Even a high oligomer (decamer) shows a poorer data fit than the polymeric model.

An attempt to prepare an NMR sample was made by dissolving the crude polymer in boiling DMSO-d₆ and allowing it to cool slowly to room temperature. Nonetheless, most of the

polymer precipitated out of the solution upon cooling; the solution was only pale yellow. The results of the 100 MHz proton NMR are summarized below and the spectrum appears in Figure 39.

TABLE 20
NMR PEAK ASSIGNMENTS FOR



Peak assignment	Peak location
α	9.0651 - 9.0719
δ	8.8421 - 8.8664
β	8.3923 - 8.4300
γ	7.8976 - 7.9538
ϵ	6.6745
water	3.1372 - 3.8938
dmsO	2.4995 - 2.5136
oligomeric	7.6569 - 7.8166
oligomeric end groups	2.7344, 2.8935

It is clear from the NMR and the elemental analysis data that this product is polymeric, and that the polymer is of fairly high molecular weight.

CHAPTER 7 POLYURETHANES

Alcohols I - V, described in Chapter 3, were also polymerized with several diisocyanates to synthesize a number of polyurethanes. Polyurethanes were chosen because this polymerization reaction affords no byproducts. This fact was used to polymerize polyurethanes under electric field. Monomeric and oligomeric species are much easier to align in the electric field than long entangled polymer chains. Better dipole alignment results in an improved SHG signal from the polymer.

Another advantage of polyurethanes is the presence of two amide linkages per every polymeric repeat unit, that results in very pronounced hydrogen bonding between the polymer chains. Hydrogen bonding can "lock in" the SHG useful side groups and slow down the dipole relaxation that is prevalent in other polymeric systems utilized for SHG. 82-87

EXPERIMENTAL

PU SERIES

PU1C15

0.033 grams (0.0002 moles) of 1,4 phenylene diisocyanate (Aldrich) and 0.045 grams (0.0002 moles) of N,N dihydroxyethyl-4-nitro-benzenamine (I) were dissolved in 5 ml of THF at room temperature. Four drops of the solution were carefully deposited on a microscope slide and THF was allowed to evaporate. The slide was then placed under a sharpened tungsten needle charged at 15000 volts. The sample was heated at 100°C for 15 minutes. The heat was then shut off and the polymer was allowed to cool for 30 minutes to room temperature. The electric field was then removed. **Figure 40** shows the structure of the PU1 polyurethane.

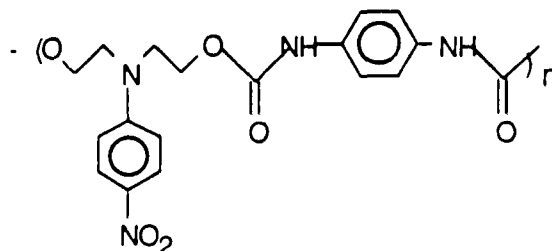


FIGURE 40: PU1

PU1C13 was similarly polymerized, but under 13000 volts. **Figure 41** shows a picture of the corona poling apparatus.

CORONA ALIGNMENT POLYMERIZATION

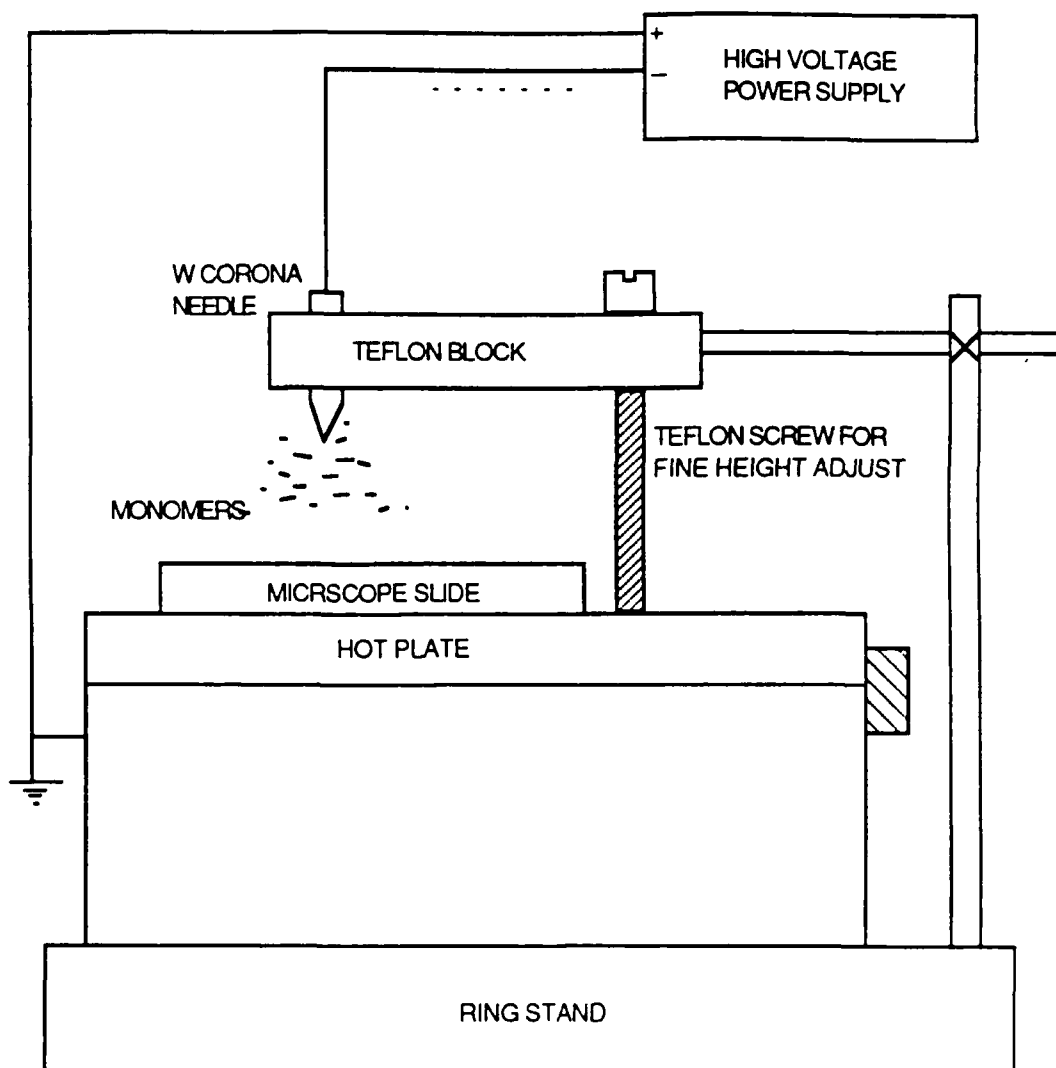


FIGURE 41

PU2C15

0.033 grams (0.0002 moles) of 1,4 phenylene diisocyanate (Aldrich) and 0.054 grams (0.0002 moles) of N,N dihydroxyethyl-2,4-dinitro-benzenamine (II) were polymerized as PU1C15 above. **Figure 42** shows the structure of PU2 polyurethane.

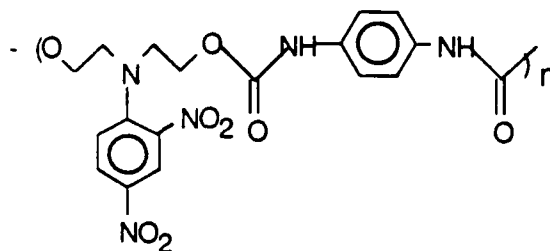


FIGURE 42: PU2

PU3C15

0.033 grams (0.0002 moles) of 1,4 phenylene diisocyanate (Aldrich) and 0.067 grams (0.0002 moles) of N,N dihydroxyethyl-4-(thio-4'-nitrophenyl)-benzenamine (III) were polymerized as PU1C15 above. **Figure 43** shows the structure of PU3 polyurethane.

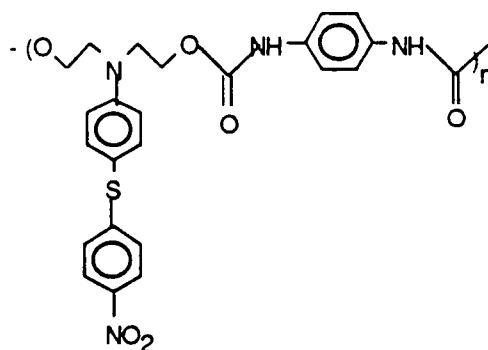


FIGURE 43: PU3

PU4C15

0.033 grams (0.0002 moles) of 1,4 phenylene diisocyanate (Aldrich) and 0.076 grams (0.0002 moles) of N,N dihydroxyethyl-4-(thio-2',4'-dinitrophenyl)-benzenamine (IV) were polymerized as PU1C15 above. **Figure 44** shows the structure of PU4 polyurethane.

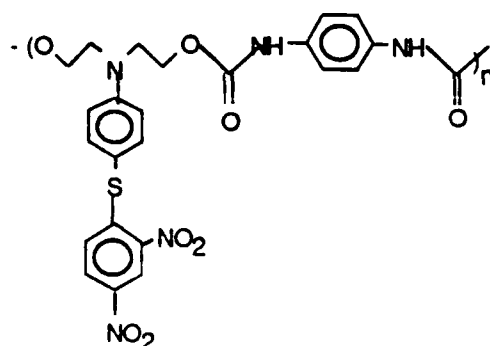


FIGURE 44: PU4

PU5C15

0.066 grams (0.0004 moles) of 1,4 phenylene diisocyanate (Aldrich) and 0.075 grams (0.0002 moles) of di-N,N dihydroxyethyl-(2,4-dinitro)-phenylene-1,3-diamine (V) were polymerized as PU1C15 above. Figure 45 shows the structure of PU5 polyurethane.

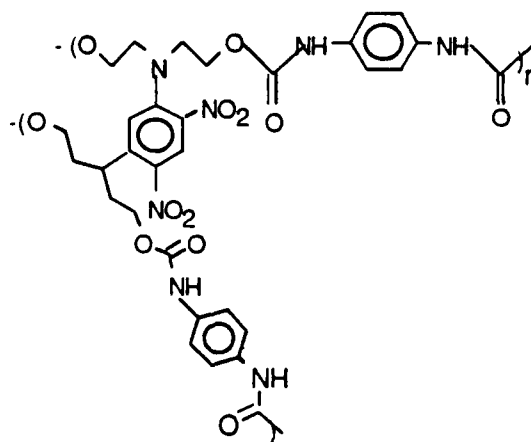


Figure 45: PU5

All of the PUXC13 polyurethanes were synthesized like their PUXC15 analogues, but the tungsten needle was charged at 13000 volts.

DU SERIES

DU1C15

0.051 grams (0.0002 moles) of diphenyl methane 4,4'-diisocyanate (Tokyo Kasei) and 0.045 grams (0.0002 moles) of N,N dihydroxyethyl-4-nitro-benzenamine (I) were polymerized as

PU1C15 above. **Figure 46** shows the structure of DU1 polyurethane.

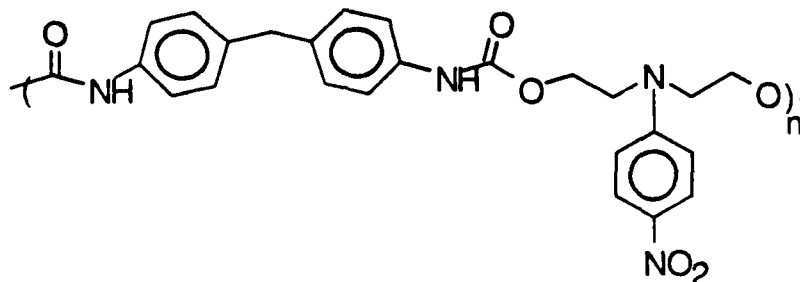


Figure 46: DU1

DU2C15

0.051 grams (0.0002 moles) of diphenyl methane 4,4'-diisocyanate (Tokyo Kasei) and 0.054 grams (0.0002 moles) of N,N dihydroxyethyl-2,4-dinitro-benzenamine (II) were polymerized as PU1C15 above. **Figure 47** shows the structure of DU2 polyurethane.

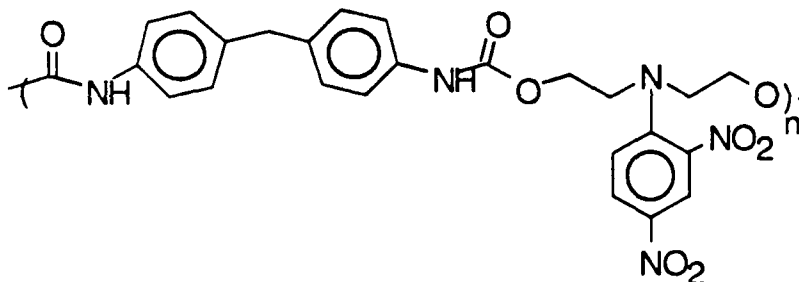


Figure 47: DU2

DU3C15

0.051 grams (0.0002 moles) of diphenyl methane 4,4'-diisocyanate (Tokyo Kasei) and 0.067 grams (0.0002 moles) of N,N dihydroxyethyl-4-(thio-4'-nitrophenyl)-benzenamine (III) were polymerized as PU1C15 above. **Figure 48** shows the structure of DU3 polyurethane.

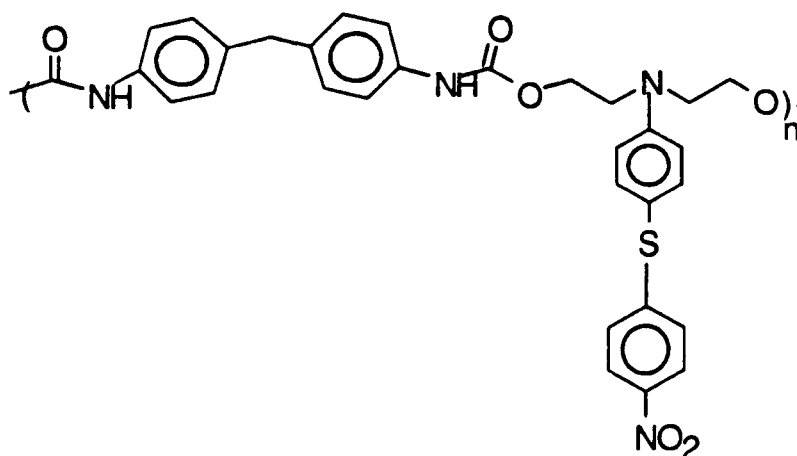


Figure 48: DU3

DU4C15

0.051 grams (0.0002 moles) of diphenyl methane 4,4'-diisocyanate (Tokyo Kasei) and 0.076 grams (0.0002 moles) of N,N dihydroxyethyl-4-(thio-2',4'-dinitrophenyl)-benzenamine (IV) were polymerized as PU1C15 above. **Figure 49** shows the structure of DU4 polyurethane.

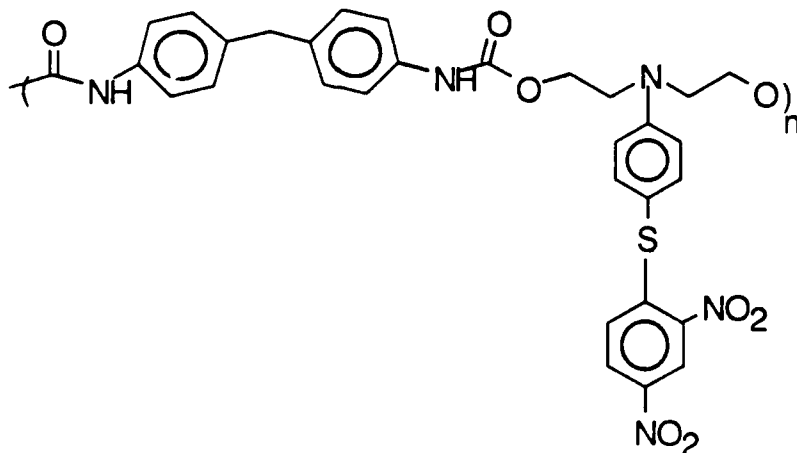


Figure 49: DU4

DU5C15

0.102 grams (0.0004 moles) of diphenyl methane 4,4'-diisocyanate (Tokyo Kasei) and 0.075 grams (0.0002 moles) of di-N,N dihydroxyethyl-(2,4-dinitro)-phenylene-1,3-diamine (V) were polymerized as PU1C15 above. **Figure 50** shows the structure of DU5 polyurethane.

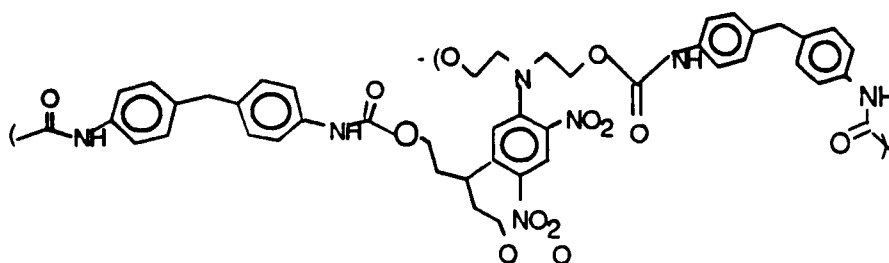


Figure 50: DU5

HU SERIES

HU1C15

33 ml (0.0002 moles) of hexamethylene diisocyanate (Aldrich) and 0.045 grams (0.0002 moles) of N,N dihydroxyethyl-4-nitro-benzenamine (I) were polymerized as PU1C15 above. **Figure 51** shows the structure of HU1 polyurethane.

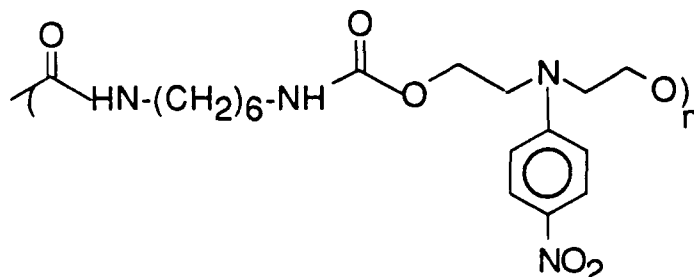


Figure 51: HU1

HU2C15

33 ml (0.0002 moles) of hexamethylene diisocyanate (Aldrich) and 0.054 grams (0.0002 moles) of N,N dihydroxyethyl-2,4-dinitro-benzenamine (II) were polymerized as PU1C15 above. **Figure 52** shows the structure of HU2 polyurethane.

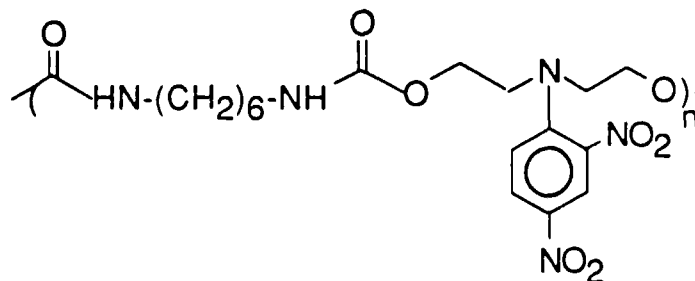


Figure 52: HU2

HU3C15

33 ml (0.0002 moles) of hexamethylene diisocyanate (Aldrich) and 0.067 grams (0.0002 moles) of N,N dihydroxyethyl-4-(thio-4'-nitrophenyl)-benzenamine (III) were polymerized as PU1C15 above. **Figure 53** shows the structure of HU3 polyurethane.

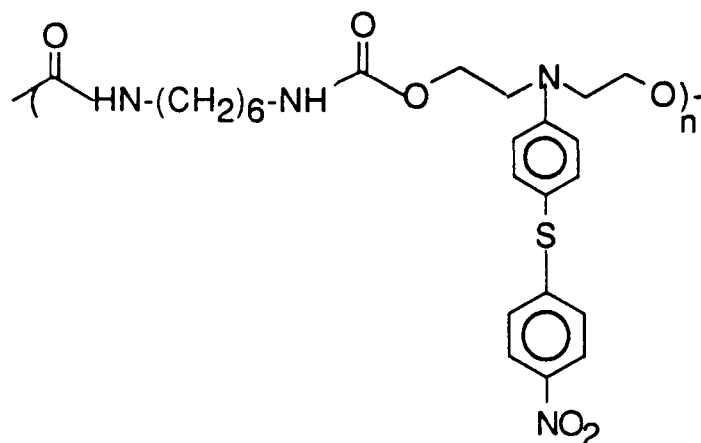


Figure 53: HU3

HU4C15

33 ml (0.0002 moles) of hexamethylene diisocyanate (Aldrich) and 0.076 grams (0.0002 moles) of N,N dihydroxyethyl-4-(thio-2',4'-dinitrophenyl)-benzenamine (IV) were polymerized as PU1C15 above. **Figure 54** shows the structure of HU4 polyurethane.

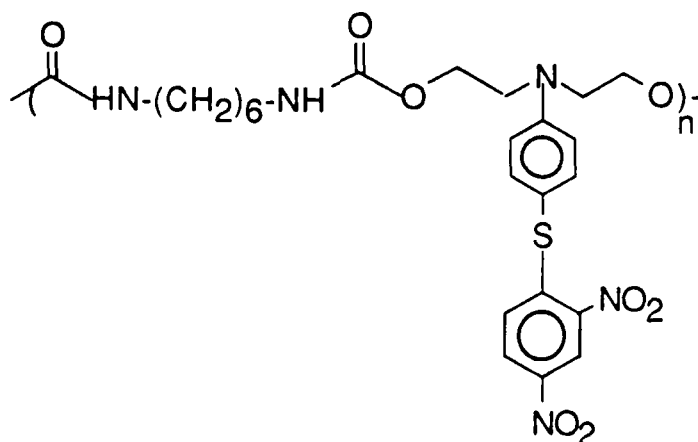


Figure 54: HU4

HU5C15

66 ml (0.0004 moles) of hexamethylene diisocyanate (Aldrich) and 0.075 grams (0.0002 moles) of di-N,N dihydroxyethyl-(2,4-dinitro)-phenylene-1,3-diamine (V) were polymerized as PU1C15 above. **Figure 55** shows the structure of HU5 polyurethane.

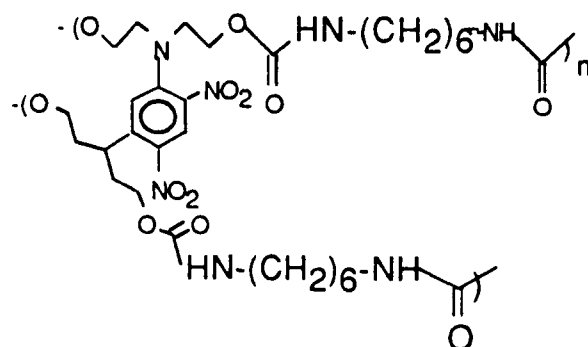


Figure 55: HU5

STRUCTURE CONFIRMATION

The 1 - 4 PU, HU AND DU series samples were scraped off the glass slide, dried in vacuo at 100°C for 12 hours and dissolved in DMSO-d₆. The soluble fractions were filtered and collected in the NMR tubes. The TMS reference was added in a capillary tube and inserted into the polymer solutions. 100 MHz spectra appear in the attached **Figures 56 - 67**. The peak assignments appear in **TABLES 21, 22 and 23**.

Another fraction of the PU polymers was submitted to Desert Analytics for elemental analysis. C, H, N, O, and S analysis was performed. Results are listed in **Table 24**.

Infrared and ultraviolet spectroscopies results appear in **Table 25 and 26 and Figures 68 - 76**.

PHYSICAL PROPERTIES

Thermal properties of these polyurethanes were investigated using differential scanning calorimetry (DSC) on the DuPont interactive DSC. Wide angle X-ray scattering was performed with the finely ground powders of PU1 - PU4 to reaffirm that the samples are amorphous.

HUPEG SERIES

Because absolute molecular weight measurements were not available, the HU series polyurethanes were copolymerized with polyethylene glycol (PEG, M.W. = 200, Aldrich). This was done to show that free standing polymeric films of high molecular weight are achievable at the synthetic conditions used for the SHG samples. A range of PEG/diol compositions was copolymerized with the hexamethylene diisocyanate and durable flexible 50 μ m films were obtained for all four (HU1PEG - HU4PEG) diols. Qualitative measurements of the films' strength and durability appear in **Table 28**.

TABLE 28
MECHANICAL PROPERTIES OF THE HUPEG SERIES

DIOL#→ % PEG	I	II	III	IV
0	brittle	brittle	brittle	brittle
5	flexible	flexible	brittle	brittle
10	n/a	n/a	brittle	brittle
15	n/a	n/a	brittle/bend	brittle/bend
20	n/a	n/a	some flex	some flex
25	n/a	n/a	flexible	flexible

SHG EVALUATION

The sample was rotated 360° under Q-switched YAG/Nd laser beam, $\lambda = 1064$ nm, pulsing @1250 Hz. Typical pulse width at that frequency is ca. 200 nanoseconds. The second harmonic signal @ 532 nm was measured as described earlier (see **Figure 2**). A sample theta scan appears in **Figure 3**. Film thickness was measured on the Dektak, an α - step stylus profilometer.

POLYURETHANE DISCUSSION

PROPERTIES AND STRUCTURE DISCUSSION

NMR

Nuclear magnetic resonance spectra of the soluble fractions of the PU, HU, and DU series polyurethanes show the onset of polymerization as evidenced by the urethane's N-H proton that appears at 9.4 - 9.5 ppm for the PU's. Similarly, these protons are seen at 9.45 - 9.80 ppm for the DU's and in the 7.0 - 7.2 ppm range for the HU's (refer to **Tables 23, 24, and 25**). This is a broad peak that is usually associated with these protons. Another broad peak, at 6.45 - 6.60 for the DU's and at 5.7 ppm for HU's, is

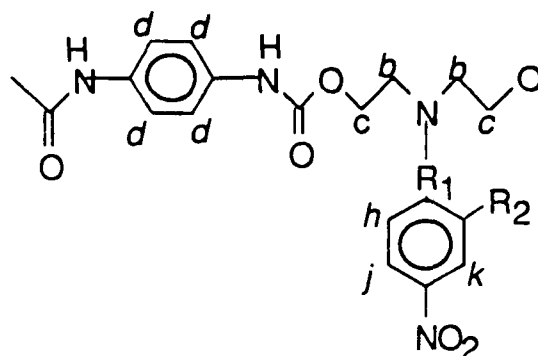
characteristic of the amine proton. This amine is the result of the reaction of water with the isocyanate group according to:⁷⁵



The peak at 4.85 - 5.15 ppm is the unreacted alcohol peak. Another area of interest is the second type of the urethane NH proton, occurring at 8.47-8.50 ppm for the PU's, 8.52-8.67 ppm for the DU's and 6.73-6.87 ppm for the HU series. This type of proton corresponds to the urethanes closest to the amine in **22**: R-O(CO)NH-R₂-NH₂.

Table 21 summarizes the peak assignments for the PU1-4 polymers.

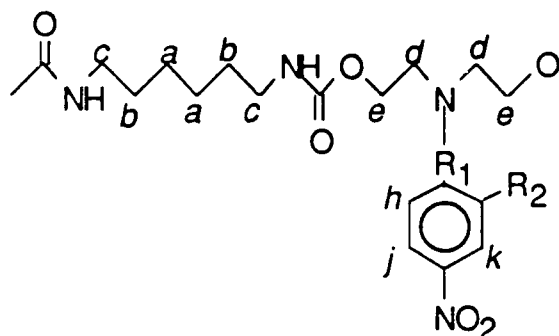
TABLE 21
NMR ASSIGNMENTS FOR THE PU SERIES



Peak assignment	1	2	3	4
$R_1 \rightarrow$	-	-		
$R_2 \rightarrow$	H_i	NO_2	H_i	NO_2
k	8.00-8.06	8.46-8.66	8.04 - 8.08	8.86-8.88
j	8.00-8.06	8.11-8.23	8.04 - 8.08	8.26-8.39
NH	9.55	9.35-9.39	9.5309	9.5370
i	6.80-7.00	-	7.13-7.18	-
h	6.80-7.00	7.45-7.52	7.13-7.18	7.02-7.11
oligomeric NH	8.50	8.49	8.47	8.4684
unreacted OH	4.90, 4.91	4.83-4.86	5.1481	4.83-4.88
g	-	-	7.36-7.40	7.36-7.40
f	-	-	6.97-7.00	6.86-6.97
d	7.34	7.24-7.36	7.3353	7.30, 7.33
oligomeric CH_2	3.59-3.62	3.58	3.59-3.63	3.49-3.63
H_2O	3.4240	3.27-3.55	2.78-3.58	3.32-3.48
c	4.28-4.30	4.2863	4.22-4.29	4.27-4.28
$dmsO$	2.51, 2.52	2.50-2.52	2.45-2.51	2.50-2.53
b	3.81-3.84	3.59-3.69	3.70-3.77	3.74-3.84

Similarly, **Table 22** lists the NMR spectra peak assignments for the HU series polyurethanes.

TABLE 22
NMR ASSIGNMENTS FOR THE HU SERIES



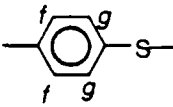
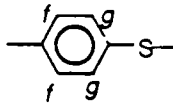
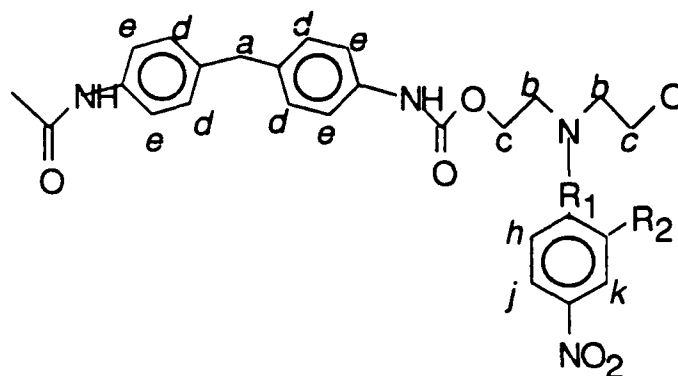
Peak assignment	1	2	3	4
$R_1 \rightarrow$	-	-		
$R_2 \text{ } \mathcal{A}$	H_i	NO_2	H_i	NO_2
<i>k</i>	8.00, 8.04	8.52-8.56	8.06-8.09	8.85-8.88
<i>j</i>	8.00, 8.04	8.18-8.24	8.06-8.09	8.32-8.41
<i>NH</i>	7.146	6.95-7.03	under <i>j</i>	7.1488
<i>i</i>	6.88-6.92	-	7.14, 7.17	-
<i>h</i>	6.88-6.92	7.45-7.52	7.14, 7.17	7.08, 7.11
<i>oligomeric NH</i>	6.84-6.80	6.74-6.73	6.85, 6.87	under <i>f</i>
<i>unreacted OH</i>	4.87-4.88	4.76-4.83	4.77-4.81	4.81-4.85
<i>g</i>	-	-	7.36, 7.33	7.35-7.38
<i>f</i>	-	-	6.90, 6.93	6.86-7.05
<i>e</i>	4.14	4.11-4.19	4.04-4.10	4.1072
<i>d</i>	3.70-3.71	4.54-4.59	3.61-3.70	3.60-3.63
<i>oligomeric CH₂</i>	3.58-3.63	<i>d</i> , 2.6-2.7	3.47-3.53	3.50-3.58
<i>H₂O</i>	3.36	3.35-3.39	3.3485	3.3484
<i>c</i>	2.92, 2.94	2.85-2.95	2.86-3.02	2.93-2.94
<i>dmsO</i>	2.51	2.49-2.51	2.509	2.50-2.51
<i>b</i>	1.32, 1.25	1.21-1.38	1.34-1.35	1.32-1.41
<i>a</i>	1.25, 1.18	1.05-1.14	1.11-1.27	1.20-1.27

TABLE 23
NMR ASSIGNMENTS FOR THE DU SERIES



Peak assignment	1	2	3	4
$R_1 \rightarrow$	-	-		
$R_2 \rightarrow$	H_i	NO_2	H_j	NO_2
<i>k</i>	8.02, 8.06	8.54, 8.55	8.03-8.10	8.85, 8.88
<i>j</i>	8.02, 8.06	8.08-8.13	8.03-8.10	8.21-8.32
<i>NH</i>	9.54, 9.59	9.35-9.45	9.56-9.81	9.58
<i>i</i>	6.95, 6.99	-	7.11 and	-
<i>h</i>	6.95, 6.99	7.47, 7.51	under d	under d
<i>oligomeric NH</i>	8.52-8.55	under j	8.67	8.52
<i>unreacted OH</i>	4.89-4.92	4.811	4.83	4.80-4.84
<i>g</i>	-	-	7.35, under e	under e
<i>f</i>	-	-	6.96-7.0	under d
<i>e</i>	7.20-7.37	7.25-7.36	7.37, under g	7.31-7.43
<i>d</i>	7.08-7.19	7.03-7.18	7.06-7.15	7.05-7.15
<i>oligomeric CH₂</i>	3.58-3.72	under b	3.60-3.63	3.54-3.68
<i>H₂O</i>	3.3904	3.35-3.46	3.36	3.35
<i>c</i>	4.22-4.38	4.20, 4.28	4.27	4.27
<i>dmsO</i>	2.50-2.52	2.49-2.54	2.51-2.52	2.50-2.54
<i>b</i>	3.80-3.95	3.57-3.66	3.7762	3.77-3.89
<i>a</i>	under b	3.77	under b	under b

Some NMR spectra show residual acetone from the tube washing near 2 ppm. Oligomers and possibly unreacted diols

manifest themselves in methylenes and alcohols, locations of which are described in the Tables above. Methylenes immediately adjacent to the alcohols are shifted downfield when a urethane is formed. This happens because the carbonyl linkage strongly withdraws electrons.

There is excellent agreement in the aromatic/aliphatic proton ratio as seen from the spectra integrations. Even for the individual protons there is good integral correspondence. This further asserts the polyurethane formation.

ELEMENTAL ANALYSIS

Elemental analysis was performed on the entire sample in the PU series, not just on the oligomeric soluble fraction, like NMR. Therefore its results are indicative of the overall polymer composition. Results are listed in **Table 24**, below.

TABLE 24
SYNOPSIS OF THE ELEMENTAL ANALYSIS RESULTS FOR PU's

PU#→ Element	I		II		III		IV		V	
	theo.	expt.	theo.	expt.	theo.	expt.	theo.	expt.	theo.	expt.
C	55.95	54.37	50.12	50.21	58.29	58.09	53.43	53.92	51.87	51.02
H	4.70	4.89	3.97	4.49	4.49	4.61	3.92	4.20	4.35	4.87
N	14.50	13.97	16.24	15.20	11.33	11.41	12.98	13.33	16.13	14.83
O	24.85	26.02	29.67	29.12	19.41	19.95	23.73	24.34	27.64	29.28
S	-	-	-	-	6.48	5.93	5.94	5.02	-	-

Experimentally determined composition closely agrees with the linear polyurethane structures of PU1 - PU4. Side reaction **22** or crosslinking via the biurette formation⁷⁴ must not occur to any appreciable extent.

UV and IR

Ultraviolet spectroscopy of the polyurethanes shows that they are nearly transparent at 532 nm, the SHG frequency of the optical experiment. Absorbance at that wavelength is detrimental to the SHG seen from the sample. They are completely transparent at 1064 nm. This is important because if the samples absorb in that range the sample will heat up and burn up under the powerful Nd/YAG beam. **Figures 72 - 76** show the UV spectra of PU1 -

PU5. The transmission characteristics of these polymers at the harmonic frequency are listed in the **Table 25** below:

TABLE 25
TRANSMISSION OF PU's AT THE HARMONIC FREQUENCY

PU#	% TRANSM. @ 520 nm	% TRANSM. @ 540 nm	maximum @ (nm)
1	91.0	96.0	410
2	65.5	88.1	410
3	67.3	83.4	380
4	8.4	20.1	390
5	42.9	67.2	400

UV spectra of the sulfide polymers PU3 and PU4 show a sulfur to nitro $n \Rightarrow \pi^*$ transition in the 350nm range that is present in their corresponding diols and ANDS. PU1 and PU2 absorb in 350 nm range like their diols, MNA and PNA. UV spectra in the near IR range shows that the samples are transparent at $\lambda = 1064$ nm, the wavelength of the fundamental beam.

TABLE 26
SUMMARY OF WAVELENGTHS (in cm^{-1}) OF PU SERIES IR ABSORPTION

PU1	PU2	PU3	PU4	GROUP PEAKS ASSIGNED TO
3331	3369	3322	3316	H-bonded amide N-H
3113	3092	3093	3100	sp^2 C-H
2947	2940	2957	2926	sp^3 C-H
2894	2902	2907	2874	sp^3 C-H
1712	1714	1716	1718	amide
1595	1602	1592	1592	amide
1516	1519	1508	1517	para benzene or 1,2,4 benzene
1483	-	-	1459	nitrobenzene
1405	1407	1405	1403	nitrobenzene
1310	1329	1335	1305	aromatic tertiary amine
1206	1217	1215	1214	aromatic tertiary amine
1113	1145	~1110	1130	para benzene or 1,2,4 benzene
1066	1063	1073	1068	nitrobenzene
1000	923	1013	1007	para benzene or 1,2,4 benzene
828	830	835	927	para benzene or 1,2,4 benzene
752	745	750	738	amide

IR spectra summaries of PU1, PU2, PU3, and PU4 are listed in **Table 26**. All four scans show that polymerization occurred. This can be monitored by the appearance of the bonds characteristic of urethanes, such as C=O, N-H, C-O, and C-N. Onset of the absorption at several wavelengths, characteristic of the amide stretches and vibrations and disappearance of characteristic absorption of the isocyanate functionality at ca. 2100 cm^{-1} are indicative of the polyurethane formation.

It is difficult to see from the IR spectra whether the side reaction depicted by **22** occurs to any appreciable extent. The primary aromatic amine has weak characteristic absorption peaks at $3400 - 3500\text{ cm}^{-1}$ due to the N-H bond stretch. This peak is hard to detect so near the strong amide stretch ca. 3300 cm^{-1} . Nonetheless, this peak is absent in all four spectra. Furthermore, 1° aromatic amine absorbs at ca. $1650 - 1580\text{ cm}^{-1}$ due to the N-H scissoring. This peak overlaps with the carbonyl stretch of the amide. These amines also absorb at $650 - 800\text{ cm}^{-1}$,³⁴ but this peak coincides with the amide absorption in that region. Finally, the strong C-N stretch in $1266 - 1342\text{ cm}^{-1}$ is identical for the 1° and 3° (from the *nitroaniline*) aromatic amines. So, IR spectroscopy is able to provide only mild evidence that **22** is not a great threat in these polymerizations.

Polyurethane formation is supported by absorptions at ($1712-1718\text{ cm}^{-1}$), ($1592 - 1602\text{ cm}^{-1}$), ($738 - 752\text{ cm}^{-1}$) and ($660 - 690\text{ cm}^{-1}$) seen in all PU series polymers. Finally, hydrogen bonded N-H and alcohol O-H are impossible to differentiate at $3316 - 3369\text{ cm}^{-1}$ region.³⁴ The absorption in that range is most likely due to urethane's N-H, because evidence for this bond is present at four other wavelengths. However, there is, probably, some unreacted OH end groups overlapping with the amide stretch.

IR spectra reaffirm the polyurethane structures dictated by the NMR and elemental analysis.

DSC

Samples showed no crystalline transitions such as melting and only slight inflections that could be glass transitions (see attached Figures). Because of the importance of the T_g for the dipole relaxation further thermal investigation was done. SHG signal relaxation vs time at room and at elevated temperatures for each of the polymers in the PU series was monitored.

SHG remained constant for all samples through 1,000,000 seconds at room temperature. At elevated temperatures only PU4C15, PU3C15 and PU1C15 were studied. Here, the corona poled samples were heated at the designated temperature for a specified time. SHG was then measured, and the sample returned to the elevated temperature for the next plot point. Results are listed in **Table 31** and **Figures 108 - 112**. They show only slight relaxation at prolonged exposures at 50°C and a major signal drop between 100°C and 135°C after 1000 seconds of heating. This strongly suggests T_g in that thermal range.

SHG signal data at elevated temperature gives a much better "feel" for the dipole relaxation in these polymers than does the DSC. From the two, T_g 's in the 100 - 135°C range are proposed.

X-RAY SCATTERING

Wide angle X-ray scattering spectra, depicted in **Figures 81 - 84**, show a broad halo typical for amorphous materials for PU2, PU3 and PU4 polymers. PU1 diffraction shows crystalline peaks at 9°, 10.35°, 11.1°, 14.15°, and possibly 19°. Application of the Scherrer equation⁷⁸ applied to these peaks reveals corresponding domain sizes between 45Å and 60Å.

$$x = \lambda / \Delta B_{\text{corr}} \cos \theta \quad 23$$

Here, x is the domain size in Å

λ is the wavelength of the X-ray source ($K_\alpha = \text{Å}$)

θ is the angle of a particular diffraction peak

$B_{\text{corr}}^2 = B_{\text{app}}^2 - B_{\text{slit}}^2$, where B_{corr} is the width of the diffraction peak, corrected by the slit width.

The size is indicative of small organic crystals, not that of the polymer chains. This data is in line with the differential scanning calorimetry, which conclusively shows that the polymers are completely amorphous.

X-ray scattering is a very sensitive technique and it can pick up a signal from less than 1/2° (degrees) of the sample composition. It is possible that some unreacted diol or other impurity from the sample processing is responsible for the scattering peaks.

POLING

Conventionally, parallel plate poling has been used in the SHG field for the polymer dipole alignment. Here, a polymer film is sandwiched between two parallel electrodes. The electrodes are either transparent or opaque at the fundamental and harmonic wavelengths. If the opaque electrodes are used, then they must be removed prior to the optical probing. A picture of a parallel plates poling apparatus appears in **Figure 85**.

The corona poling technique has been used in the past to produce piezoelectric polymeric films⁷⁹ and more recently, specifically for the dipole orientation of polymer films for SHG.¹² The authors were able to achieve better dipole orientation and, therefore, better harmonic signal from the corona poling than from the conventional parallel plates technique.¹²

Better alignment occurs for a number of reasons under the corona. Firstly, higher poling fields at the polymer surface are obtainable because the corona poling takes place at the voltages near the dielectric breakdown of air. In the parallel plate method, breakdown of the sample typically occurs as a burn through the film. This happens because of the short circuiting caused by local defects, such as pinholes and impurities.¹² Therefore, the theoretical film breakdown voltages are not achievable in this method. So, the alignment is limited to lower voltages between the plates. Even in good quality films this could be ten times lower than the maximum electric field.

Secondly, conducting indium tin oxide glass (ITO), commonly used for electrodes, is typically 300Å thick. Even the minute milliamp currents caused by the discontinuities in the film heat up and degrade the ITO at the poling voltages. This local decomposition creates a short circuit that, in turn, draws in more amperage and heat and burns the rest of the sample.

Thirdly, poling usually takes place at elevated temperatures that are necessary to elevate the polymer above its glass transition point. Dipole movement and reorientational response takes place in the polymer only in that temperature range or above. This molecular motion can create defects that are not present at room temperature. Defects could also appear as a result of nonuniform sample heating that, in turn, could be caused by nonuniform film thicknesses among other things. Even if these

do not occur, the polymer dielectric breakdown voltage is lowered significantly at the elevated temperatures.¹²

Finally, in this work, monomer mixtures were cast from the THF solutions. The coating was never a smooth film upon deposition, and often, even the resulting polymers were not wetting the surface. Therefore, the conventional parallel plate poling was not advisable in this case.

Instead, a number of modified parallel poling methods were attempted. One involved covering the reacting region with a thin polyethylene terephthalate (PET) film. PET in the thickness range of 18 μm to 130 μm was used. In this approach the poling voltages were limited by the dielectric breakdown of the PET film used. Also, the choice of PET limited the temperatures to less than 80°C. Specific geometry of this method is shown on **Figure 86**.

Limits of this poling approach were not only PET's thermal limitations. The electric field was "shared" by the polyurethane and PET according to 24:⁸⁰

$$E_T/D = t_1/\epsilon_1 + t_2/\epsilon_2$$

24

So, polyurethanes received only a fraction of the poling voltage applied. Another limitation was placed by the top (live) electrode. A non bonded top electrode did not provide a uniform contact across the poling area (please refer to **Figure 86** in the Appendix) . This resulted in poling aberrations around the poling surface. If the electrode was bonded to PET (as in sputtered aluminum on PET) it decomposed at voltages below 5000 volts. This resulted in a fatal discontinuity in voltage to the sample. Often, this loss of contact was not easily detectable until the sample was optically evaluated. PET could not be peeled off the sample because of the excellent bonding properties of polyurethanes.

This meant that polyurethane thicknesses could not be measured optically or profilometrically. If PET was forcefully pried off it removed the "best poled" surface of the polyurethanes. In light of these reasons, this approach was of only passing interest.

Another poling strategy was employed by Dr. Wnek at Rensselaer Polytechnical Institute . He used thin glass microscope

cover slips as insulators between the polymer and electrodes. This poling set up is shown on **Figure 87**. Glass plates were 100 mm thick each. The poling voltages were limited to 2000 volts by the glass dielectric breakdown strength. The effective poling field applied to the polyurethane is given by **24**.

If polyurethane thickness (not accurately directly measurable) is on the order of 50 mm and glass's dielectric constant is assumed to be comparable to that of the polyurethane, then the effective poling field on the polymer is ca. 80,000 V/cm or between one and two order of magnitudes lower than that attainable with the conventional parallel plates poling of polymers. This is unfortunate, because extra alignment, bought by the increased mobility of poling smaller species, is negated by the earlier loss of the poling effectiveness as the polymerization progresses. 80 KV/cm is not enough of a force to reorient large oligomers as they condense. It is not clear how soon in the course of the polymerization the poling efficiency is lost, because good SHG response was obtained.

There are other non-trivial concerns about the modified parallel plate poling. In order to get better, more uniform and higher polymer films better monomer mixture and more uniform monomer deposition is necessary. This is not possible in the melt polymerization between the plates. Better polymer films are typically cast from solution than from the melt. The top plate severely limits this. Monomers could be solution cast onto the top glass slide and the solvent allowed to evaporate. However, great care must be taken to remove all of the solvent. Once the sandwich is made, evaporation of the trapped solvents can not take place without catastrophic failure of the sample.

Diisocyanates are very reactive species. The chosen diisocyanates were selected (among other things) for their tailored reactivity. Wide range of diisocyanate reactivities is available (see **Table 27⁸¹**). Some of the fastest ones are all aromatic. Chosen systems use diphenyl methane diisocyanate and para-phenylene diisocyanate, which react very quickly.

TABLE 27
RELATIVE REACTIVITIES FOR THE CONSECUTIVE REACTIONS
OF DIISOCYANATES WITH TWO REPRESENTATIVE ALCOHOLS

DIISOCYANATE	RELATIVE RATE CONSTANTS			
	ethanol		1-butanol	
	k ₁	k ₁ /k ₂	k ₁	k ₁ /k ₂
m-phenylene	-	-	11	8.4
p-Phenylene	-	-	7.7	9.2
4,4'-Diphenylmethane	2.3	3.2	2.4	2.9
2,6-Tolylene	-	-	2.2	6.1
2,4-Tolylene	3.0	25	4.9	11.9
3,3'-Dimethyl-4,4'-diphenylmethane	-	-	0.41	2.4
Durene	-	-	0.05	2.6
1,5-Naphthalene	2.7	3.5	-	-
1,3-Xylylene	0.2	2.5	-	-
1,4-Xylylene	0.18	1.9	-	-
5-t-Butyl-1,3-xylylene	0.19	2.7	-	-
1,6-Hexamethylene	-	-	0.001	2.0
Phenyl isocyanate (std)	1	-	1	-

Here, k_1 is defined as the rate constant for a reaction of an alcohol with the diisocyanate. k_2 is the rate constant for the monofunctional isocyanatourethane, formed in k_1 , and the second alcohol. The reactions with ethanol were carried out in toluene at 30°C. The reaction rates of 1-butanol were measured in 40°C toluene. All rates are relative to the phenyl isocyanate standard. Therefore, paraphenylene diisocyanate reacts 4 orders of magnitude faster than the hexamethylene diisocyanate.

If the isocyanates are exposed to air for a long time, they are converted to an acid according to **22**, which is not only less reactive, but gives off water upon decomposition. This water can not evaporate in a sandwich and destroys the sample. Incidentally, open poling systems, like corona poling, allow liquids to evaporate. This is could be useful in future "alignment polymerizations" that, unlike polyurethane condensations, give off water, gas or some other liquid of polymerization.

Lack of a precise thickness measurement technique for sandwiched samples makes accurate SHG comparison impossible.

As can be seen from data in the present work, structural changes in the molecular design of the polymer often produce a subtle change in SHG response, which can not be evaluated without an exact thickness measurement. Another concern is not knowing the thickness of the sample. The variation in poling ability with the film thickness is seen in **Figure 113** in Chapter 8.

At present, it certainly seems like the corona poling is able to optimize the benefits of the maximized orientation achieved by the "alignment polymerization". Its advantages are numerous and it is much more open to any future system modifications.

CHAPTER 8

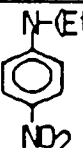
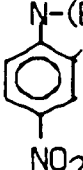
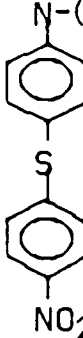
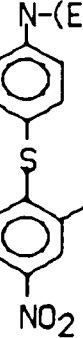
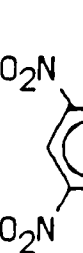
POLYURETHANE SHG MEASUREMENTS AND DISCUSSION

Several key studies were considered when the polyurethanes were designed for SHG. The first was the comparison of sulfide polyurethanes with the nitroaniline polyurethanes. The second issue to be addressed was the addition of a second nitro group in the ortho position to the electron donor and its effect on SHG. Thirdly, the effect of optimizing the number of NLO side groups in the polymeric backbone was investigated. Another issue was the effect of the poling field strength on the SHG from the polyurethanes. SHG signal relaxation was to be studied versus time and temperature. Finally, the thermally relaxed samples were to be reoriented under the original alignment polymerization poling conditions and the SHG from these repoled samples was to be compared to the original SHG's from the alignment polymerization.

It is appropriate to explain the role that the various polyurethane series (PU, DU and HU) played in this work. PU was the main series investigated. Paraphenylene diisocyanate provides a very stiff hydrogen bonded urethane linkage upon reaction with an alcohol. The diphenyl methane (DU series) polymer offers a bit more flexibility by allowing an added degree of freedom as a rotation around the sp^3 methylene link. The DU series was prepared to see the effect of the dilution of the number of SHG active entities per repeat unit in the backbone. The HU series was prepared to study the flexibility vs stiffness of the polyurethane backbone and its effect on SHG. **Table 29** shows the polymer structures and the assigned name abbreviations. It also lists the SHG values obtained for these thin (2-4 μ m) 15 KV corona poled polyurethane films. The corresponding θ - scans are included in **Figures 88 - 102**.

TABLE 29

RELATIONSHIP BETWEEN THE POLYURETHANE STRUCTURE AND ITS
SHG for 15KV corona polyurethanes in 2 - 4 μm thickness range

DIISOCYANATE ALCOHOL		$(\text{CH}_2)_{26}(\text{NCO})_2$	$(\text{OCN}-\text{C}_6\text{H}_4)_2\text{CH}_2$	$\text{OCN}-\text{C}_6\text{H}_4-\text{NCO}$
 I NAME: SHG:	NAME: SHG:	HU1 1.4 mV/ μ	DU1 81 mV/ μ	PU1 178 mV/ μ
 II NAME: SHG:	NAME: SHG:	HU2 8.2 mV/ μ	DU2 36 mV/ μ	PU2 48 mV/ μ
 III NAME: SHG:	NAME: SHG:	HU3 9.0 mV/ μ	DU3 21 mV/ μ	PU3 40 mV/ μ
 IV NAME: SHG:	NAME: SHG:	HU4 21 mV/ μ	DU4 61 mV/ μ	PU4 52 mV/ μ
 V NAME: SHG:	NAME: SHG:	HU5 none	DU5 67 mV/ μ	PU5 14 mV/ μ

At the time of this work, absolute SHG measurements, such as χ_2 or d_{33} , were not available for films thinner than a coherence length. Normally, for the thicker films, coherence length can be obtained from a Maker-fringe experiment.⁶ Since no fringes are seen from thin films, using optical waveguiding techniques¹² were used previously to measure the refractive indexes of the harmonic and the fundamental wave.

As a reference, several commonly used materials were measured for SHG in the present system. These results appear below:

TABLE 30
REFERENCE SHG MATERIALS

MATERIAL	SHG SIGNAL
QUARTZ	15 mV
POWDER KDP	40 mV
POWDER UREA	34 mV
POWDER ANDS	750 mV
POWDER MNA	1500 mV

A) Relaxation Studies

Table 31 shows how some of the polyurethane samples lost their SHG efficiency after prolonged exposures to elevated temperatures. At room temperature all of the polyurethanes in the FU series showed no signal decay over the first 10^6 seconds of their life, see **Figure 106**. Dipole alignment relaxation of poled polymers at temperatures near glass transition is well documented in the literature.^{10,11,12,82,83} In this thermal range, molecular motion of the macromolecules is allowed. This viscous flow is utilized in the conventional poling processes.

FIGURE 106
SHG SIGNAL RELAXATION FOR
PU's AT ROOM TEMPERATURE

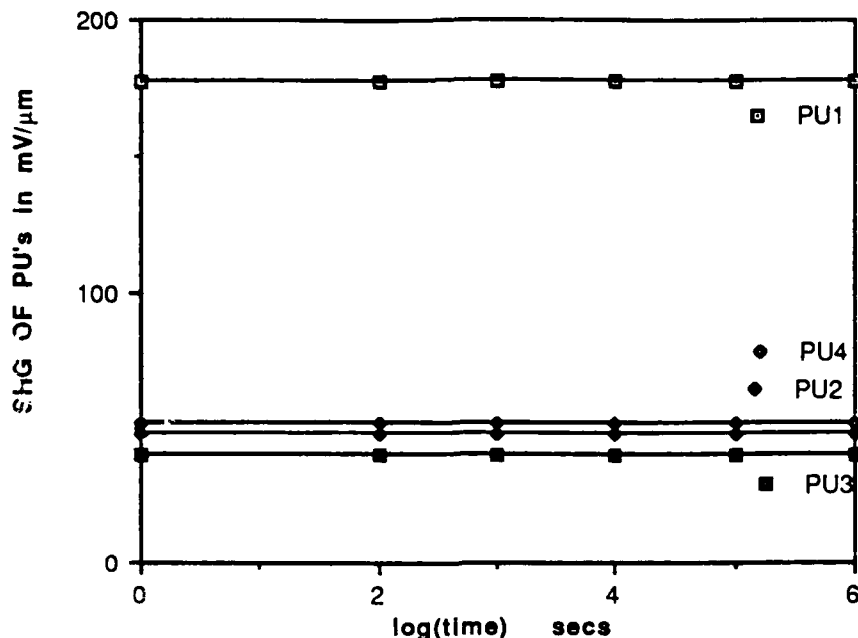


TABLE 31
DIPOLE ALIGNMENT RELAXATION IN THICK POLYURETHANES
POLED AT 15 KV AS A FUNCTION OF SHG (mV/μ)

TRTMNT → POLYMER	NONE	10 ⁶ sec @ RT	10 ⁴ sec @50°C	10 ³ sec @100°C	10 ³ sec @135°C
PU1	178	178	128	12	0.3
PU2	48	48	n/a	n/a	n/a
PU3	40	40	n/a	n/a	n/a
PU4	52	52	43	36	1.9

At room temperature, synthesized polymers were well below their T_g 's and dipoles were "frozen in". In practice, however, some relaxation does indeed take place. This is the most obvious in the SHG systems where the active entities are small polar guest molecules, such as MNA, dissolved in a transparent polymer matrix, such as PMMA. Hampsch and coworkers⁸⁴ observed a 80% signal drop in just 10 hours. Their system was 4% DANS (4-dimethylamino-4'-nitro stilbene) dissolved in PMMA. After

0.5×10^6 seconds at room temperature the harmonic signal decayed virtually to zero.

Marks and coworkers, in an attempt to improve the SHG relaxation parameters, dissolved DANS in an optical grade epoxy resin. Here, the SHG signal decreased down to 40% of the original in the 3.6×10^6 second time span.⁸⁵ Amorphous polymers with covalently bonded NLO side groups performed a bit better, but still showed appreciable dipole relaxation at room temperature.^{85,86}

This is why the temporal performance of the studied polyurethanes is so encouraging. At 50°C after 10,000 seconds samples lost 17 - 28% of their original SHG efficiency, indicating that some dipole relaxation was slowly taking place. This is in sharp contrast to Meredith's work that examined the SHG relaxation at elevated temperatures.⁸⁷ Meredith's system consisted of DANS trapped in a "polymeric cage" of a thermotropic nematic liquid crystalline host. Its SHG signal relaxed to 1.5% of the original at 50°C.

After 1,000 seconds at 100°C, almost 3/4 of the signal loss was recorded, showing that the original anisotropy in the sample was mostly randomized due to diffusion. Finally, the exposure of the samples to 135°C completely averaged out all preferred orientation in the linear polyurethanes. Conversely, the crosslinked samples, such as DU5C15, did not lose any of the induced orientation even after a 1000 second heating at 120°C; please refer to **Figure 107**. **Figures 108 - 112** shows how some of the polyurethanes relaxed their dipole alignment after variable time exposures to 100°C and 50°C.

FIGURE 107
DU5 SHG SIGNAL RELAXATION AT 120°C

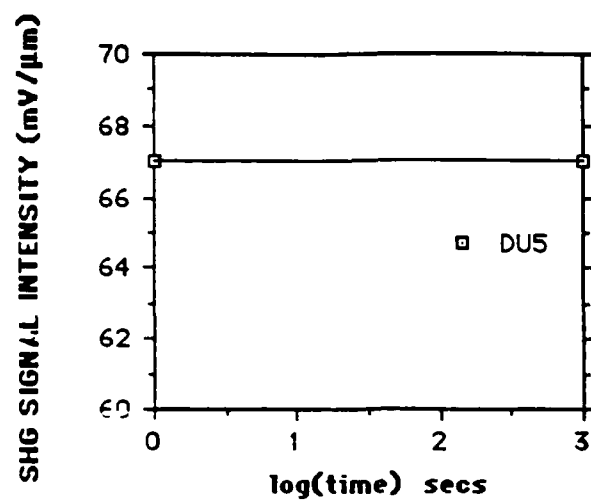


FIGURE 108

PU RELAXATION @ 50°C

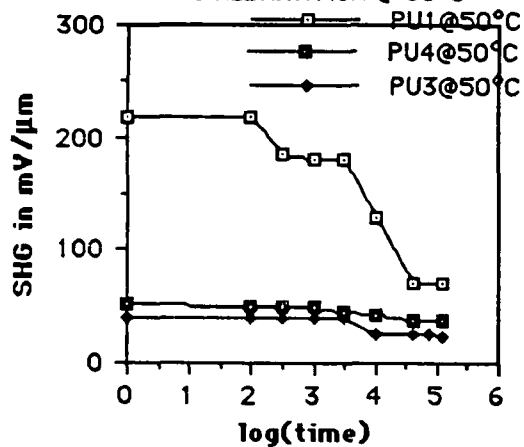


FIGURE 109

PU RELAXATION AT 100°C

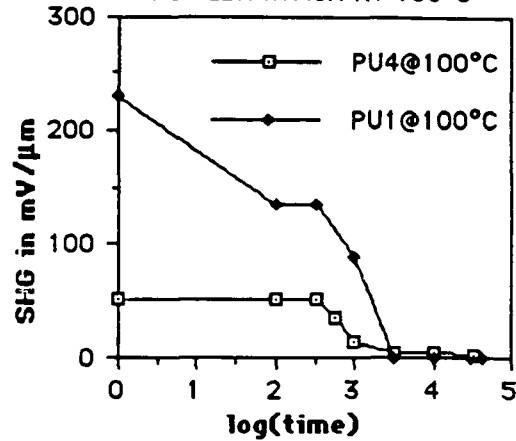


FIGURE 110

PU4 RELAXATION

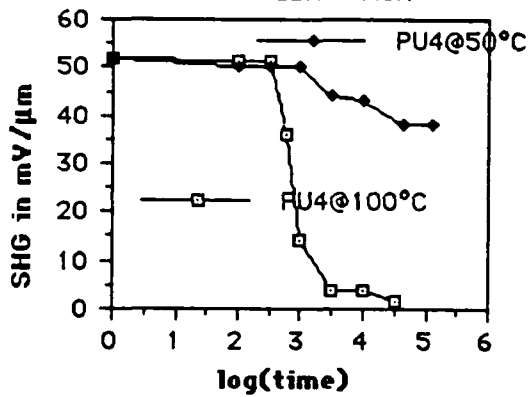


FIGURE 111

PU1 RELAXATION

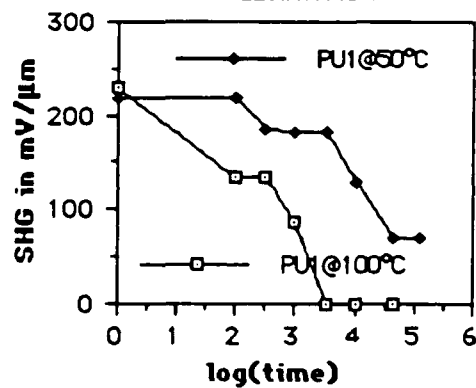
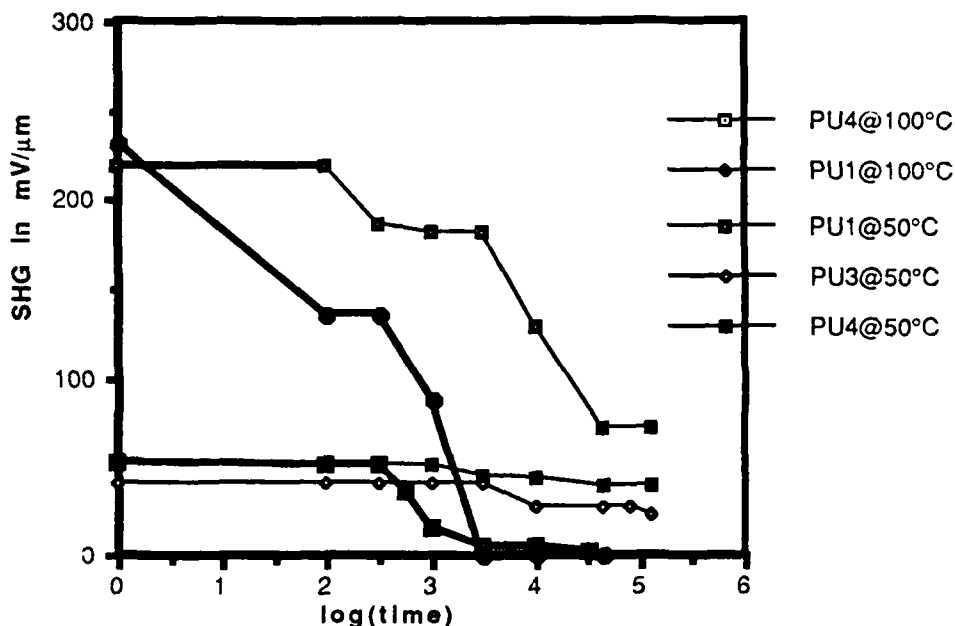


FIGURE 112

TIME AND TEMPERATURE DEPENDENT SHG
RELAXATION OF THE PU SERIES POLYMERS



These data, combined with the DSC results, indicate glass transition in the 100 - 135 °C range for the para-phenylene polyurethanes.

B) POLING FIELD EFFECT

Poling electric field strength has a great effect upon the degree of alignment of the polymers. In traditional polymer poling to obtain piezoelectric films or for SHG, usually a saturation level was reached where increasing the voltage did not result in improved orientation as indicated by the leveling of the materials' non-linear response.¹² In these processes the polymer films, spun on substrates, were heated above their T_g's under the applied voltage.

In present work, polymerization proceeded under the poling voltage. This means that a monomeric mixture, not a polymer, was cast on the substrate. When heat and corona were applied two competing processes could have taken place. The first is the desired dipole alignment during the course of the polymerization

due to the field. The second process electrostatically charges small monomeric particles and disperses them under the needle. This results in a blank spot directly under the needle, where the SHG signal should be optimal upon the completion of poling.

Clearly, good alignment during polymerization must be optimized by minimizing this effect while maximizing the dipole alignment. SHG saturation voltage conditions were studied in detail for all PU series polyurethanes.

These studies were complicated by several factors. Firstly, the maximum corona voltage is limited ultimately by the dielectric breakdown of air around the tungsten needle. Dielectric strength is influenced by humidity and temperature. For instance at the distances of 2-3 mm between the corona tip and the sample, voltages of up to 20KV could be produced at room temperature without arcing. In the 100°C-110°C range this voltage drops to 15KV-17KV. At 300°C, only 7KV levels could be reached.

Air breakdown results in an ionized glowing purplish blue cloud that arcs to the ground. With voltages above air breakdown strength the size of the "clouds" grows and the arcs are able to reach farther and farther.

Another important factor needs greater understanding at present. There appears to be a dependence of the poling efficiency on the sample thickness. With the thicker samples the degree of alignment seems to decrease. **Figure 113** shows the drop of the poling efficiency with the increasing sample thickness as monitored by the SHG response of PU1C15. The dependence appears to be linear for PV1C15 polyurethanes.

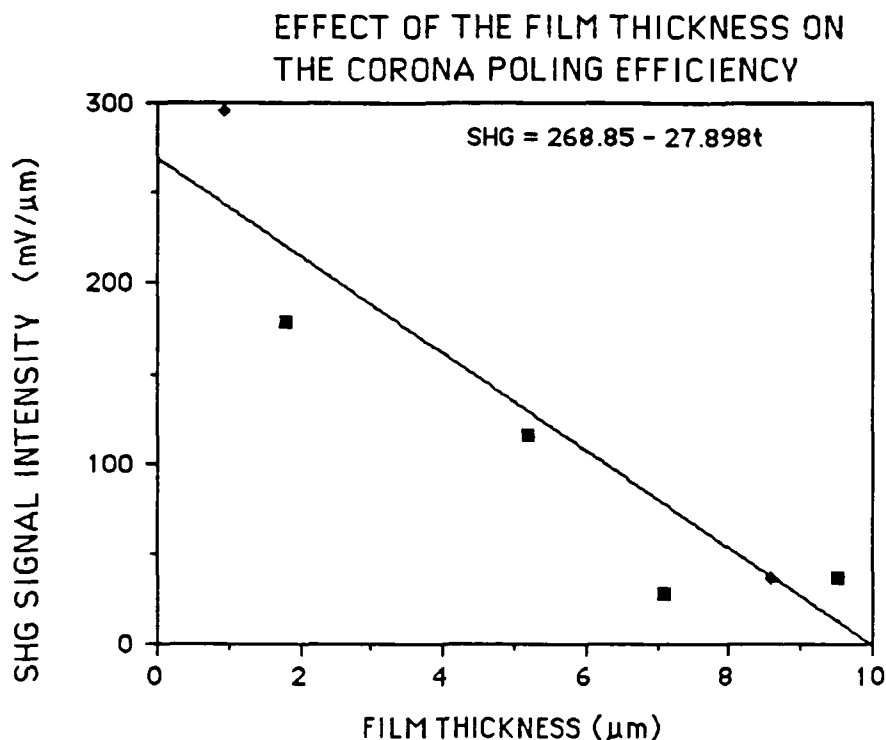


FIGURE 113 : EFFECT OF THE FILM THICKNESS
ON SHG DENSITY OF PU1C15

Since the entire reacting surface is radially charged around the corona tip, there is a strong radial SHG signal dependence. It does not appear that corona poling of these polyurethanes is solely a surface alignment technique. If that were the case, the SHG values would be approximately the same for samples of all thicknesses.

For these reasons, all samples studied were in the same thickness range. The results appear in **Table 32**. There is a remarkable drop from 15 KV to 13 KV for all PU polymers and at 10 KV the polyurethanes studied showed virtually no harmonic signal. Because of static charging and arcing at 100°C, it was not possible to raise the poling voltage above 15,000V. Therefore, the commonly observed saturation of the non-linear effect is not seen here.

TABLE 32
EFFECT OF THE POLING FIELD STRENGTH ON SHG
OF THIN PARAPHENYLENE POLYURETHANES (PU'S)

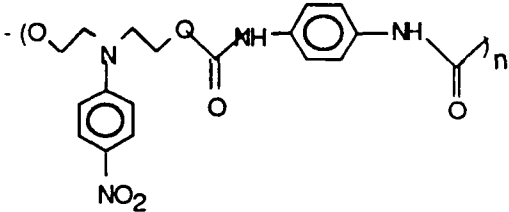
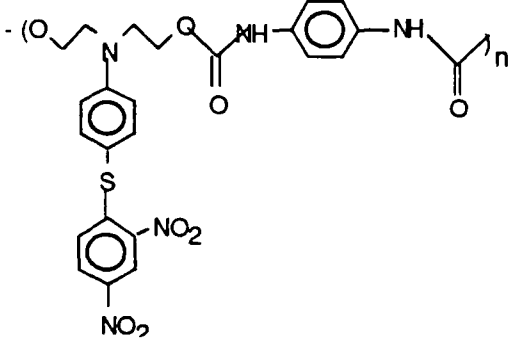
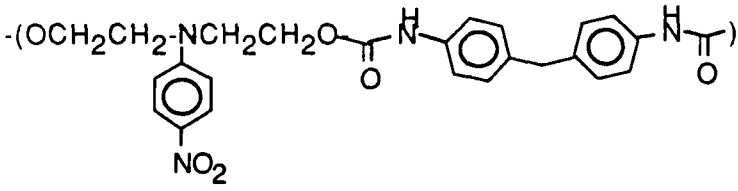
CORONA POLING FIELD	15,000 VOLTS	13,000 VOLTS	10,000 VOLTS
PU1	178 mV/ μ	78 mV/ μ	n/a
PU2	48 mV/ μ	15 mV/ μ	n/a
PU3	40 mV/ μ	6.5 mV/ μ	n/a
PU4	52 mV/ μ	12 mV/ μ	n/a
PU5	14 mV/ μ	5 mV/ μ	0.41 mV/ μ

Samples of PU1C15 and PU4C15 were thermally relaxed at 135°C for 15 minutes. There, the anisotropies were thermally removed as indicated by the disappearance of the harmonic response at 532 nm. The samples were re-poled at 135°C and 15KV for 15 minutes. The heat was shut off and the samples were cooled to room temperature under the E-field. After 45 minutes the E-field was removed. The samples were rotated under a pulsed YAG laser as described previously. The results of these scans appear in **Figures 103, 104 and 120**.

The signal from these samples was drastically (40-80%) lower than that from the alignment polymerization. Results are listed in **Table 33**. These results indicate that the alignment polymerization provides particularly superior dipole alignment to the conventional poling with the stiffer polymeric backbones. For instance, DU1C15 shows ca. 40% SHG improvement with alignment polymerization, while more rigid alignment polymerized PU1C15 shows over 5 times stronger SHG than its conventionally poled counterpart.

In light of the need for stiff, high T_g polymers for thermally and temporally stable SHG, these results appear especially attractive.

TABLE 33
COMPARISON BETWEEN THE ALIGNMENT POLYMERIZATION
AND THE CONVENTIONAL POLING SHG's, 15 KV CORONAS

POLYURETHANE STRUCTURE	ALIGNMENT POLYMERIZATION SHG	CONV. POLING SHG
	178 mV/ μ	35 mV/ μ
	52 mV/ μ	25 mV/ μ
	67 mV/ μ	39mV/ μ

It is interesting to note here that the SHG signal from the PU1C15 repoled was much stronger than the one from PE1C15 (**FIGURE 104**) prepared under similar conditions (35 vs 9.6 mV/ μ , **Table 34**).

TABLE 34

POLYESTERS VS POLYURETHANES FOR SHG

POLYMER STRUCTURE	SHG
<p>PE1C15-"REPOLE"</p>	9.6 mV/ μ
<p>PU1C15-"REPOLE"</p>	35 mV/ μ

This could be attributed to two phenomena. Firstly, in the urethanes better dipole alignment is possible because of the hydrogen bonding in the urethane linkage. This bonding can be responsible for better "locking in" the urethane C=O dipole parallel to the nitroaniline dipole. In these polyurethanes there are two C=O linkages per every nitroaniline. So, ultimately, there are two carbonyls contributing for SHG along with every nitroaniline.

Secondly, the two added sp^3 nitrogens in the urethane renders the carbonyl dipole more flexible with respect to the backbone above T_g . Also these spacers in a fairly stiff aromatic backbone could help the mobility of the nitroaniline by rendering the whole chain more flexible above T_g . Finally, the hard segment/soft segment model of PUs can be enlisted to summarize the role of the hydrogen bonding "locking in" the dipole orientation below T_g .

C) Effect of the Second Nitro

Table 35 summarizes the effect of the addition of the second nitro group in the ortho position to the electron donor. In the DU15, PU13, and PU15 series a general drop in SHG is observed upon addition of the second nitro group. The most dramatic drop is seen in PU1C13 \rightarrow PU2C13 (78 \rightarrow 15 mV/ μ , \downarrow 81%). PU1C15 \rightarrow PU2C15 shows a 73% drop (178 \rightarrow 48 mV/ μ). DU1C15 \rightarrow DU2C15 decreases the harmonic signal 56% (81 \rightarrow 36 mV/ μ).

TABLE 35
COMPARISON OF THE SHG'S (mV/ μ) FROM THE
MONO AND DINITRO POLYURETHANES

SUBSTITUENT	ANILINES		SULFIDES	
DIOL# \rightarrow POLYMERS	I	II	III	IV
HU15	1.4	8.2	9.0	21
DU15	81	36	21	61
PU13	78	15	6.5	12
PU15	178	48	40	52

These results were counterintuitive; one would expect a universal increase in SHG upon addition of a second nitro group due to an increased dipole moment in the dinitroanilines. This certainly was the intention behind the molecular design. However, recently published β measurements of dinitroaniline⁹⁰ show that the polarizability of this molecule (21×10^{-30} esu) is roughly half of that of the p-nitroaniline.

Upon a closer examination of these polyurethanes, a relationship between the stiffness of the polymer backbone and the SHG drop due to the second nitro group can be established. As mentioned earlier, paraphenylene polyurethane has the stiffest backbone of the polyurethanes in the present study. The addition of the second nitro group to create the 2,4 dinitro aniline not only increases the dipole moment of the molecule; it also rotates the direction of the dipole moment. This new net dipole direction is at an odd angle to the chain. Stiff chains can not sterically allow a perfect alignment of these dipoles.

Instead, the poling process must align the para-nitroaniline dipole moment with the electric field. When the excitation takes place under the laser beam, polarization probably chooses the shortest path because this is such a fast process. The shortest polarization in this entity is between the amine and the ortho nitro group, see **Figure 114** below.

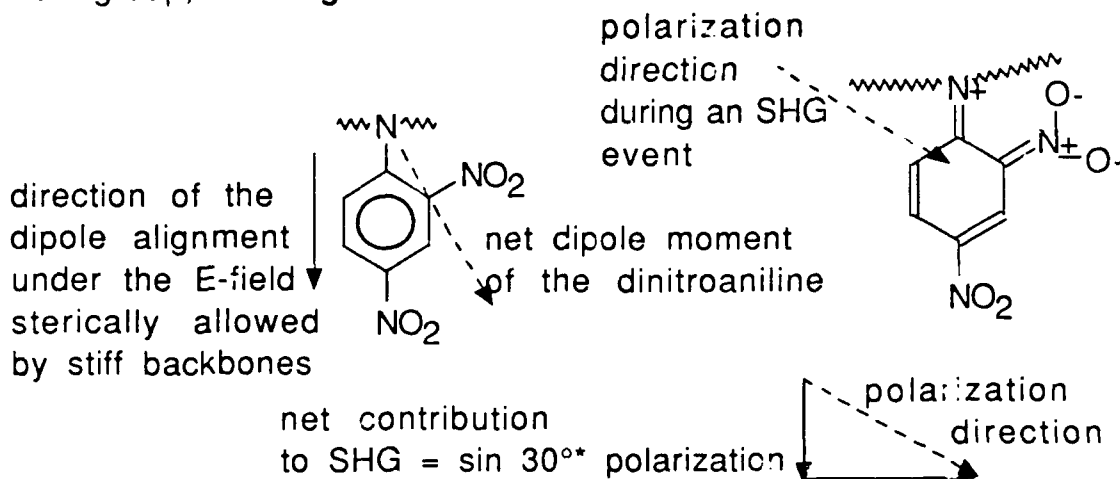


FIGURE 114: ALIGNMENT AND POLARIZATION OF THE DINITROANILINES ATTACHED TO STIFF POLYURETHANE BACKBONES

Therefore, only a fraction of the dipole moment is seen for the SHG in the excited state. For the SHG, the difference between the excited and the ground dipole moment is important, as is the transition dipole moment:

$$\beta = |\mu_{ge}|^2(\mu_e - \mu_g) / \text{dispersion term} \quad \text{from 13}$$

Since the excited state dipole moment contributing to the SHG is reduced, and the ground state dipole moment is increased by the addition of the second nitro group the β is drastically lowered as seen from 13.

In the more flexible urethanes, better dipole alignment can be achieved during the poling as seen in **Figure 115** below:

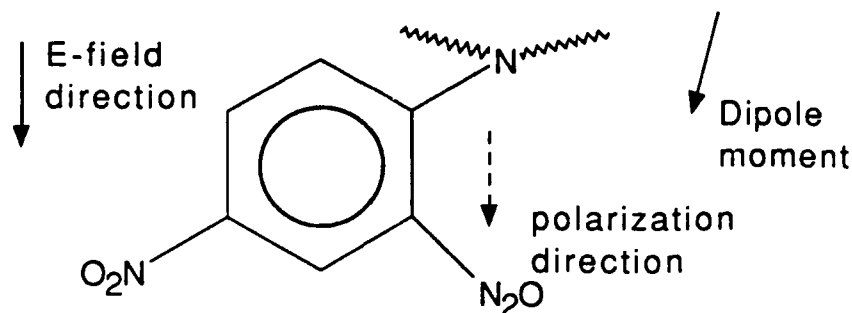


FIGURE 115: ALIGNMENT AND POLARIZATION OF THE DINITROANILINES ATTACHED TO FLEXIBLE POLYURETHANE BACKBONES

Even if the transition state and the excited state dipole moments are solely directed by the amine \rightarrow ortho nitro polarization, the SHG contribution from them is larger than that from the similar polarization in the stiff chains.

As the stiffness is relaxed and more flexibility is allowed the signal loss is lessened. This is seen in going from the paraphenylene to the diphenyl methane polyurethanes (PU \rightarrow DIJ). PU1C13 \rightarrow PU2C13 shows the biggest drop because 13,000 volts is not as sufficient to "fight" the polymer stiffness as 15,000 volts. The electric field does "fight" the stiffness; in poling the polymer in a sterically impossible direction, the stiffness of the chain works against you, not for you.

Hexamethylene series (HU's) have a very flexible all- sp^3 backbone. These chains can adapt to the odd angles of the dinitroaniline dipoles. As a result, a large increase is seen in SHG of HU1C15 \rightarrow HU2C15 (1.4 \rightarrow 8.2 mV/ μ).

In the sulfides, there is a net increase in SHG when a second nitro group is added. Unlike the nitroaniline polyurethanes, these side groups have an added degree of freedom around the sp^3 sulfur. Therefore, they have an ability to rotate to perfectly adjust to the new dipole moment direction. The amount of the increase of SHG is in general agreement with the decrease of the chain stiffness.

D) Role of Sulfur

In the mononitro compounds, the insertion of a thiophenyl group between the nitro group and the aniline ring drastically reduces the SHG response. (See Table 36) This effect is evident in the paraphenylene polyurethanes poled at 15,000 V and 13,000 V and also in the diphenyl methane urethanes. The HU series synthesized with the more flexible hexamethylene diisocyanates showed a dramatic increase in the second harmonic response.

TABLE 36
COMPARISON OF THE ANILINE AND SULFIDE
POLYURETHANE SUBSTITUENTS SHG (in mV/ μ)

SUBSTITUENT	MONONITRO		DINITRO	
	I	III	II	IV
DIOL#→ POLYMER				
PU15	178	40	48	52
PU13	78	6.5	15	12
DU15	81	21	36	61
HU15	1.4	9.0	8.2	21

The largest SHG drop was seen in PU1C13 → PU3C13 (78 → 6.5 mV/ μ down 92%). The second largest drop was observed in PU1C15 → PU3C15 (178→40mV/ μ down 78%) . In the DU series, DU1C15 → DU3C15 the signal drops from 81mV/ μ → 21mV/ μ down 74%. Finally, in HU1C15 → HU3C15 an increase is seen; 1.4 → 9.0mV/ μ up 543%. The trend here is, once again, that with the increasing stiffness of the backbone, the SHG drop increases in anilines vs diphenyl sulfides.

This happens because the nitroaniline entity in the U1 series has a dipole moment which is more orthogonal to the backbone than that of the sulfides. In stiffer chains ideal alignment of the sulfide dipole moment parallel with that of the carbonyls becomes impossible. Here, again, the stiffness of the backbone works "against you". Nitroanilines are easier to align parallel to the carbonyls, so that the dipole moments add up constructively. In the very flexible hexamethylene urethanes parallel alignment becomes possible and as a result an SHG increase is seen. Finally, β of p-amino-p'-nitro diphenyl sulfide group, 27×10^{-30} esu, is

about 25% lower than that of the nitroaniline ($35-42 \times 10^{-30}$ esu). This also lowers the SHG of the sulfide polyurethanes compared to that of the similar nitroaniline polymers.

HU series polyurethanes have a completely unsaturated sp^3 backbone that results in HU1, HU2, and HU5 polyurethanes being near their glass transition at room temperature. This is indicated by viscoelastic behavior that can be visually observed in the HU's. Another problem with the HU series is the lower reactivity of hexamethylene diisocyanate vs that of its aromatic counterpart. Hexamethylene diisocyanate is a liquid at room temperature with higher volatility than the solid paraphenylene and diphenyl methane diisocyanates. Combined, these two reasons probably result in a lower molecular weight polyurethanes due to an upset stoichiometry.

The diphenyl sulfide bearing HU urethanes (HU3 and HU4) have a stiffer SHG side group than HU1, HU2, and HU5. In light of the flexibility of the sp^3 backbone, this stiffness of the diphenyl sulfides begins to dominate the SH behavior of the polyurethanes.

In the dinitro polyurethanes similar chain stiffness effects are observed. In the PU series, PU2C13 ($15 \text{ mV}/\mu$) and PU2C15 ($48 \text{ mV}/\mu$) show SHG signal comparable to that of PU4C13 ($12 \text{ mV}/\mu$) and PU4C15 ($52 \text{ mV}/\mu$), their dinitro counterparts, respectively. DU4C15 shows an increased signal over that of DU2C15 ($61 \text{ mV}/\mu \leftarrow 36 \text{ mV}/\mu$, up 69%). HU4C15 ($21 \text{ mV}/\mu$) shows a marked improvement over HU2C15 ($8.2 \text{ mV}/\mu$, up 149%).

In the stiffest paraphenylene urethane chains, dinitroanilines are comparable to the dinitro sulfides in their harmonic response because both offer active dipole moments at an odd angle to the backbone. It is also sterically impossible to align the active dipoles parallel to that of the carbonyls. The added degree of freedom, afforded by the rotation around the sulfur in PU3 does very little to improve the alignment of the dipole and polarization direction parallel to the electric field. In PU4, however, better alignment of the polarization direction with the E-field is possible because of the polarization to the ortho nitro as seen in **Figures 114, 115 and 116**. Unfortunately, as seen in **Table 25** in Chapter 7, PU4 absorption is much greater than that of the other polyurethanes (I-III) in the green region. Therefore,

there is virtually no SHG difference between the two types of urethanes.

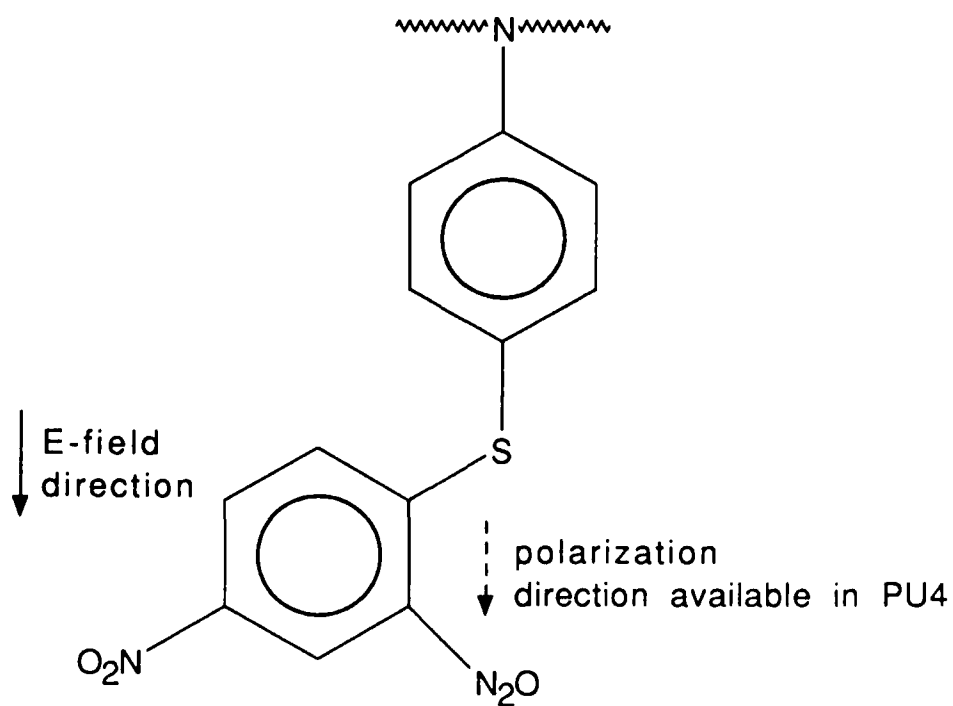


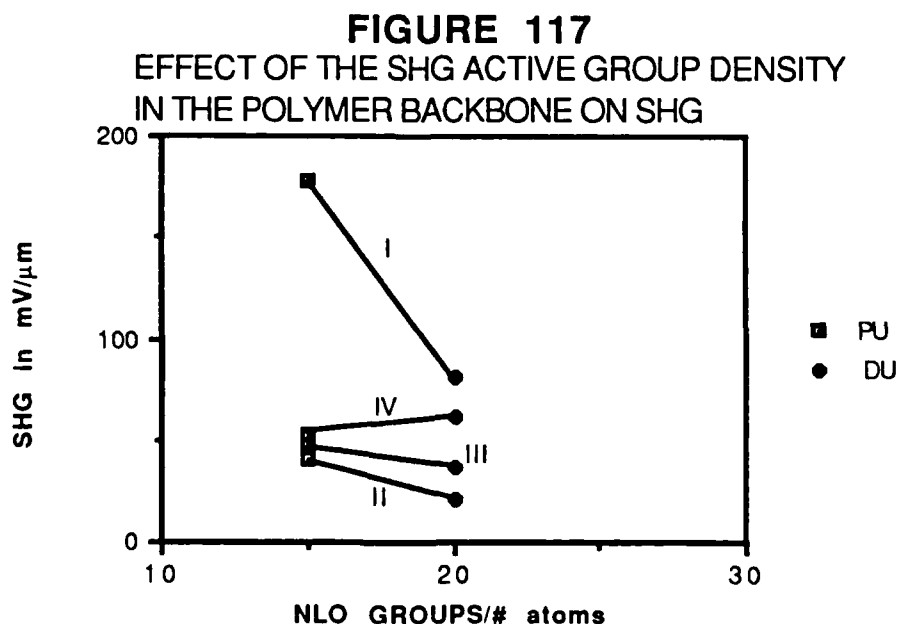
FIGURE 116: PU4 POLARIZATION UNAVAILABLE FOR PU3

It could be argued that a slight drop in PU13's and a slight increase in PU15's could be related to the increasing ability to align the active groups with the higher electric field. Rather than asserting this fact, it should be pointed out that the effect is so slight that it is within the error range of the experiment.

As in the mononitro compounds, the added flexibility of the DU backbones sterically allows a better alignment of the SHG groups in the electric field. This results in an increased sulfide harmonic response vs that of the nitroanilines. Here, once again, the flexibility issue dominates the harmonic response. Sulfides are better able to align the dinitrobenzene dipole moments due to an added degree of freedom provided by the rotation ability around the sp^3 sulfide. This does not do much in the PU4C15 and PU4C13 because the sulfur rotation alone can not bring the dipole alignment. However, in the diphenyl methane urethanes it is coupled with the rotational ability of the methylene link and dipoles are sterically alignable.

In the HU2C15 \rightarrow HU4C15 a 149% increase can also be attributed to the stiffness of the diphenyl sulfide group in the very flexible backbone. This stiffness helps to preserve the dipole alignment and slower the relaxation process in the HU sulfides.

E) Density Study



CHAPTER 9

FUTURE WORK

Optimization of the second harmonic response from the polymers can be approached from several directions. The presently described alignment polymerization systems can be improved by a more uniform film deposition and by reactivity tailored poling. Synthetic improvements fall into two categories. Firstly, the existing synthetic conditions can be modified to yield higher molecular weight polymers, especially in case of cyclopolymerizations, polyesterifications and poly(ANDS) condensations. Secondly, the active "ingredients" can be modified to produce altered polymers with possibly increased molecular weights or increased harmonic response.

Thirdly, a more uniform polymeric dipole alignment is possible with several variations of the corona poling. Only a relatively small radial polymeric region below the corona tip is optimally aligned. If the corona discharge takes place from a sharp edge of a wire instead of a point source, a narrow polymeric strip is aligned. Furthermore, this approach can be extended to a grid of coronas. Here, an array of strategically positioned point sources of voltage create overlapping radial polymeric regions that span the entire film surface. If the corona poling apparatus is enclosed in a sealed container filled with gas, which has higher dielectric strength than air, the breakdown will occur at higher voltages. This might result in increased dipole alignment.

During the alignment polymerization of urethanes, the poling voltage can be ramped with the temperature. As mentioned in Chapter 7, the dielectric breakdown of air takes place at lower voltages as the temperature is increased. Consequently, if the voltage is increased as the heat is shut off in the polyurethane poling, slight SHG improvement could be seen.

Similarly, if the polymerization of urethanes is carried out with the tailored reactivity diisocyanates, then specific voltage vs temperature and time profiles can be developed for each polymeric system. The importance of optimizing the diisocyanate reactivity was demonstrated in Chapter 7. If the diisocyanate reacts too slow, then the side reactions with water and other impurities become increasingly important.

If it reacts too quickly, then the polymerization will take place too early, either in the monomeric solution prior to the deposition or as the solvent evaporates. In both cases,

polymerizations occur prior to the application of the aligning voltage. Certainly, more diisocyanates need to be examined to better balance the reactivity tradeoffs.

More solvent systems should be evaluated for better monomer deposition. Presently, uniform films are very difficult to obtain from the alignment polymerization. This is because four diols (I-IV) and the tetrol V display a surprisingly wide array of solubilities. In particular, IV was especially difficult to dissolve in THF. A high volatility solvent capable of high diol and diisocyanate solubility will deposit a more uniform monomeric coating, yielding a smoother polymeric film.

Another polyurethane SHG improvement can be brought about by using a diisocyanate with an SHG active group. For instance, N,N di(2-isocyanatoethyl) 4-nitroaniline can be obtained:

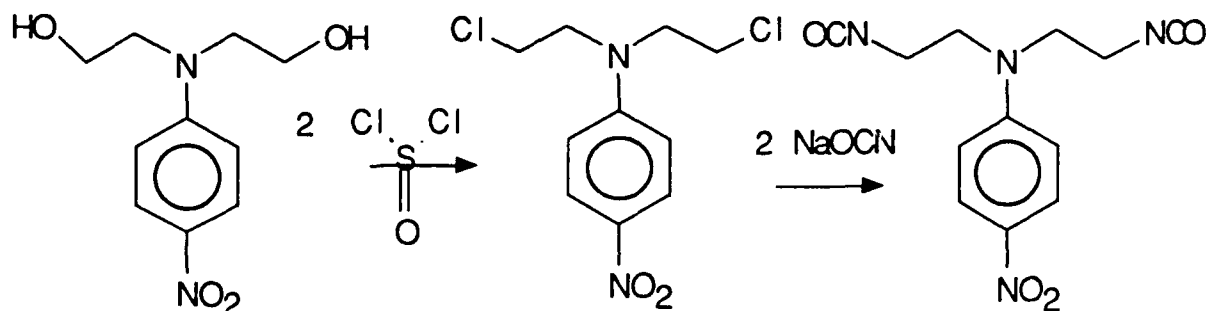


FIGURE 118: SYNTHETIC ROUTE TO A NLO DIISOCYANATE

The first part of this synthesis has been successfully carried out, as described below. The second stage is readily obtained from the literature⁸⁸ is a standard route to isocyanates. This diisocyanate doubles the SHG active group density in the polyurethanes and hopefully further improving the polymer harmonic response.

Diamines have been prepared from the I diol according to:

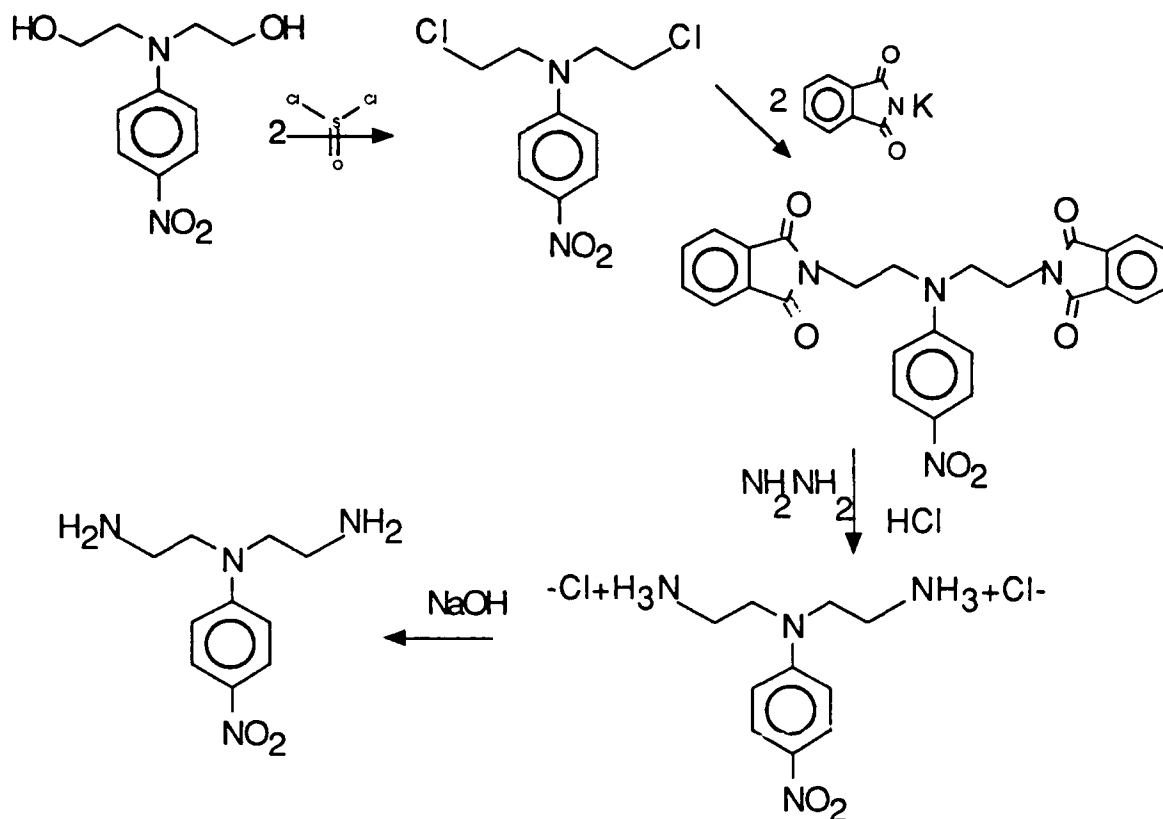


FIGURE 119: SYNTHETIC ROUTE TO A NLO DIAMINE

This synthetic route was proposed and carried out by Dr Wei.⁸⁹ He had difficulty isolating the free amine in the last reaction step. When the free amine is obtained, it can be used to prepare nylons, polyimides and epoxies.

The new polymeric systems not only expand the range of polymer classes for SHG, they provide an interesting intermediate between the polyesters and polyurethanes in the polyamides. With the NLO polyimides, a new class of thermally stable SHG polymers is insured. Finally, epoxies will provide another class of the crosslinked polymers with permanently aligned dipoles. As an added benefit, these new classes will provide more data on the effect of increasing the SHG group density in the polymer backbone.

Also, if the conditions for cyclopolymerization of VI and VII are determined, yet another class of linear SHG polymers with a high density of NLO groups will be obtained. These cyclopolymerization conditions must exist because a crosslinked product was readily obtained at higher temperatures.

Finally, poly(ANDS) is only one synthetic step away from fruition. Poly(DNDS) synthesis proves the feasibility of poly(ANDS) polymerization. Both poly(ANDS) and poly(DNDS) should be excellent SHG polymers, if either their crystallinity is disrupted or utilized for the phase matching. Certainly, they warrant more work because of their superb SHG potential. Similarly, more effort in polymerization of poly(ANDS vinylene) will bring equally high dividends.

In conclusion, it is interesting to point out that molecular engineering of polymers for SHG, and polyurethanes in particular, brought very satisfying results. The corona alignment polymerization yielded excellent results. It yielded significantly higher SHG values than the conventional corona poling in all of the polymeric systems tested.

At the same time it provides a unique tool for dipole alignment of the rigid backbone polymers. Such aromatic polymeric systems offer temporal and thermal SHG longevity that was lacking for this class of materials before. High T_g polymers are almost impossible to align via conventional corona or parallel plates poling, because of the high temperatures required. Corona alignment polymerization offers the only way to efficiently pole these polymers. It definitely has high potential for other NLO polymerization systems. It can also be extended to ceramic systems, such as sol-gels.

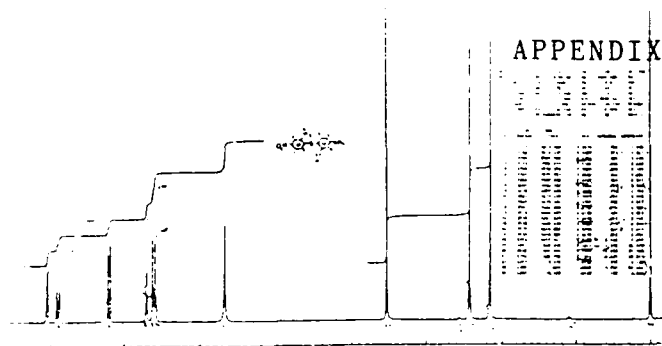


FIGURE 10: NMR of B

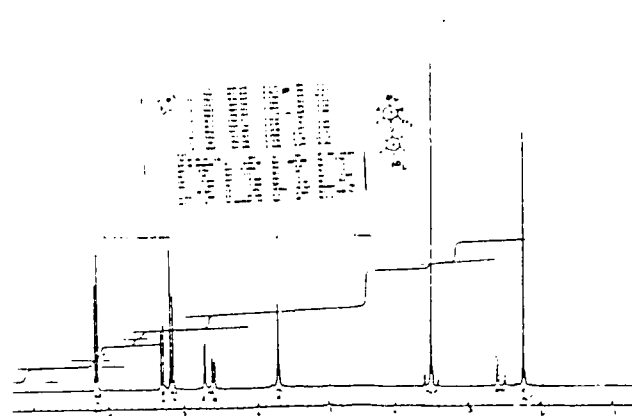


FIGURE 11: NMR of C

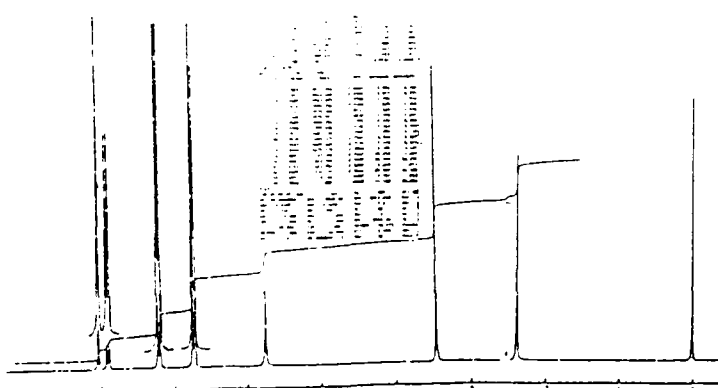


FIGURE 12 : NMR of D

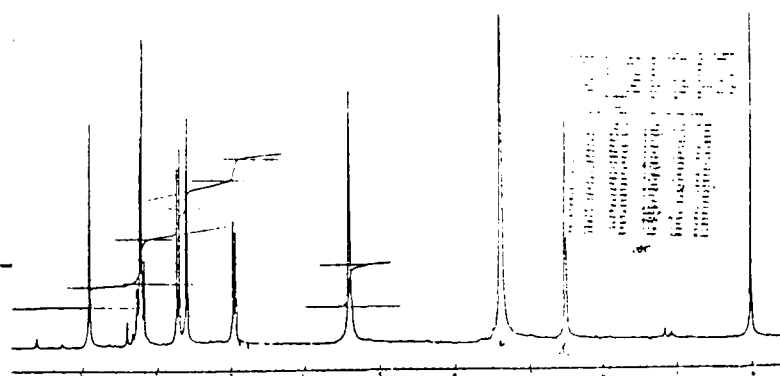


FIGURE 13: NMR of E

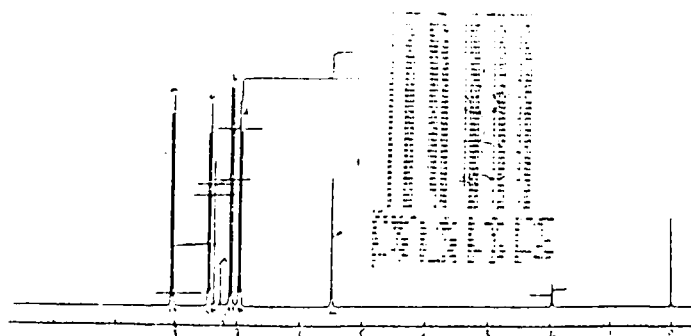


FIGURE 14 : NMR of F

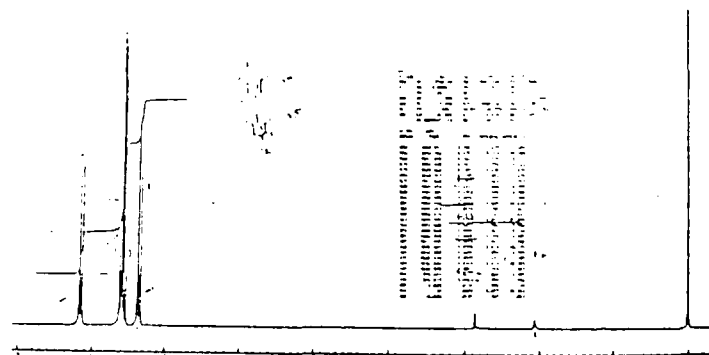


FIGURE 15: NMR of G



FIGURE 18: NMR of I

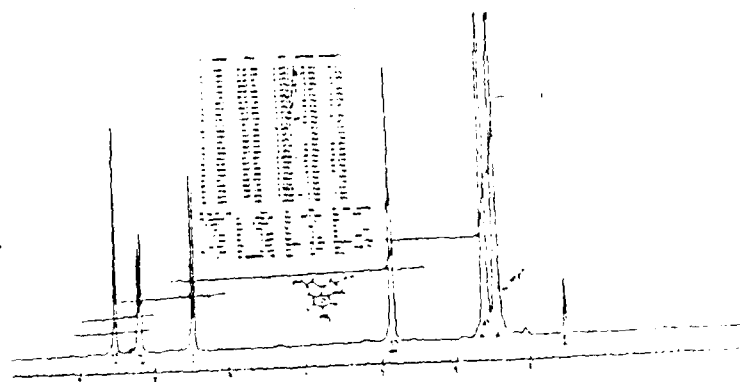


FIGURE 19: NMR of II

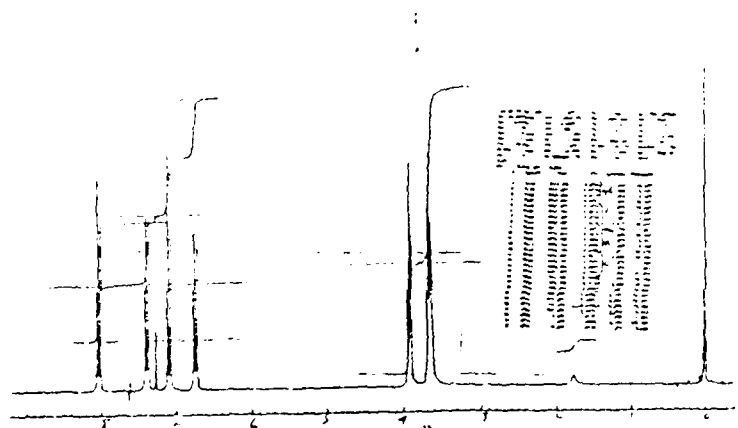


FIGURE 20: NMR of III

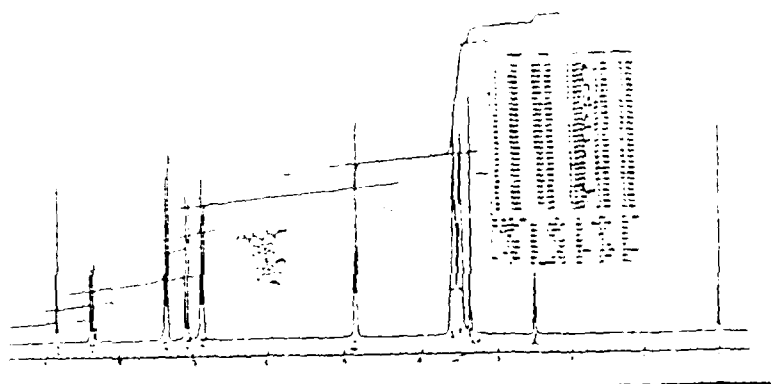


FIGURE 21: NMR of IV

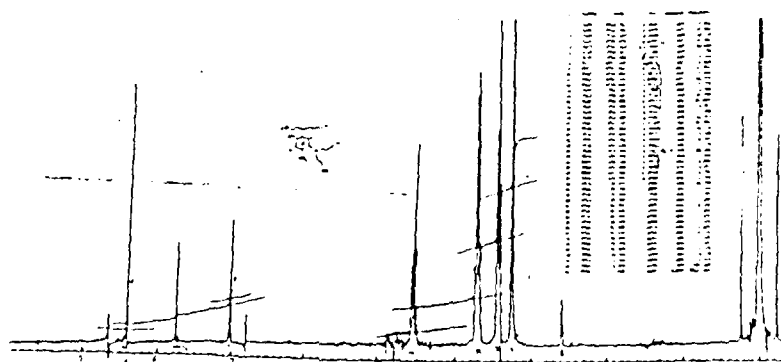


FIGURE 22: NMR of V

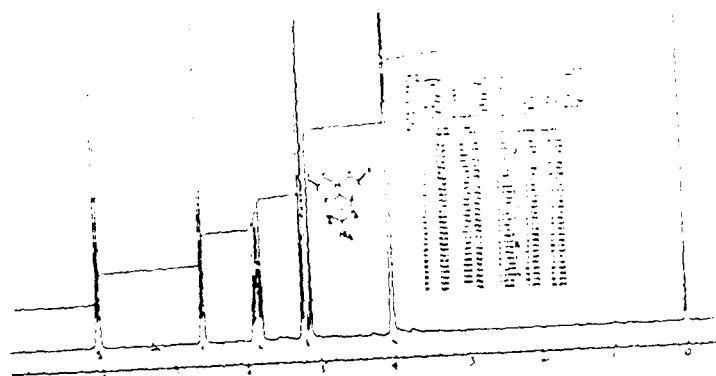


FIGURE 24: NMR of VI

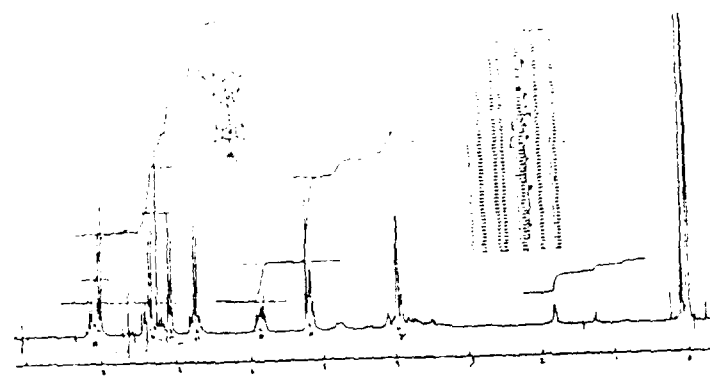


FIGURE 25: NMR of VII

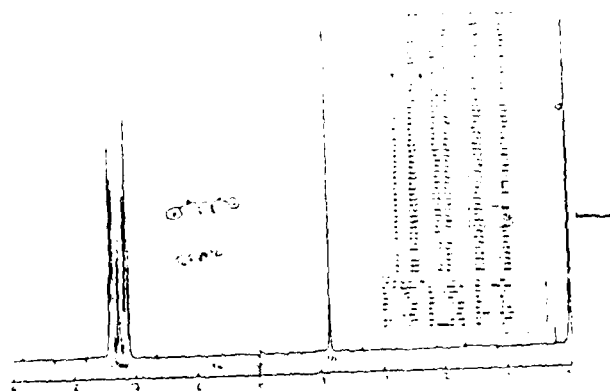


FIGURE 27: NMR of Diphenyl Malonate

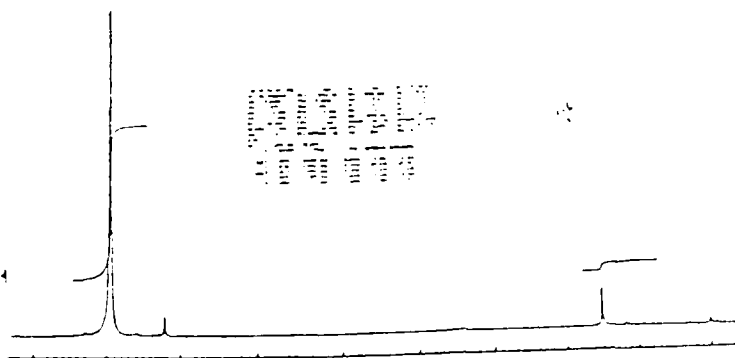


FIGURE 29: NMR of 2,6-dinitro-1,4-dichlorobenzene

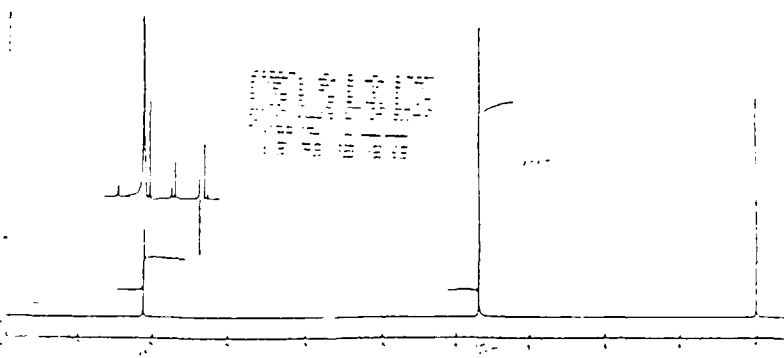


FIGURE 30: NMR of 2,5-dinitro-1,4-dichlorobenzene*2dioxane

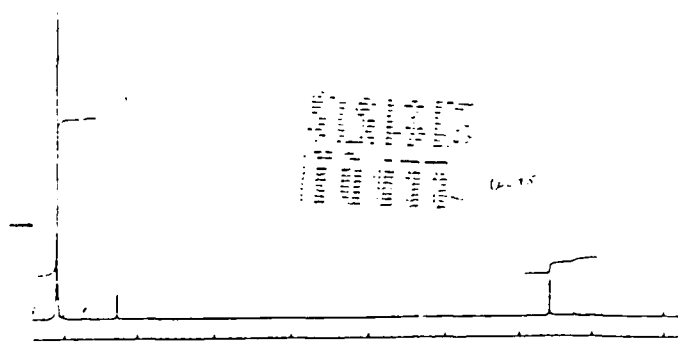


FIGURE 31: NMR of clean 2,5-dinitro-1,4-dichlorobenzene

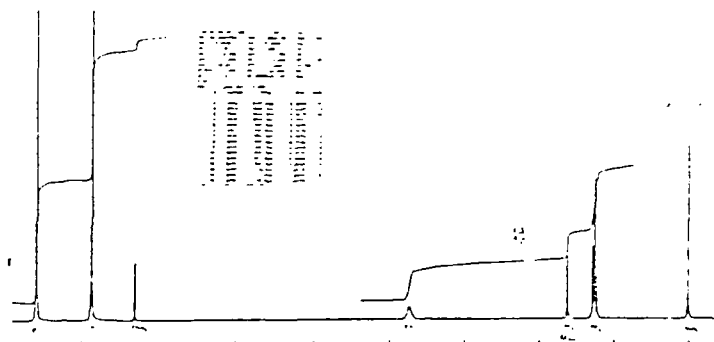


FIGURE 32: NMR of 1,3-dichloro-4,6-dinitrobenzene

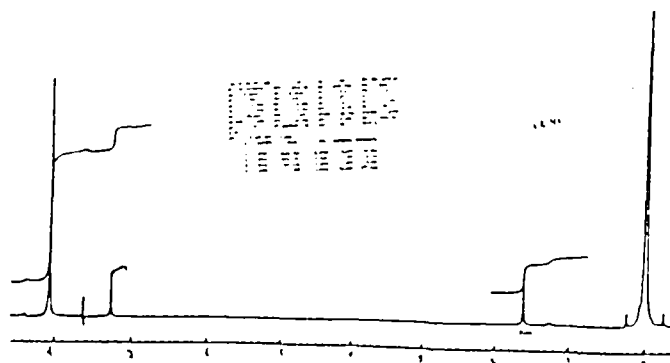


FIGURE 33: NMR of 1,2-dichloro-4,5-dinitrobenzene

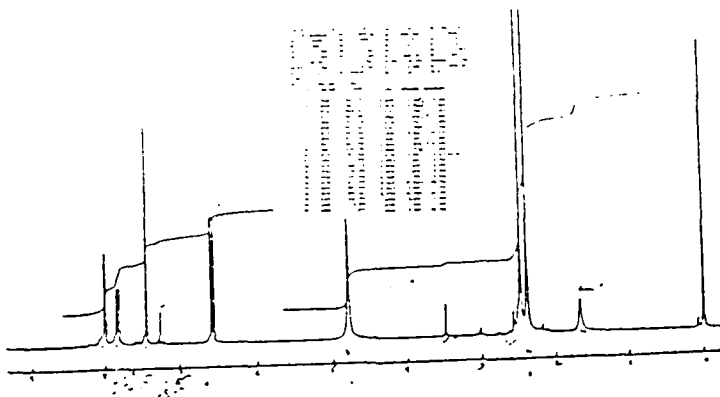


FIGURE 36: NMR of 3,5-dichloro-
2,2'-dimethyl-4'-nitro-
4'-nitro diphenyl sulfide

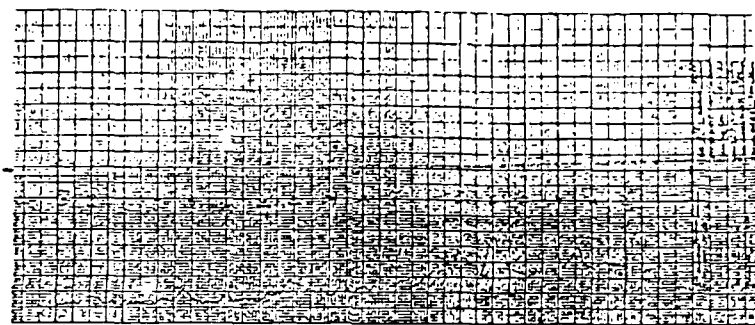


FIGURE 38: WAX of Poly(DNDS)

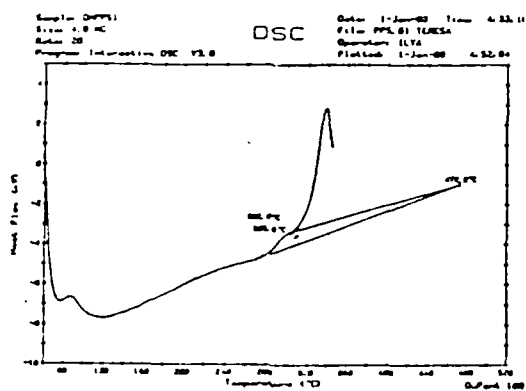


FIGURE 37: DSC of Poly(DNDS)

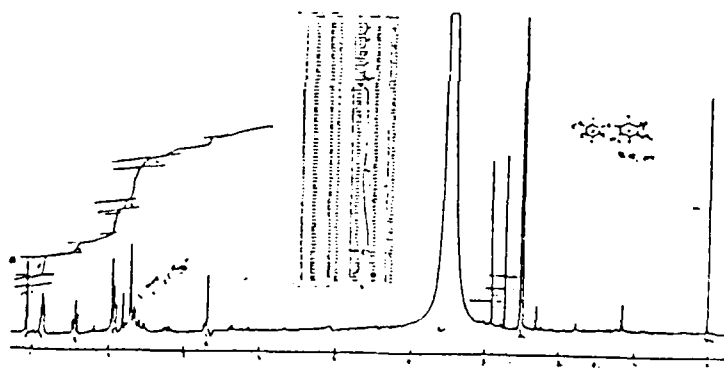


FIGURE 39: NMR of Poly(DNDS)

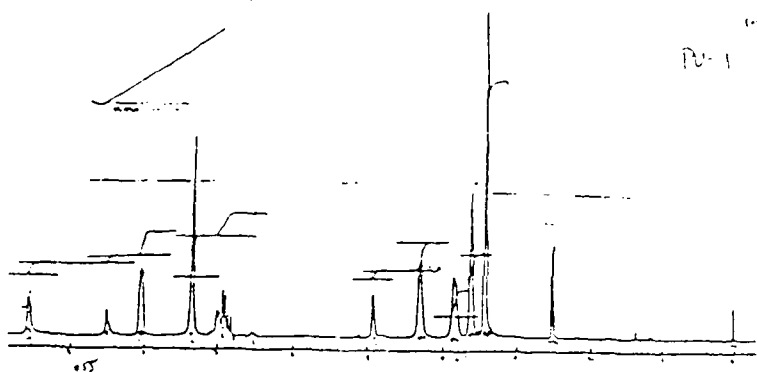


FIGURE 56: NMR of PU1

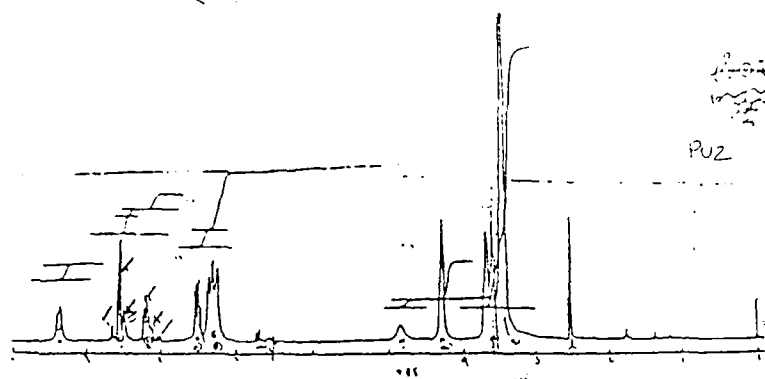


FIGURE 57: NMR of PU2

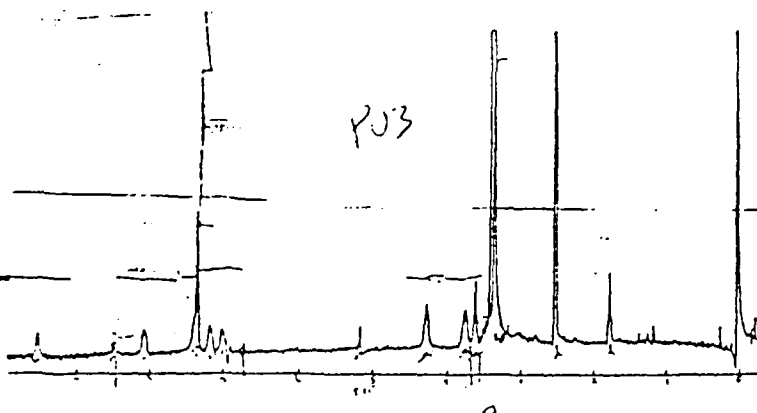


FIGURE 58: NMR of PU3

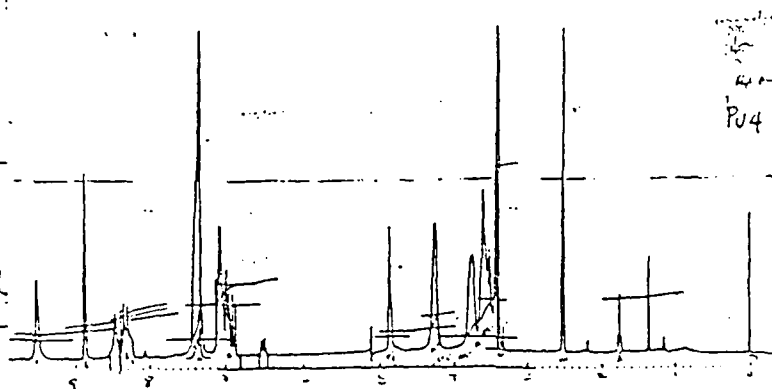


FIGURE 59: NMR of PU4

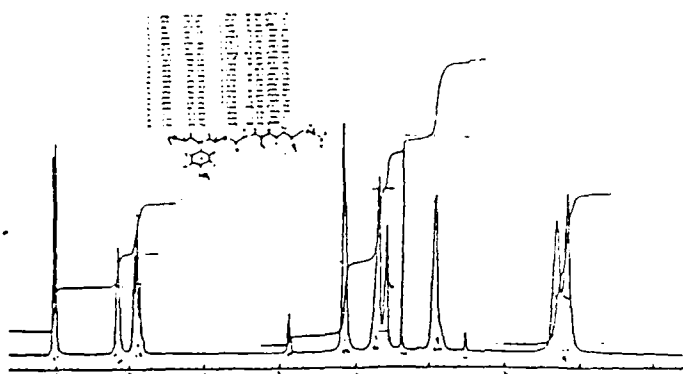


FIGURE 60: NMR of HU1

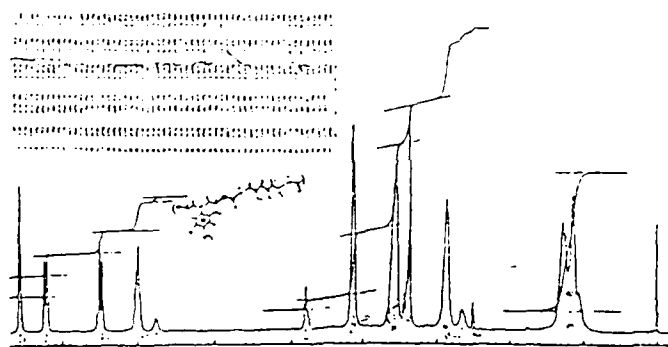


FIGURE 61: NMR of HU2

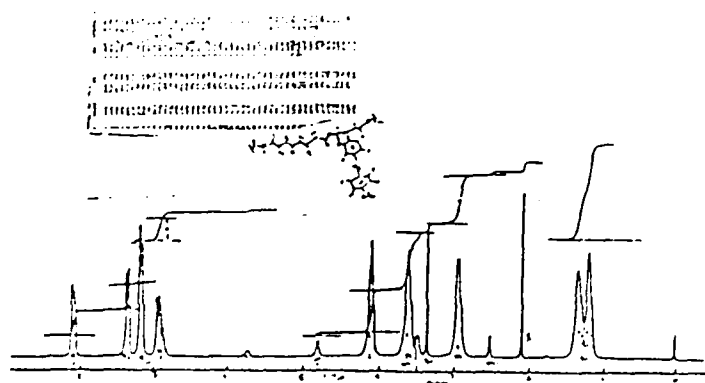


FIGURE 62: NMR of HU3

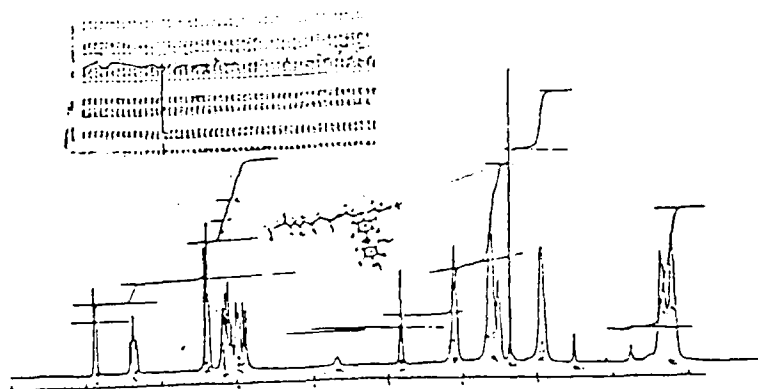


FIGURE 63: NMR of HU4

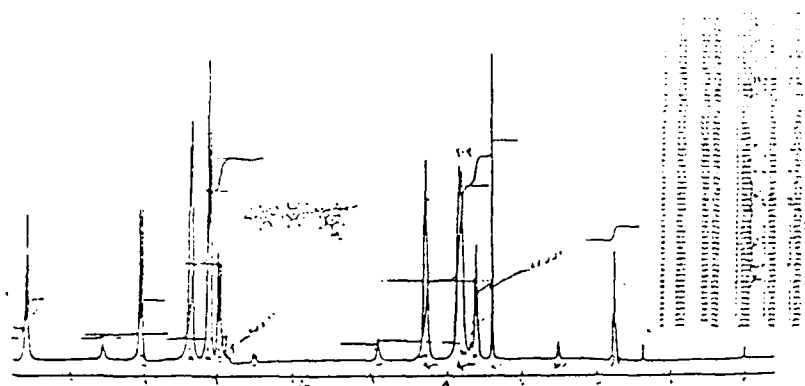


FIGURE 64: NMR of DU1



FIGURE 65: NMR of DU2

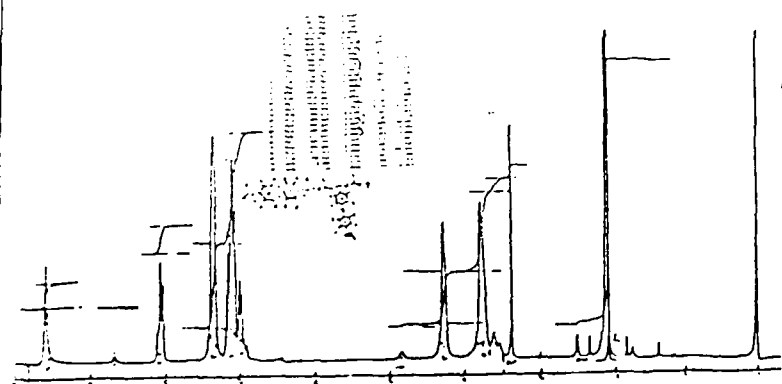


FIGURE 66: NMR of DU3

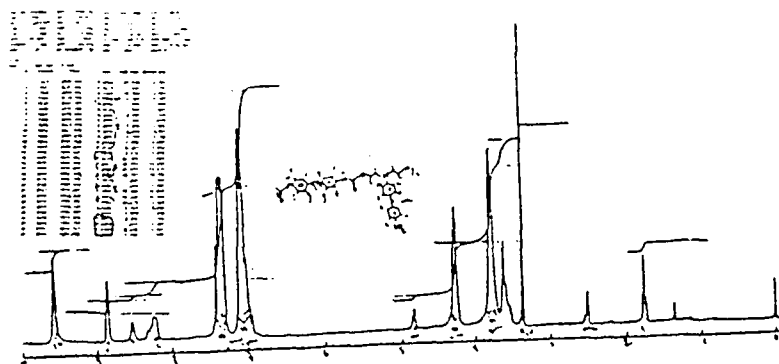


FIGURE 67: NMR of DU4

Scan Name: REG001 Resolution: 4.000 cm⁻¹ Scan Time: 01:12 100 scans
 Start: 4000.00 End: 400.00
 No additional information
 16:09:54 14 NOV 1989

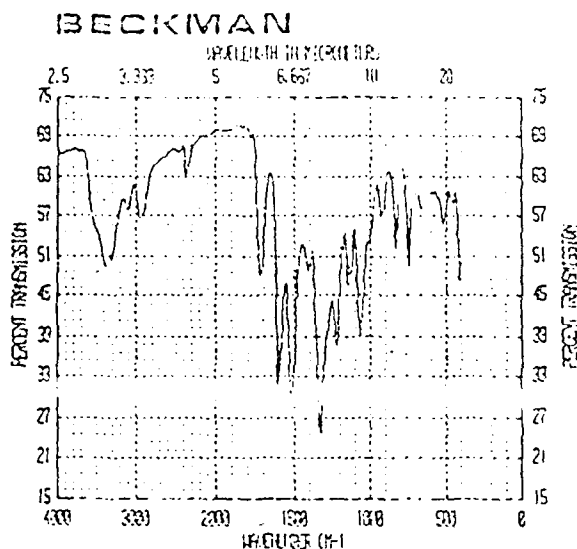


FIGURE 68: IR Spectrum of PU1

Scan Name: REG001 Resolution: 4.000 cm⁻¹ Scan Time: 01:12 100 scans
 Start: 4000.00 End: 400.00
 No additional information
 16:09:54 14 NOV 1989

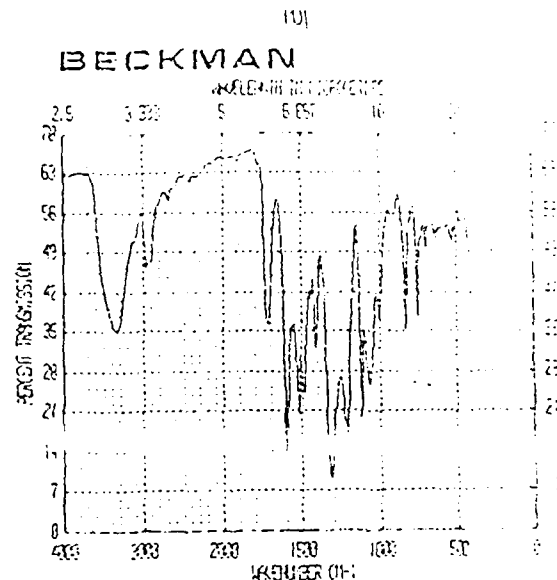


FIGURE 69: IR Spectrum of PU2

Scan Name: REG001 Resolution: 4.000 cm⁻¹ Scan Time: 01:12 100 scans
 Start: 4000.00 End: 400.00
 No additional information
 16:09:54 14 NOV 1989

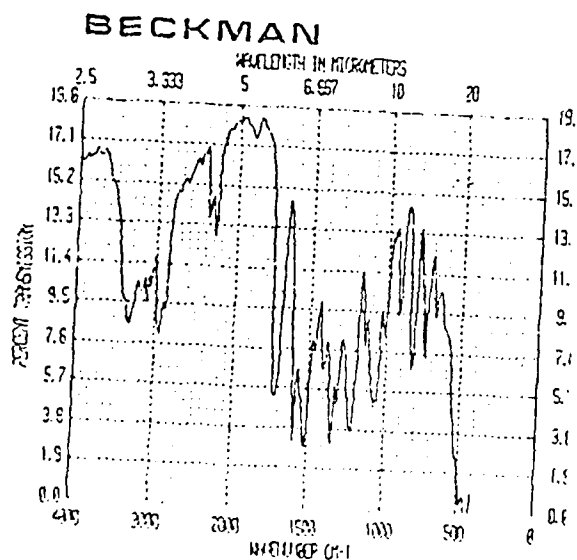


FIGURE 70: IR Spectrum of PU3

Scan Name: REG001 Resolution: 4.000 cm⁻¹ Scan Time: 01:12 100 scans
 Start: 4000.00 End: 400.00
 No additional information
 16:09:54 14 NOV 1989

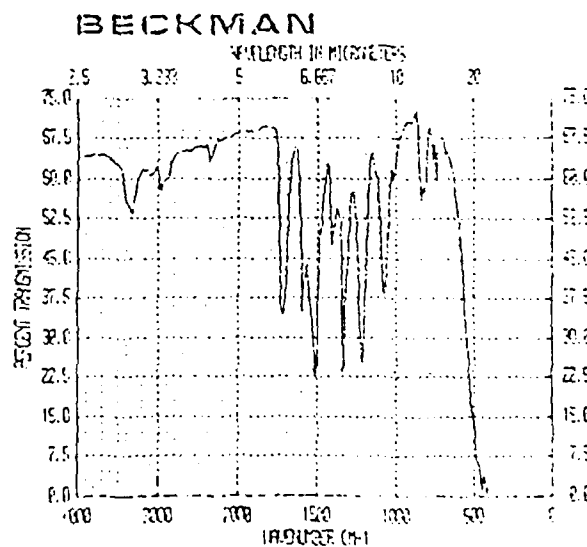


FIGURE 71: IR Spectrum of PU4

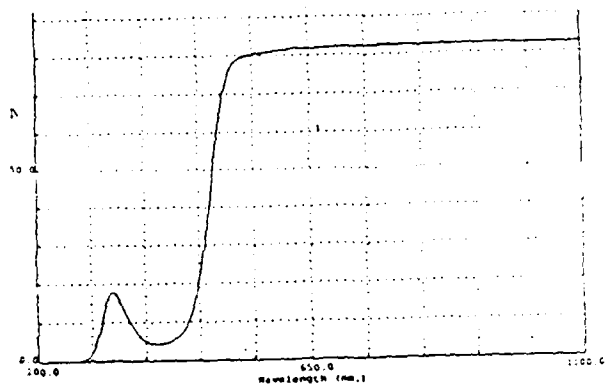


FIGURE 72: UV Spectrum of PU1

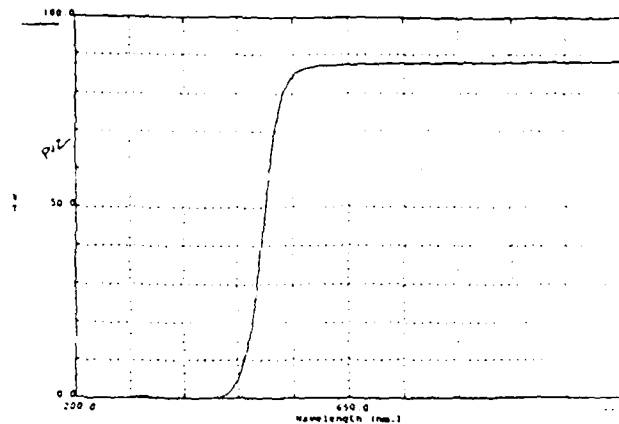


FIGURE 73: UV Spectrum of PU2

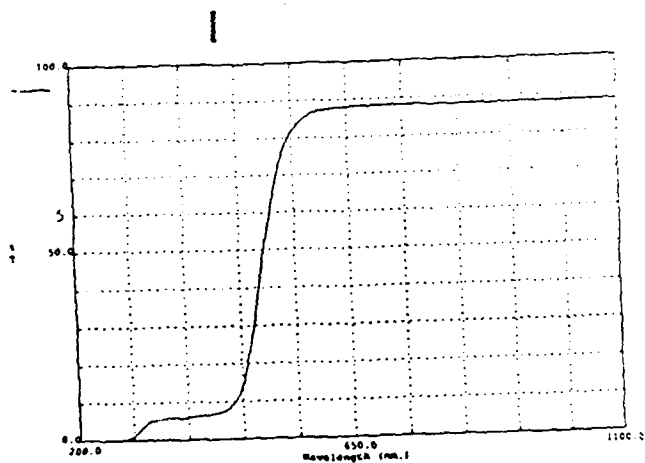


FIGURE 74: UV Spectrum of PU3

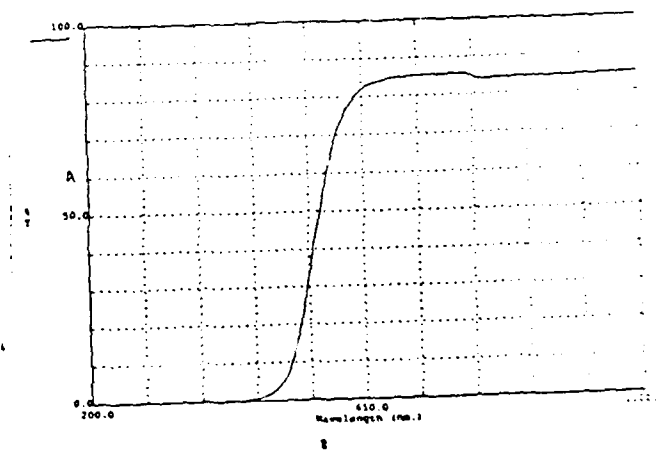


FIGURE 75: UV Spectrum of PU4

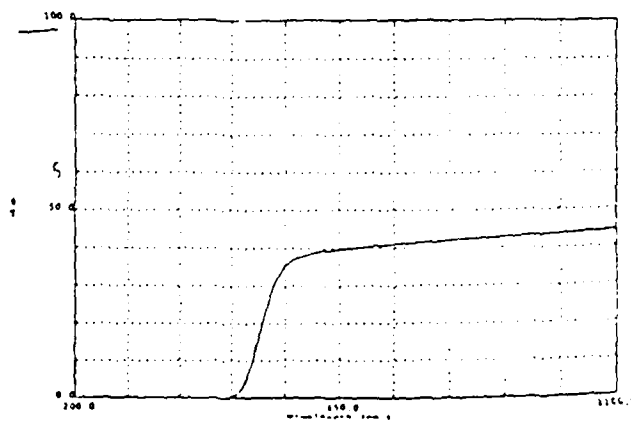


FIGURE 76: UV Spectrum of PU5

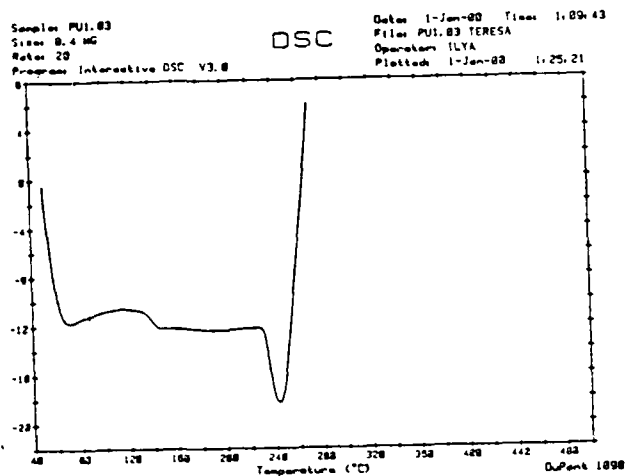


FIGURE 77: DSC of PU1

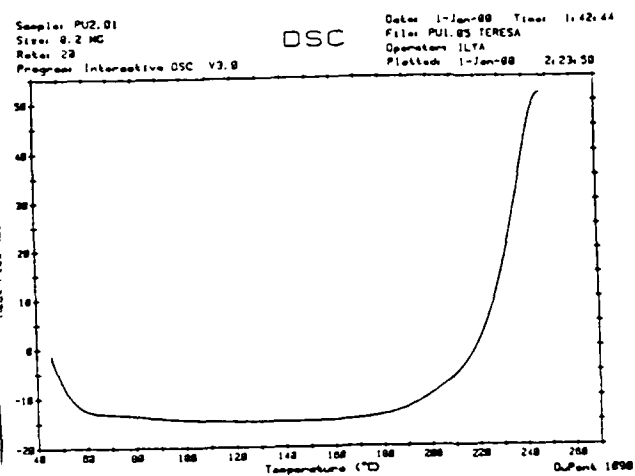


FIGURE 78: DSC of PU2

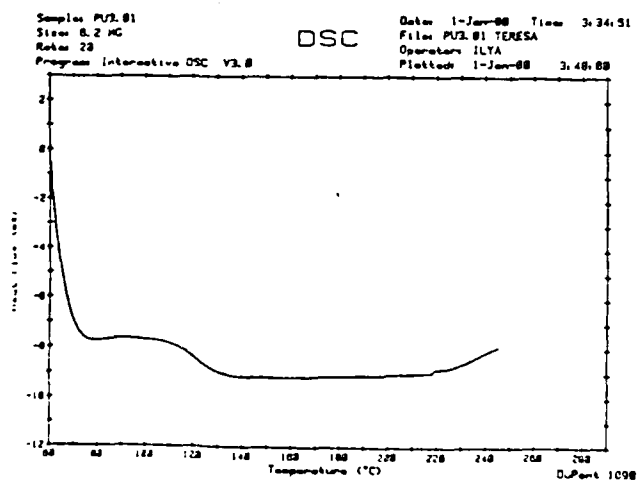


FIGURE 79: DSC of PU3

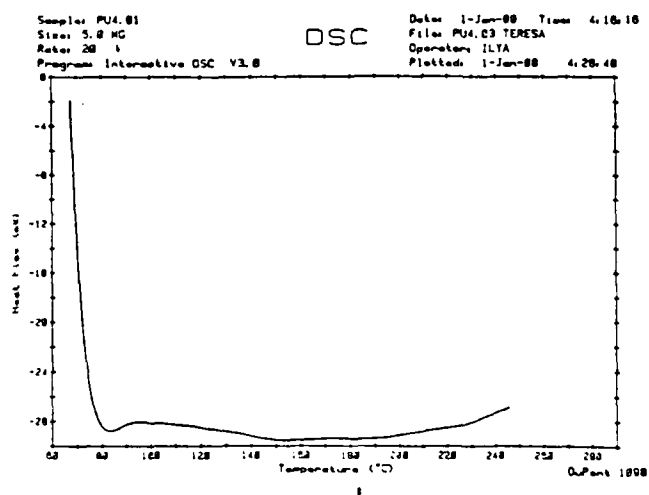


FIGURE 80: DSC of PU4

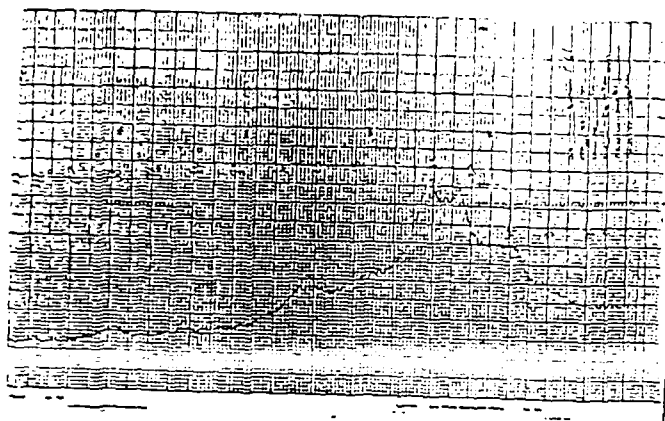


FIGURE 81: SAX from PU1

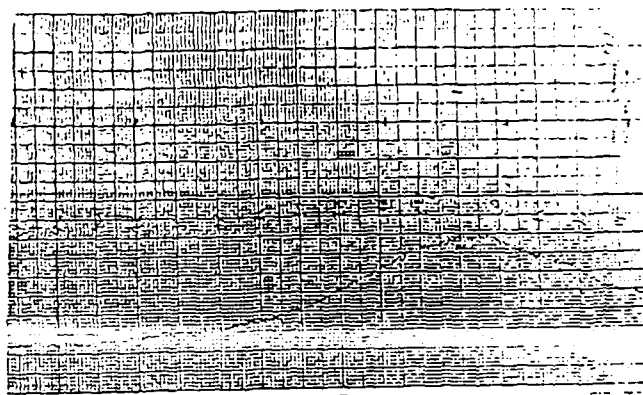


FIGURE 82: SAX from PU2

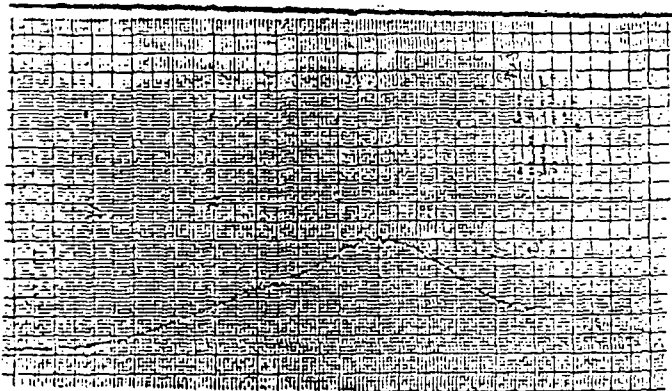


FIGURE 83: SAX from PU3

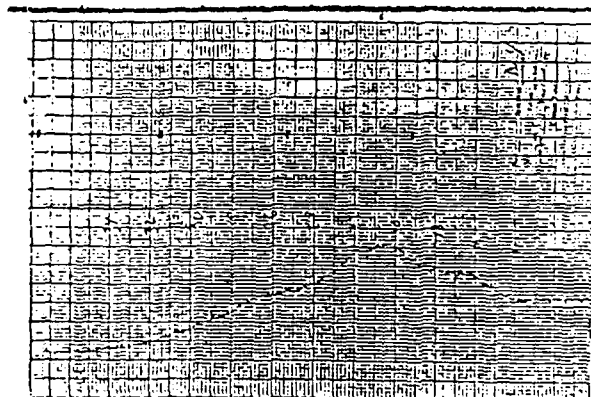


FIGURE 84: SAX from PU4

FIGURE 85

PARALLEL PLATES POLING

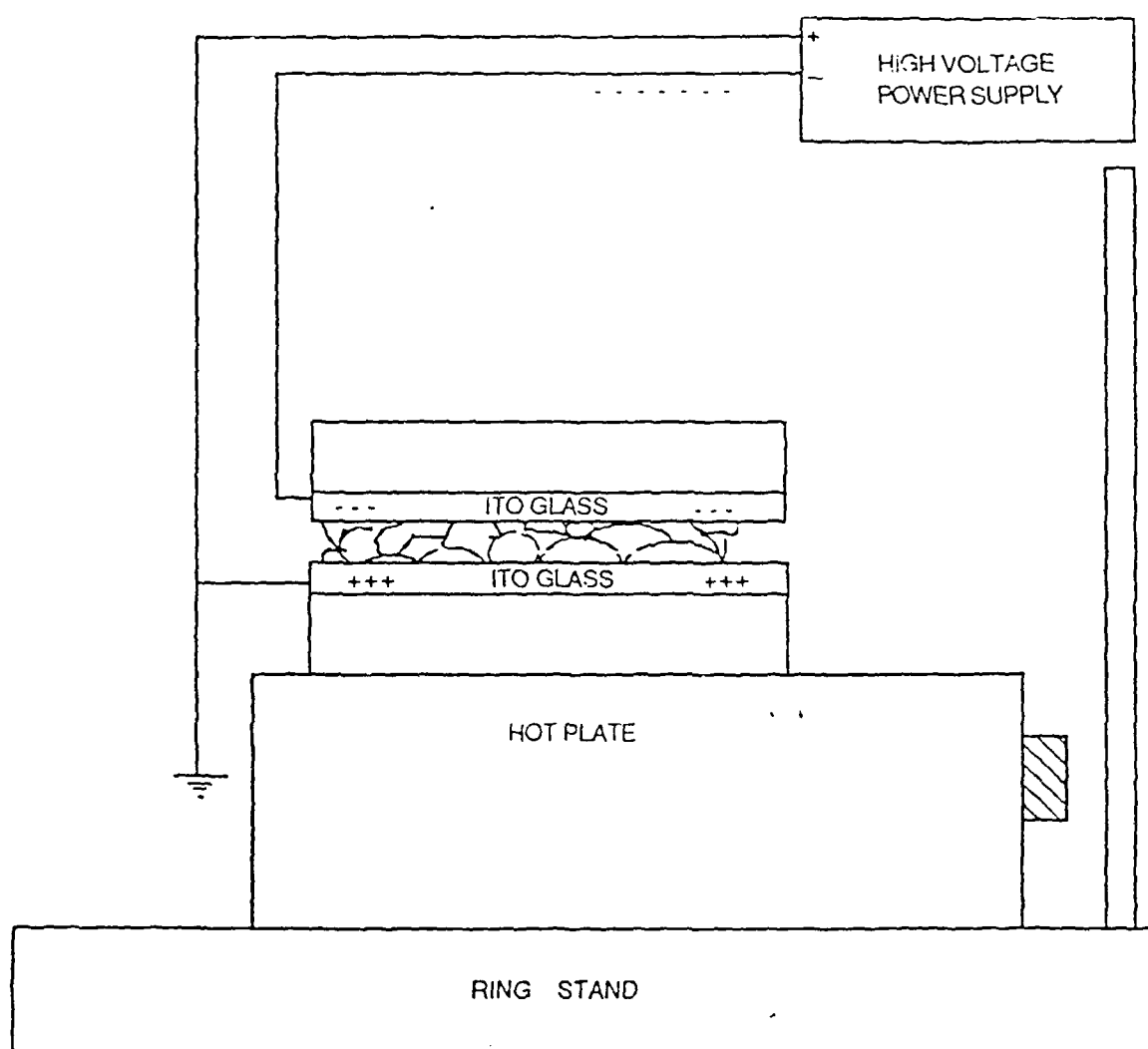


FIGURE 86

PARALLEL PLATES ALIGNMENT POLYMERIZATION WITH PET

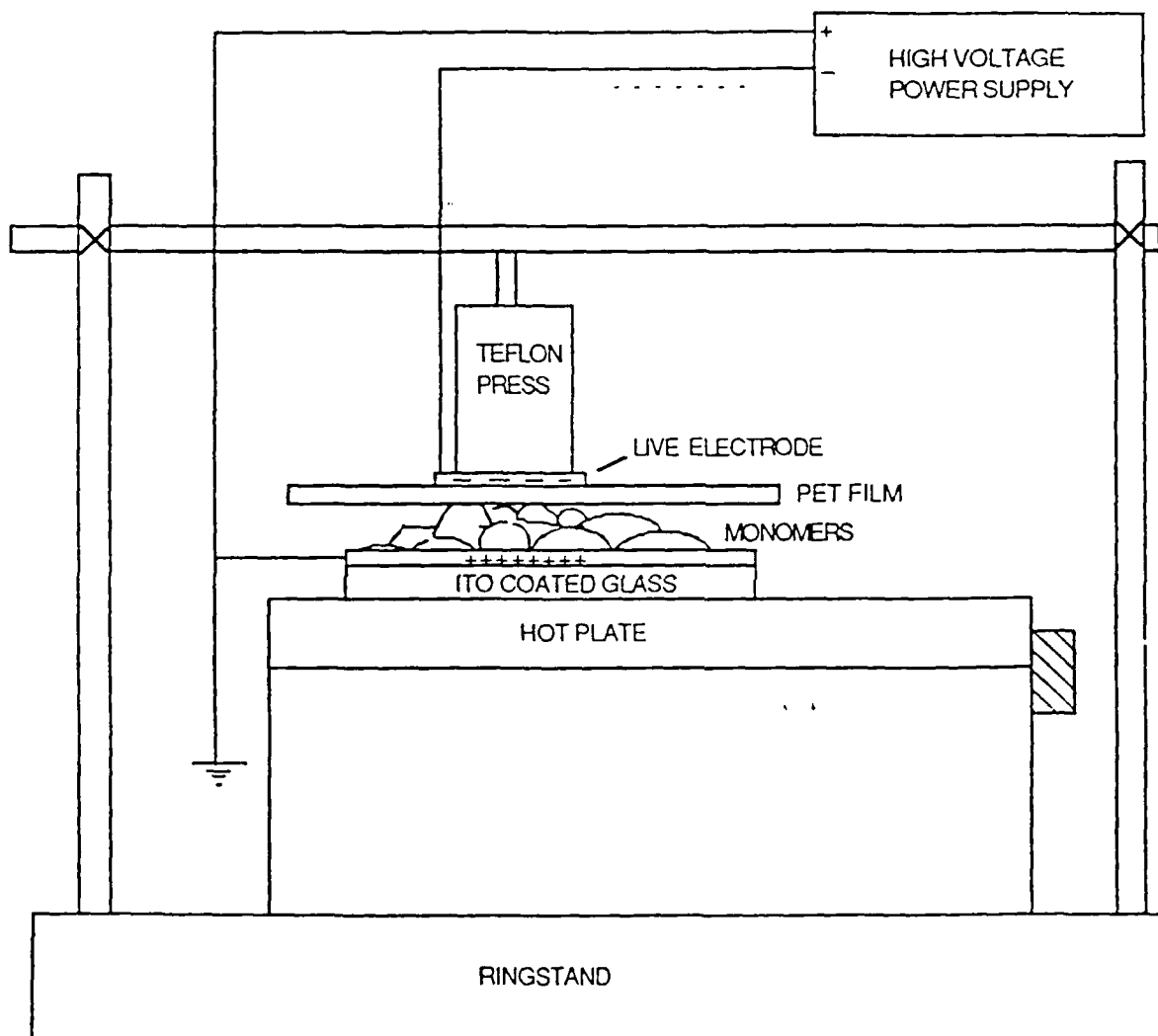
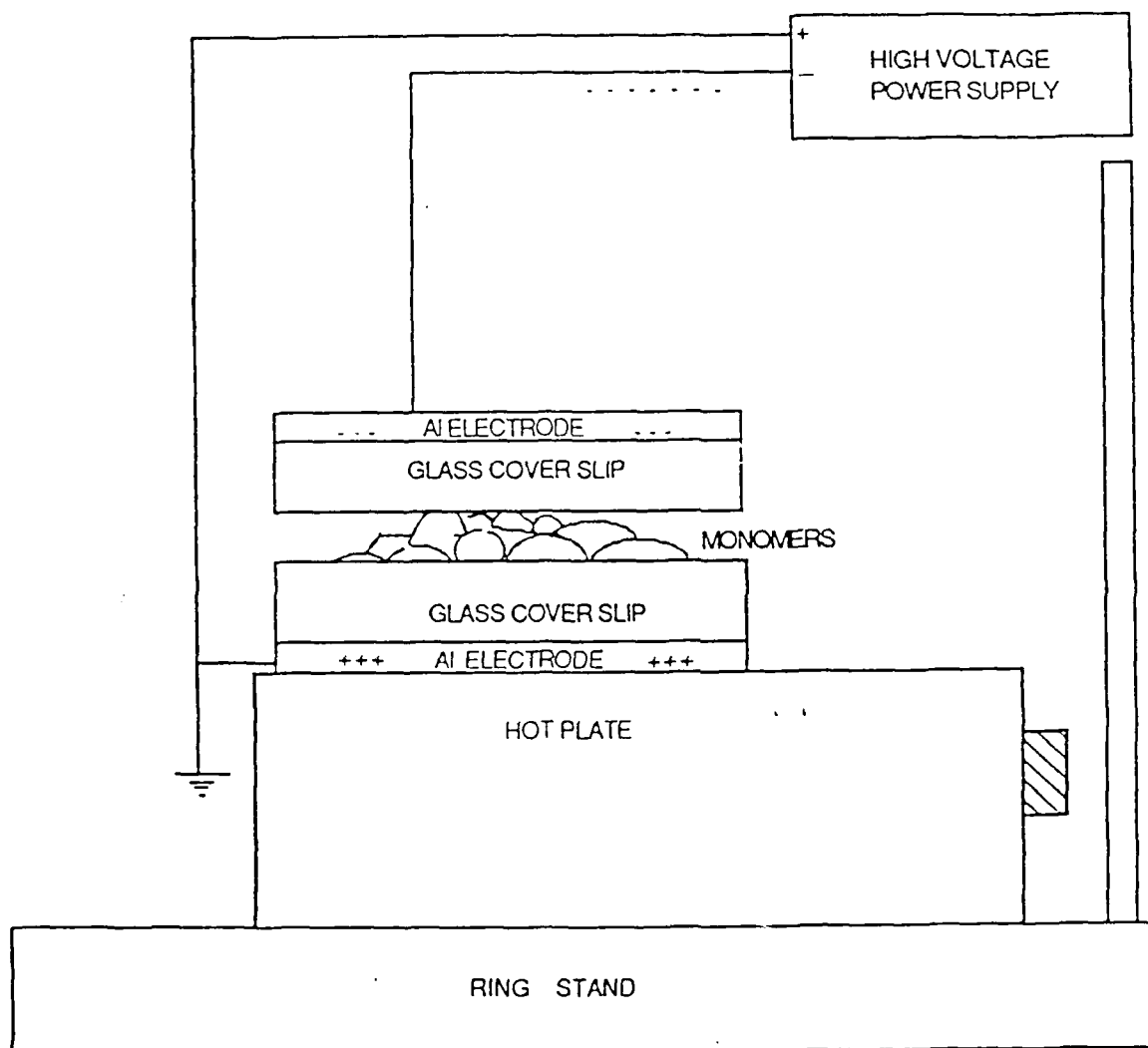


FIGURE 87

PARALLEL PLATES ALIGNMENT POLYMERIZATION, WNEK METHOD



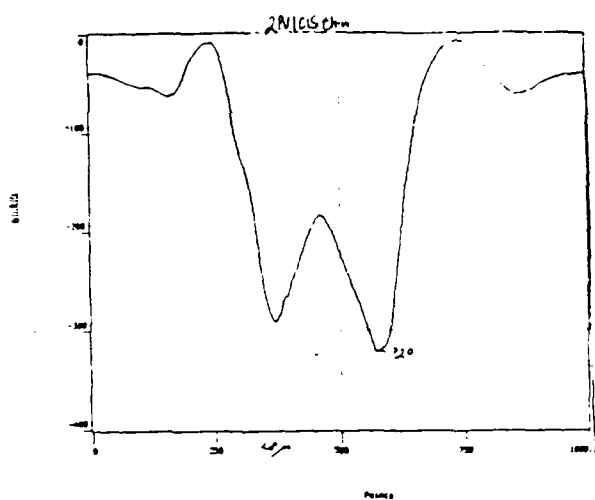


FIGURE 88: SHG from PU1C15

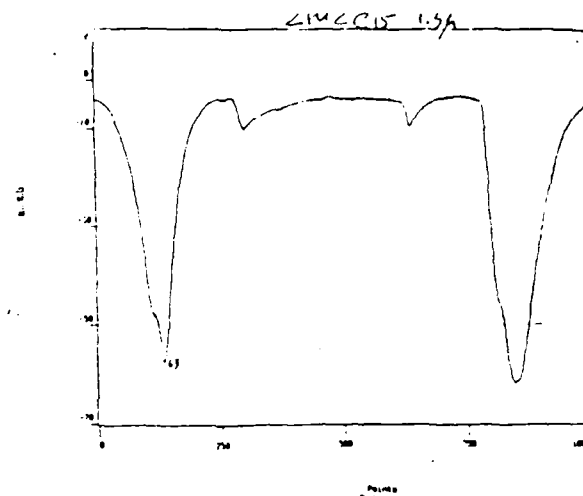


FIGURE 89: SHG from PU2C15

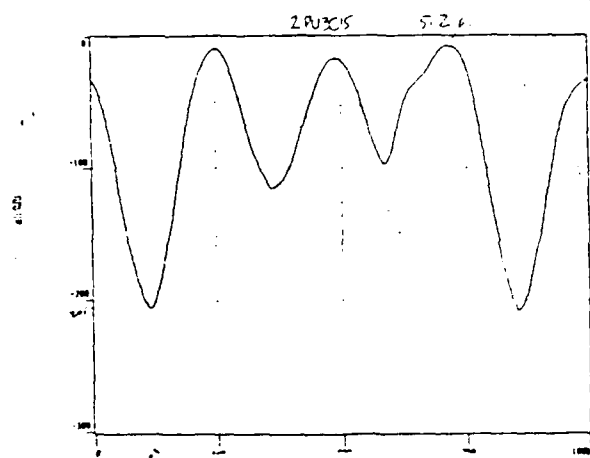


FIGURE 90: SHG from PU3C15

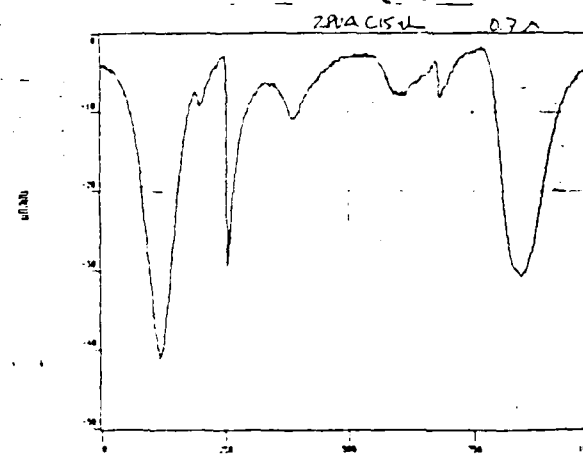


FIGURE 91: SHG from PU4C15

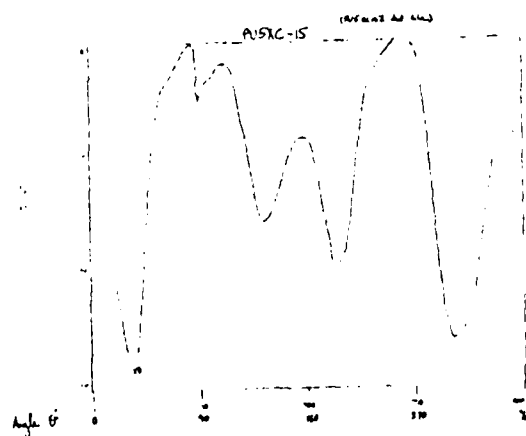


FIGURE 92: SHG from PU5C15

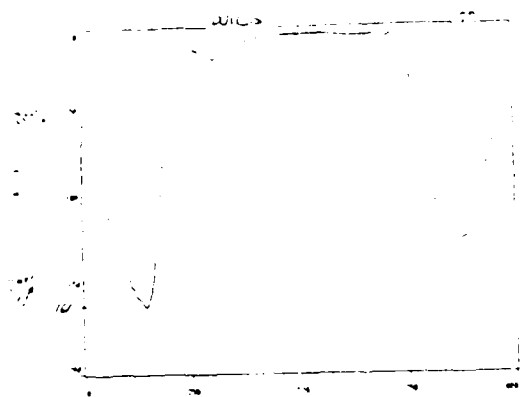


FIGURE 93: SHG from DU1C15

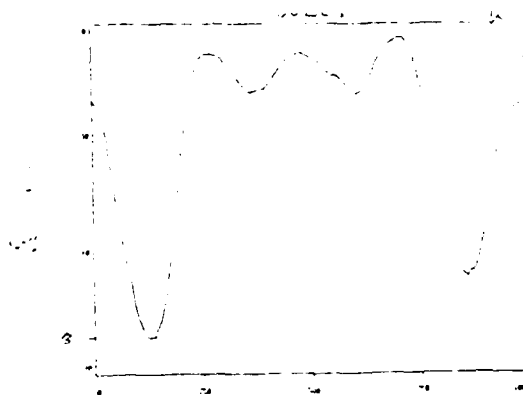


FIGURE 94: SHG from DU2C15

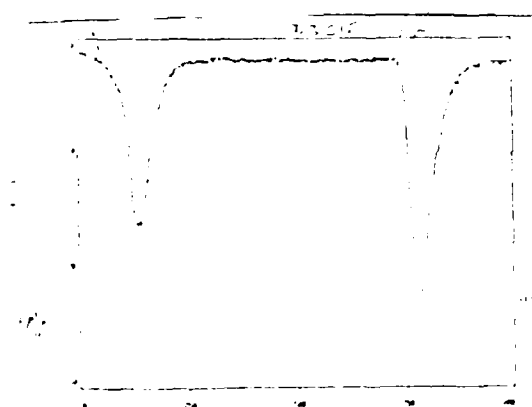


FIGURE 95: SHG from DU3C15

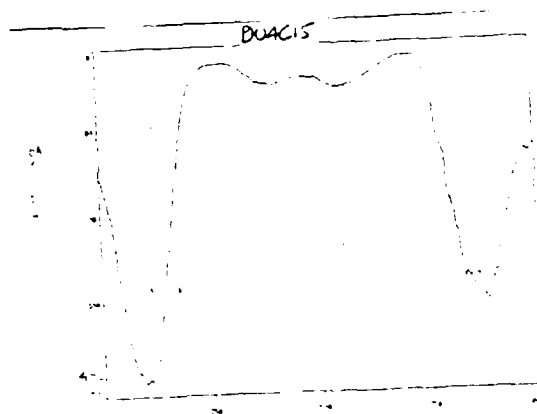


FIGURE 96: SHG from DU4C15

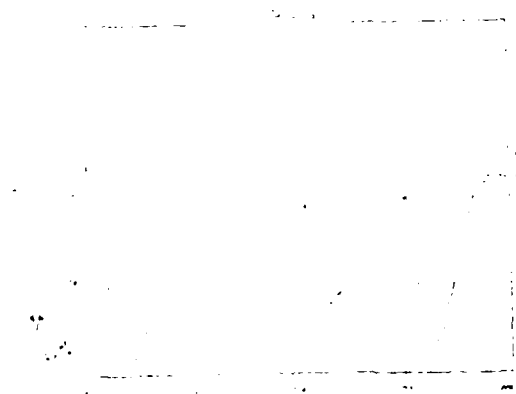


FIGURE 97: SHG from DU5C15

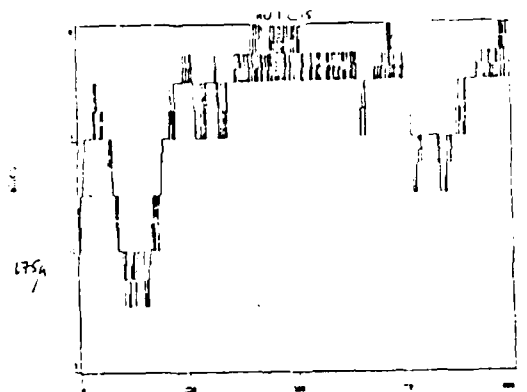


FIGURE 98: SHG from HU1C15

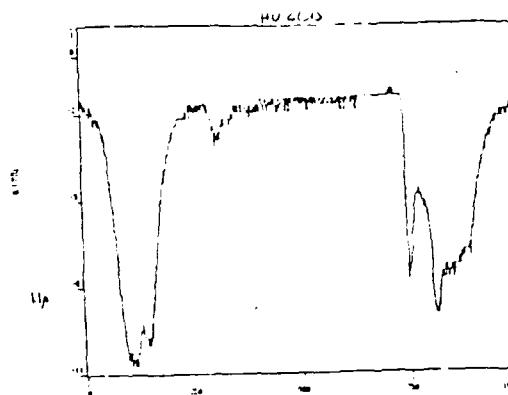


FIGURE 99: SHG from HU2C15

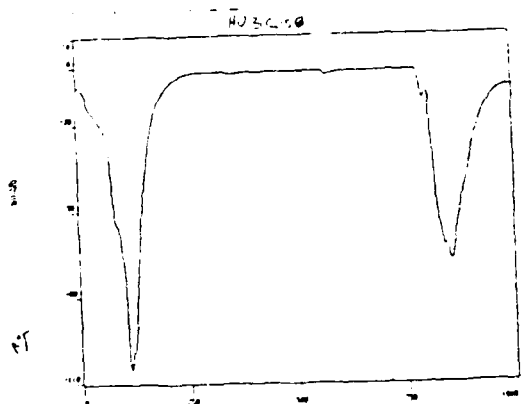


FIGURE 100: SHG from HU3C15

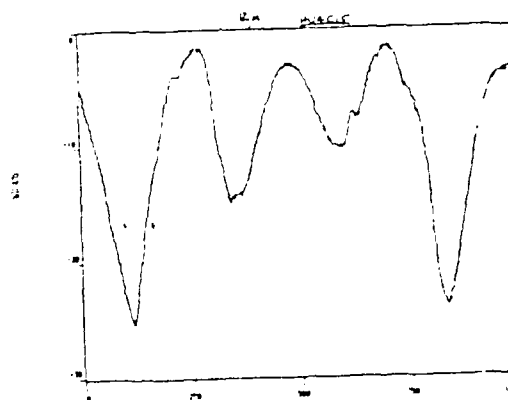


FIGURE 101: SHG from HU4C15

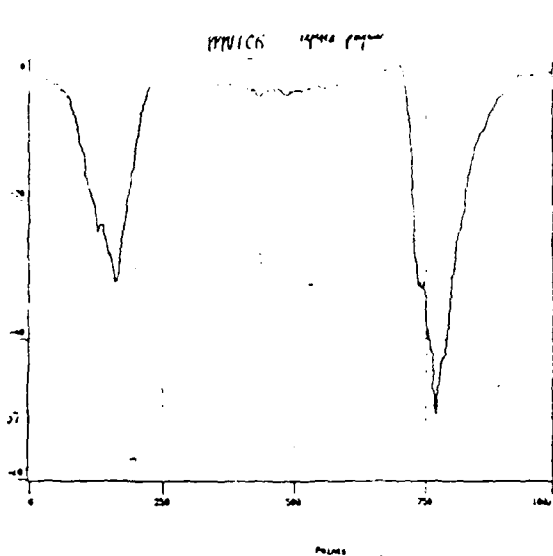


FIGURE 103: SHG from Repoled
PU1C15

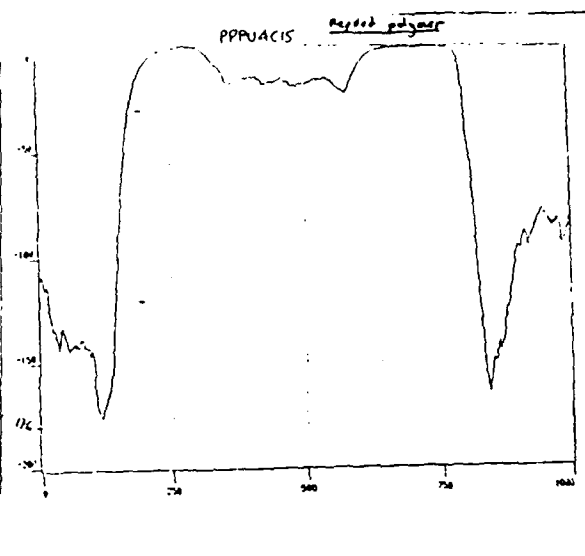


FIGURE 104: SHG from Repoled
PU4C15

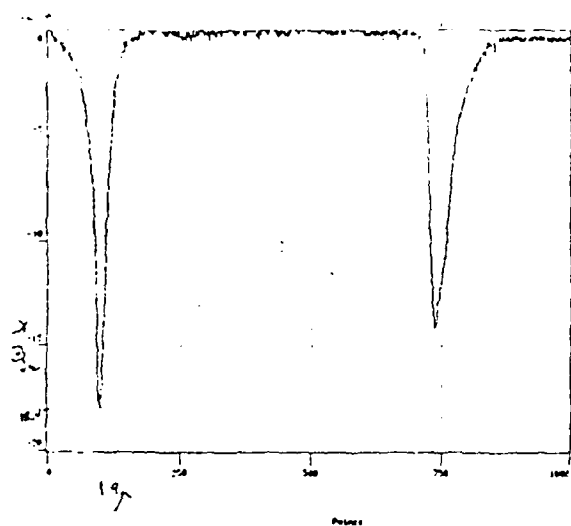


FIGURE 105: SHG from PE1C15

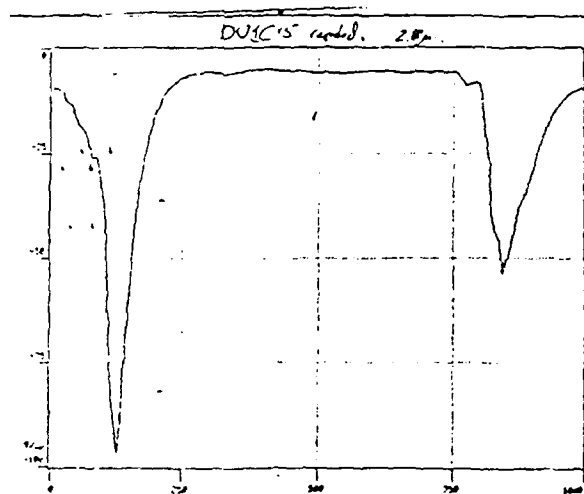


FIGURE 120: SHG from Repoled
DU1C15

REFERENCES

1. Nonlinear Optical Properties of Organic and Polymeric Materials, ACS Symposium Series, Polymer Chemistry Division, September 1982, Kansas City.
2. Molecular and Polymeric Optoelectronic Materials: Fundamentals and Applications, SPIE's 30th International Symposium on Optical and Optoelectronic Applied Sciences and Engineering, 21 - 22 August 1986, San Diego, CA.
3. Nonlinear Optical Properties of Organic Materials, SPIE's 32nd Annual International Technical Symposium on Optical and Optoelectronic Applied Science and Engineering, 14 -19 August 1988, San Diego, CA.
4. A.F. Garito, K.D. Singer and C.C. Teng in Nonlinear Optical Properties of Organic and Polymeric Materials, D.J. Williams, ed., ACS Symposium Series, Polymer Chemistry Division, September 1982, Kansas City.
5. S.K. Kurtz and T.T. Perry, *J. Appl. Phys.*, **39** (8), 3798 (1968).
6. J.Jerphragnon and S.K. Kurtz, *J. Appl. Phys.*, **41** (4), 1667 (1970).
7. E.E. Havinga and P. Van Pelt, *Ber. Bundsesenges. Phys., Chem.* **83**, 816 (1979).
8. G.R. Meredith, J.G. Vandusen, and D.J. Williams in Nonlinear Optical Properties of Organic and Polymeric Materials, D.J. Williams, ed., ACS Symposium Series, Polymer Chemistry Division, September 1982, Kansas City.
9. D.J. Williams, *Angew. Chem. Int. Ed. Engl.* **23**, 690 (1984).

10. J.B. Stamatoff et al., in Molecular and Polymeric Optoelectronic Materials: Fundamentals and Applications, G. Khanarian, ed., Proceeding of the SPIE's 30th International Symposium on Optical and Optoelectronic Applied Sciences and Engineering, 21 - 22 August 1986, San Diego, CA.
11. K.D. Singer, J.E. Sohn and S.J. Lalama, *Appl. Phys. Lett.*, **49** (5), 248 (1986).
12. M. Eich et al., *J. Appl. Phys.*, **66** (6), 2259 (1989).
13. I. Gorodisher, Master's Thesis, MIT.
14. F. Zernike and J.E. Midwinter, Applied Nonlinear Optics, John Wiley & Sons; New York, 1973, p. 26.
15. R.J. Twieg and K. Jain in Nonlinear Optical Properties of Organic and Polymeric Materials, D.J. Williams, ed., ACS Symposium Series, Polymer Chemistry Division, September 1982, Kansas City.
16. Reference 4, page 5.
17. Reference 15, pages 60, 61.
18. Reference 14, pages 3 and 29 - 31.
19. *ibid*, p. 43.
20. Buckley et al, Proceeding of the ACS Symposium on Solid State Polymerization, New York, April 13-18, 1986.
21. A.Yariv and P. Yeh, Optical Waves in Crystals, Wiley, 1984.
22. Reference 4, p. 7.
23. J.D. Swalen et al, *IBM Research Report*, Physics, September 27, 1989.

24. G.E. Wnek et al in A.J. Heeger, J. Orenstien and D.R. Ulrich eds., *MRS Symposium Proceedings*, **109**,139, (Boston1988).
25. H. Abdel-Halim et al., *J. Phys. Chem.*, **90**, 5654 (1986),
26. A. Mangini and R. Passerini, *J. Chem. Soc.*, 4954 (1956).
27. A. Mangini and R. Passerini, *J. Chem. Soc.*, 1168 (1952).
28. G. Modena, *Proc. 4th Intern. Meeting Mol. Spectry.*, Bologna, pp. 483- 490 (1952), *Chem. Abstr.* **59**: 4688h.
29. H.H. Szmant and J.J. McIntosh, *J. Am. Chem. Soc.*, **73**, 4356 (1951).
30. A.E. Lutski, E.M. Obuhova, and R.C. Cheshko, *Zhur. Fiz. Khim.* **42(8)**, 1861, (1968).
31. V. Baliah and V.M. Kanagasabapathy, *Indian Journal of Chemistry*, **16B**, 810 (1978).
32. L.M. Litvinenko and R.C. Cheshko, *Zhur. Obshchei Khim.* **30**, 3682, (1960); L.M. Litvinenko and R.C. Cheshko, *Izvest. Vysshikh. Ucheb. Zavedenii, Khim. i Khim. Technol.*, **3(1)** 99, (1960).
33. J.B. Hyne and J.W. Greidanus, *Canadian Journal of Chemistry*, **47**, 803, (1968).
34. R.M. Silverstein, G.C. Bassler, and T.C. Morrill, *Spectrometric Identification of Organic Compounds*, J. Wiley and Sons, N.Y. 1981, pp. 305 - 308.
35. Jerry March, *Advanced Organic Chemistry*, Wiley, New York, 1985, pp. 238 - 245.
36. S. Inoue et al., *Synthetic Metals* **28**, p. D231, (1989).

37. A. Mangini, *Pure Appl. Chem.*, p.103, (1963).
38. J.-L. Bredas, in Handbook of Conducting Polymers, edited by T. Skotheim (Dekker 1986), pp. 893-894.
39. C.B. Duke and A. Paton, in *Conductive Polymers*, edited by R.B. Seymour, (Plenum, 1981), pp. 162-165.
40. K. Ikawa, *Yakugaku Zasshi*, **79**, 764 (1959); **Chem. Abstr.** **54**, 10922h (1960).
41. G.W. Raiziss et al., *J. Am. Chem. Soc.*, **61**, 2763, (1939).
42. R. Lantz, U.S. Patent # 1,965,776.
43. L.M. Litvinenko et al, *Zhur. Obschei Khim.*, **29**, 1470, (1959),
Chem. Abstr. **54**, 8721c, (1960).
44. L.M. Litvinenko and N. F. Levchenko, *Zhur. Obschei Khim.*, **29**, 3079, (1959).
45. Y.O. Gabel and F.L. Grinberg, *J. Appl. Chem. USSR English Transl.*, **12**, 1481 (1939); **Chem. Abstr.** **34**, 6244 (1940).
46. M.S. Zhedek, *Zh. Prikl. Khim.* **25**, 109 (1953); **Chem. Abstr.** **47**, 867a, (1953).
47. Porter, *Organic Reactions* **20**, pp.455 - 481, (1973).
48. Dr. Yen Wei, unpublished results.
49. Dr. G.E. Wnek, unpublished results.
50. Dr. G.E. Wnek, private communication.
51. H. Gilman and J.F. Nobis, *J. Am. Chem. Soc.*, **71**, 274, (1949).
52. A. Mangini and R. Passerini, *Gazzetta Chim. Ital.*, **84**, 606, (1954).

53. D.J. Pasto and C.R. Johnson, Laboratory Text for Organic Chemistry, Prentice Hall, N.J., 1979, p.48.
54. G.B. Butler and F.L. Ingley, *J. Am. Chem. Soc.*, **73**, 895, (1951).
55. W.E. Gibbs and R.J. Van Deusen, *Journal of Polymer Science*, **54**(159), S1, (1961).
56. G.B. Butler and R.J. Angelo, *J. Am. Chem. Soc.*, **79**, 3128, (1957).
57. G. Odian, Principles of Polymerization, Wiley-Interscience, N.Y. 1981, p. 239.
58. *ibid*, pp. 243 - 246.
59. Dr. H. Hall, private communication.
60. T. Sulzberg and R.J. Cotter, *Macromolecules* **1**(6), 554 (1968).
61. T. Sulzberg and R.J. Cotter, *Macromolecules* **2**(2), 146 (1969).
62. Reference 86, pp. 103 - 105.
63. H.R. Allcock and F.W. Lampe, Contemporary Polymer Chemistry, Prentice-Hall, N.J., 1981, pp. 29 - 31.
64. R.W. Lenz, Organic Chemistry of Synthetic High Polymers, Wiley-Interscience, N.Y. 1967, pp.86 - 88.
65. S.R. Sandler and W. Karo, Polymer Synthesis, pp. 66 - 67, and pp. 74 - 84, Academic Press, N.Y. 1974.
66. C.A. Bischoff and A. von Hedenstrom, *Berichte der Deutschen Chemischen Gesellschaft* **35**(3), 3452 (1902).
67. J.F. Wolfe, B.H. Loo, and F.E. Arnold, *Macromolecules* **14**, 915 (1981).

68. G.T. Morgan, *Journal of the Chemical Society* **81**, 1382 (1902).
69. P. Hartley and J.B. Cohen, *Journal of the Chemical Society* **85**, 868 (1906).
70. E.H. Nason, *J. Am. Chem. Soc.* **40**, 1602 (1918).
71. M.J.J. Blanksma, *Recueil des Travaux Chimiques des Pays-Bas*, **21**, 419.
72. G.S. Hammond and F.J. Modic, *J. Am. Chem. Soc.*, **75**, 1385, (1953).
73. R.A. Wessling and R.G. Zimmerman, U.S. Patents # 3,401,152 and 3,706,677.
74. J.D. Capistran et al., *ACS Polymer Preprints* **25**(2), 282 (1984).
75. Reference 86, p.108.
76. *ibid.*, p.136, reference 93, p.187.
77. Reference 34, pp. 105 -128.
78. B.D. Cullity, Elements of X-ray Diffraction, Addison-Wesley, MA, 1978, p. 102.
79. D.K. Das-Gupta and K. Doughty, *IEEE Transactions On Industry Applications* **1A-14** (15), 448 (1978).
80. D. Kingery, K. Bowen and D. Uhlmann, Introduction to Ceramics, p.947, Wiley-Interscience, N.Y. 1976.
81. Reference 64, p. 185
82. G.T. Boyd, *Thin Solid Films* **152**, 295 (1987).
83. D.J. Williams, *Angew. Chem. Int. Ed. Engl.* **23**, 690 (1984).

84. Hampsch et al., *Macromolecules* **21**, 526 (1988).
85. Marks et al., in Nonlinear Optical Properties of Organic Materials, G. Khanarian, ed., Proceedings of SPIE's 32nd Annual International Technical Symposium on Optical and Optoelectronic Applied Science and Engineering, 14 -19 August 1988, San Diego, CA.
86. References 10,11,12; also D.A. Ender et al. in Nonlinear Optical Properties of Organic Materials, G. Khanarian, ed., Proceedings of SPIE's 32nd Annual International Technical Symposium on Optical and Optoelectronic Applied Science and Engineering, 14 -19 August 1988, San Diego, CA.
87. G.R. Meredith, J.G. VanDusen, and D.J. Williams, *Macromolecules* **15**, 1385, (1982).
88. Reference 43, p. 380.
89. Dr. Yen Wei, unpublished results.
90. David Pugh and John O. Morley in Nonlinear Optical Properties of Organic Molecules and Crystals, D.S. Chelma and J. Zyss. editors, Academic Press, Inc., Orlando, Florida, 1987, p. 220.